12-2014

Oxidative Damage to DNA 2´-Deoxyribose by Carbonate Radicals: Reaction Mechanisms and Products

Terence J. Moore
East Tennessee State University

Oxidative Damage to DNA 2´-Deoxyribose by Carbonate Radicals: Reaction Mechanisms and Products

---

A thesis

presented to

the Faculty of the Department of Chemistry

East Tennessee State University

In partial fulfillment

of the requirements for the degree

Master of Science in Chemistry

---

by

Terence Joshua Moore

December 2014

Dr. Marina Roginskaya, Chair

Dr. Scott Kirkby

Dr. David Close

Keywords: DNA damage; oxidative stress; reactive oxygen species; carbonate radical anion

ABSTRACT

Oxidative Damage to DNA 2´-Deoxyribose by Carbonate Radicals: Reaction Mechanisms and Products

by

Terence Joshua Moore

The carbonate radical anion ($CO_3^{\bullet -}$, CR) is an important reactive oxygen species produced *in vivo* by one-electron oxidation of CO_2 or bicarbonate, constituents of the major physiological buffer. It was demonstrated for the first time by using an HPLC-based analysis of low-molecular products of DNA damage that CRs react with DNA 2´-deoxyribose by the hydrogen abstraction mechanism. CRs exhibit a ~ 800-fold preference for one-electron oxidation of guanine over hydrogen abstraction from DNA sugar, in sharp contrast with •OH. CRs also have, as compared to •OH, an increased preference for the H1´ abstraction, which is the most thermodynamically favorable due to the highest stability of the respective deoxyribosyl radical but kinetically the slowest due to low solvent accessibility, by the expense of the decreased preference for the H5´ abstraction. All these findings are in agreement with the characteristics of CR as a potent oxidant and selective hydrogen abstractor.

DEDICATION

To my mother, Diana, and my father, Terry, for showing me the value of education from an early age. None of my accomplishments would have been possible without each of you.

To the rest of my family for their love and support throughout my entire academic career.

To Justin for your unwavering support and encouragement. You have been my rock throughout this process, and I know you will only continue to inspire me to achieve great things.

ACKNOWLEDGEMENTS

I am endlessly grateful to Dr. Marina Roginskaya for her superb mentorship during my graduate studies at ETSU and for allowing me the opportunity to pursue my dreams under her guidance. Many thanks to Drs. Scott Kirkby and David Close for their time serving on my advisory committee. I am also indebted to Dr. David Close and Yuriy Razskazovskiy for use of their laboratory spaces and to Dr. Razskazovskiy for synthesizing the carbonato-cobalt complexes used extensively in my research. I am also grateful to Mr. Derrick Ampadu-Boateng, my lab mate, for his work on 8oxoG kinetics.

To the faculty and staff of the Chemistry Department for sharing their advice and wisdom with me, I am unceasingly appreciative. Many thanks to Mr. Ryan Alexander, Ms. Jillian Quirante, and Dr. Sandy Eagle for everything they do for the students and faculty in the Chemistry Department. Your tireless dedication to my colleagues and myself has not gone unnoticed.

I am also beholden to all my fellow graduate students in the Chemistry Department for their emotional and academic support. I know each of you will continue to amaze me as I follow your careers.

TABLE OF CONTENTS

Page

LIST OF TABLES

LIST OF FIGURES

Figure Page

LIST OF ABBREVIATIONS

FBR ..... free base release

SDP ..... sugar damage products

dL ..... 2´-deoxyribonolactone

5MF 5-methylenefuran-2-one

5´-Ald ..... 5´-aldehyde

Fur ..... furfural

C4´-OAS ..... C4´-oxidized abasic site

MDA ..... malondialdehyde

Lac 1-N-oxycarbonylmethyl-5-methyleneazacyclopent-3-ene

TBARS ..... thiobarbituric acid reactive substances

TBA ..... 2´-thiobarbituric acid

CR ..... carbonate radical anion

8oxoG 8-oxo-7,8-dihydroguanine

polyL ..... poly-L-lysine

NHE ..... normal hydrogen electrode

CHAPTER 1

INTRODUCTION

Oxidative Stress and DNA

The adverse side effect of living in an oxygenated environment is the oxidation of biologically important macromolecules within aerobic organisms. While it has been shown that oxidation of these molecules is necessary to promote cellular signaling processes and hence is beneficial to the organism, excessive production of species capable of oxidizing biomolecules may be defined as a state of *oxidative stress*. This oxidative stress may be the result of endogenous or exogenous factors, including environmental pollution[1], UV light[2], and ionizing radiation[3,4]. The typical stressor is a *reactive oxygen species (ROS)* that is usually free radical in nature. ROS such as the hydroxyl radical (HO•), the superoxide radical ($O_2^{\bullet-}$), hydrogen peroxide (H_2O_2), nitric oxide (NO), and peroxynitrite ($ONOO^-$) have been implicated in a number of pathologies including inflammatory diseases, ischemia and reperfusion[5,6], neurodegenerative diseases (like Huntington's disease[7] and Alzheimer's disease[1,8]), cancers[6], stroke[5], respiratory diseases[9], and aging processes[6].

Among all biomolecules subjected to oxidative stress conditions, deoxyribonucleic acid (DNA) as the major hereditary unit is the major focus of studies in this field. A multitude of oxidative modifications to DNA may be initiated by interaction with ROS, including damage to the deoxyribose moiety of the sugar-phosphate backbone of the DNA double helix, nucleobase modifications within the DNA sequence, single- and double-strand breaks (SSB and DSB,

respectively), and DNA-protein crosslinks[6]. These types of oxidative damage to DNA are usually repaired by the cells under normal metabolic conditions, but during oxidative stress the repair mechanism is unable to cope with the volume of DNA lesions, and some DNA lesions are left unrepaired. It is these unrepaired DNA lesions that can lead to the development of the disease conditions listed above. In the specific case of cancers, this oxidative damage to DNA is believed to be the precursor to oncogene activation and tumor-suppressor gene inactivation, resulting in unregulated cellular growth (tumorigenesis)[10].

Types of Oxidative Damage to DNA: Sugar and Base Damage

DNA damage occurs when ROS attack the DNA at one of two loci: the deoxyribose moiety (sugar damage) or the nucleobase moiety (base damage). Base damage is estimated to account for 2/3 of the total damage, while sugar damage comprises the remaining 1/3 of total damage[11]. Sugar damage has been implicated as the precursor to DNA SSBs and DSBs, which have traditionally been acknowledged as important biomarkers for cellular DNA damage. The double-strand breaks initiated by sugar damage have also been considered to be mutagenic in nature due to possibility of base deletion, and contribute to increased genomic instability.

Sugar Damage

Upon reaction with 2′-deoxyribose (Figure 1, page 17), ROS can abstract a hydrogen from one of the five carbons present, resulting in a 2′-deoxyribosyl radical. Typical sugar lesions occur at the C1′, C4′, and C5′ positions of 2′-deoxyribose[12]. Although there is the potential for sugar damage at the C2′ and C3′ positions as well, the overall contribution of these pathways is

negligible as compared to the others, likely due to the lesser stability of the 2′-deoxyribosyl radicals formed after hydrogen-abstraction[12]. The relative stability of the radical formed follows the trend of •C1′ > •C4′ > •C5′ ~ •C3′ > •C2′, where the relative energies of these radicals were calculated by Colson and Sevilla at the ROHF/3-21G level of theory, and the stability of the C1′ and C4′ radicals is crucial due to the role of these radicals as the primary species responsible for base release and strand break, respectively[13]. Structures of the possible radicals formed by H-abstraction from 2′-deoxyribose are shown in Figure 2.

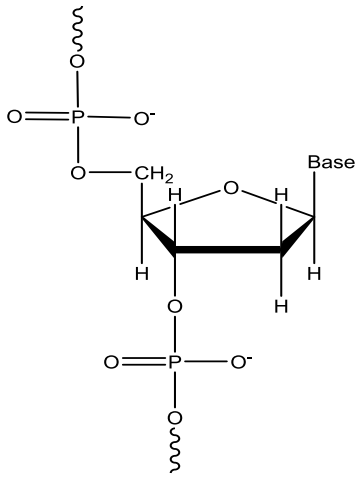

Figure 1: The structure of the 2′-deoxyribose moiety of the sugar-phosphate backbone of DNA, indicating the numbering of the five deoxyribose carbons

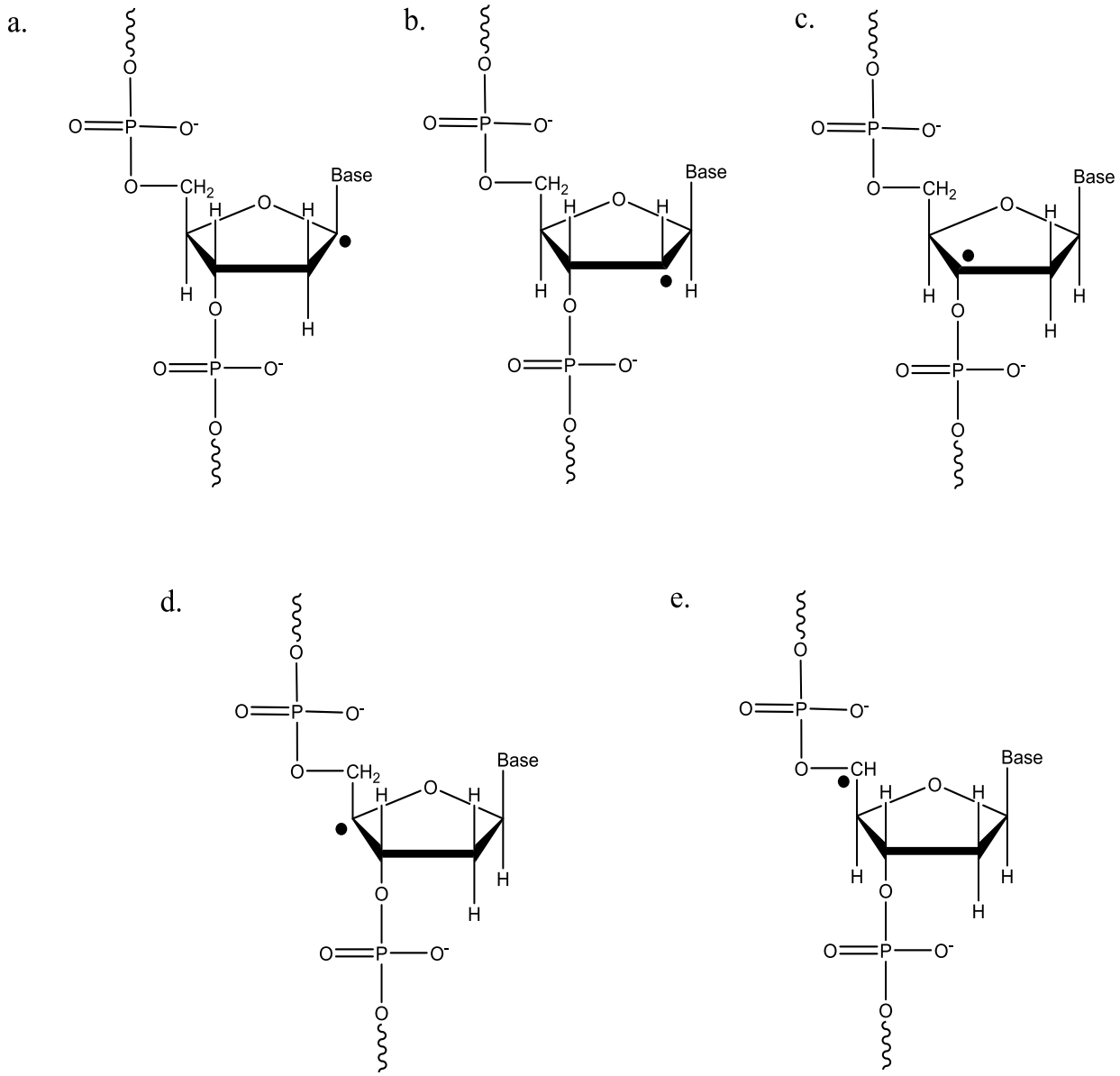

Figure 2: The structures of deoxyribosyl radicals formed via hydrogen abstraction. The radicals are arranged in increasing numerical order: a) C1′-radical; b) C2′-radical; c) C3′-radical; d) C4′-radical; and e) C5′-radical

The question of which DNA sugar hydrogen is preferentially abstracted during ROS attack has been studied extensively by our research group[14-17] and other research groups, and this

query is key to the study of DNA degradation by ROS attack. The debate is not without its share of controversy amongst the research community, but the nature of DNA oxidative lesions is heavily dependent on the position where hydrogen abstraction from 2′-deoxyribose occurs. The resulting consequences from each type of DNA damage are also dependent on the position of initial hydrogen abstraction.

The bulk of evidence suggests that DNA sugar damage occurs via combination of three major competing pathways: C1′, C4′, and C5′ sugar H-abstraction by ROS. Until recently, the focus of this research has been on the interaction between hydroxyl radicals (considered by many to be the most biologically important ROS), and these radicals specifically oxidize DNA sugar in the preferential order of C4′ > C1′ > C5′ >> C2′ ~ C3′.[14-18] The predominance of one pathway over the other is a combination of thermodynamic and kinetic factors: the thermodynamic preference of hydrogen abstraction from each position of 2′-deoxyribose is decreased in the order C1′ > C4′ > C2′ > C3′> C5′.[13,19] Solvent accessibility decreases in the order C5′ > C4′ ~ C3′ ~ C2′ ~ C1′, and this parallels the reactivity of the corresponding hydrogens to hydroxyl radicals.[12]

C1′ Pathway. The formation of a C1′deoxyribosyl radical is preceded by hydrogen abstraction from the C1′ position of the parent sugar. However, the C1′ hydrogen of 2′-deoxyribose is buried within the minor groove of the DNA beta helix (in B-DNA), and solvent accessibility to this locus is limited.[12] The reactivity at this position of 2′-deoxyribose is limited to minor groove-binding molecules in which the oxidant was generated within the groove and oriented toward the H1′ hydrogen.[12] Once the C1′ deoxyribosyl radical is formed it will proceed

down one of two pathways: the C1′ radical can be further oxidized to form a carbocation, while in the presence of molecular oxygen, a peroxyl radical is formed, followed by release of a superoxide anion and formation of a carbocation at the C1′ position. The carbocation formed by either of the previous two pathways is hydrolyzed by water; this process is accompanied by release of a free base (free base release, FBR). The resulting intermediate, 2′-deoxyribonolactone (dL), is relatively unstable and will undergo β- and δ-elimination of 5′-phosphate and the 3′-phosphate upon heating or at basic pH to form 5-methylenefuran-2-one (5MF). This reaction scheme is summarized in Figure 3.[18]

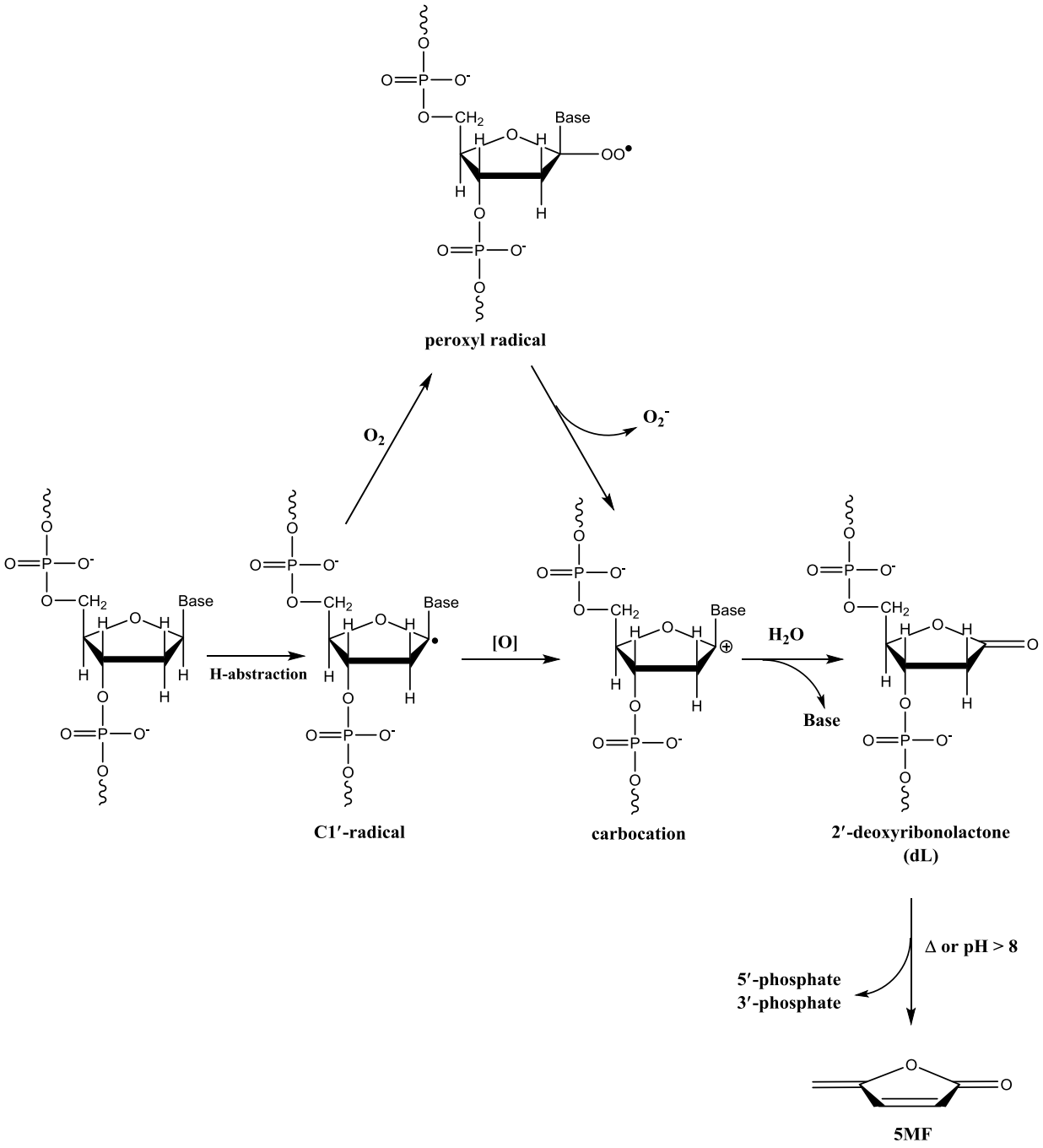

Figure 3: The formation of 5MF from a C1´ radical and dL precursor lesion[18]

C5′ Pathway. The formation of a C5′-deoxyribosyl radical is preceded by hydrogen abstraction from the C5′ position of 2′-deoxyribose. The two hydrogen atoms attached to the 5′-carbon atom are highly accessible in a B-DNA helix, and consideration of the surface areas of both of these atoms leads to even greater solvent accessibility[12]. Despite the fact that both atoms are accessible from the minor groove of the DNA double helix, one atom points away from the groove toward the solvent[12], and it stands to reason that this hydrogen will be the primary focus of hydrogen abstraction by aqueous oxidants. Pathways involving the abstraction of hydrogen from the 5′-position have been proposed for DNA scission mediated by enediyne antibiotics, Fenton-generated hydroxyl radicals, gamma radiolysis, cationic metal porphyrins, and the hydroperoxyl radical (•OOH)[12].

The radical formed by the abstraction of H5′ can undergo a second one-electron oxidation, resulting in the formation of a carbocation intermediate that is reactive to water. The hydroxylated C5′-position then undergoes 3′-phosphate elimination to yield an oligonucleotide of 5′-aldehyde (5′-Ald), which can then undergo FBR and phosphate elimination to generate furfural (Fur). This proposed reaction scheme is presented in Figure 4.

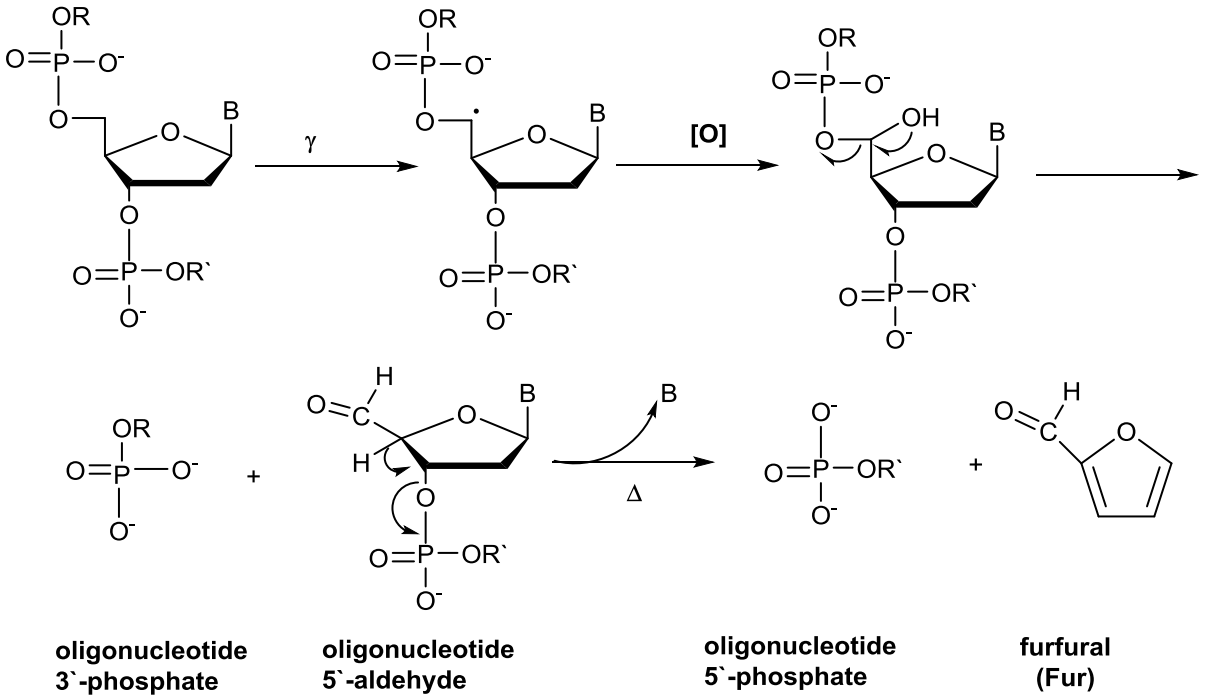

Figure 4: The formation of 5′-aldehyde (5′-Ald) from the precursor C5′-deoxyribosyl radical. This radical undergoes base and phosphate elimination reactions to generate furfural[18]

C4′ Pathway. The C4′ pathway is initiated by hydrogen abstraction from the C4′-position of the DNA 2′-deoxyribose. Due in large part to the accessibility of this site in B-DNA, many DNA-cleaving molecules can attack DNA at this position[12]. Systems involving ionizing radiation-induced damage, methidiumpropyl(EDTA)•Fe(II), Fenton-generated hydroxyl radicals, and several drugs (including bleomycin, calicheamicin, neocarzinostatin, elsamicin A, and C1027) have been proposed to undergo 4′-hydrogen abstraction to yield DNA damage[12].

The von Sonntag research group proposed a pathway based on alkyl phosphate and ribose 5′-phosphate chemistry that was independent of the presence of oxygen[20]. In this pathway, an alkyl radical generated adjacent to a phosphate ester underwent hydrolysis followed by β-

elimination of phosphate[12]. Extrapolating this proposed mechanism from model systems to DNA, von Sonntag *et al.* hypothesized a C4′-radical was formed followed by β-elimination of one – or both – phosphate group(s)[12,20]. Also in this model, a radical cation intermediate is generated followed by an addition reaction of water and release of a proton[12,21,22]. The radical is believed to be stabilized due to the lone pairs of electrons on the oxygen heteroatom in the ring[12]. The phosphate elimination and radical cation formation were also observed in model studies by Giese *et al.*[23], where the final product is dependent on whether water adds to the carbocation or the carbon-centered radical.

The C4′ pathway has been established as a fundamental mechanism of DNA immediate strand breaks initiated by radiation-produced HO•, and this pathway is estimated to participate in approximately 50% of immediate strand breaks in dilute aqueous solutions[24], in contrast to the findings of Tullius *et al.* (~21%)[25]. This pathway can be divided into two component pathways: formation of malondialdehyde or formation of a C4′-oxidized abasic site.

C4′-Oxidized Abasic Site Formation. Despite being initially identified in γ-irradiated aqueous solutions of DNA[26,27], the C4′-oxidized abasic site (C4′-OAS) has also been found as a product of bleomycin-facilitated anaerobic DNA cleavage[17]. Upon formation of this lesion, DNA-DNA cross-linking reactions have been observed[28-30], and the product of this cross-linking has been shown to block DNA replication and repair mechanisms[17,31,32], which increases the potential for the C4′-OAS to act mutagenically.

The role of the C4′-OAS in radiation-induced DNA damage remains at a minimum, unclear, if not controversial, due to lack of directly comparable data in the literature on the yields of the C4′-OAS[17]. Fluorimetric assays performed by Dhar *et al.*[33] found the yield of C4′-OAS in

DNA to be 27.5% of all radio-induced aldehyde-reactive probe (ARP) carbonyl groups, while gas chromatography-mass spectrometry (GC-MS) techniques used by Chen *et al.*[34] found the C4′-OAS to be only 3% of all 2′-deoxyribose damage. Both of the procedures used by these two research groups rely on multiple derivatization steps and, perhaps most important of all, require calibration using well-characterized authentic oligonucleotides containing chemically incorporated C4′-oxidized abasic sites[17].

While the exact mechanism for the formation of a C4′-OAS remains unclear, the mechanism proposed by our research group is found in Figure 5, below. In the presence of molecular oxygen, a C4′-deoxyribosyl radical will undergo an addition of molecular oxygen to form a peroxyl radical, which proceeds through an undetermined mechanistic pathway to form the C4′-OAS. The peroxyl radical can also undergo elimination of molecular oxygen to form a C4′-deoxyribosyl carbocation that can eliminate the nucleobase in the presence of water to form the C4′-OAS.

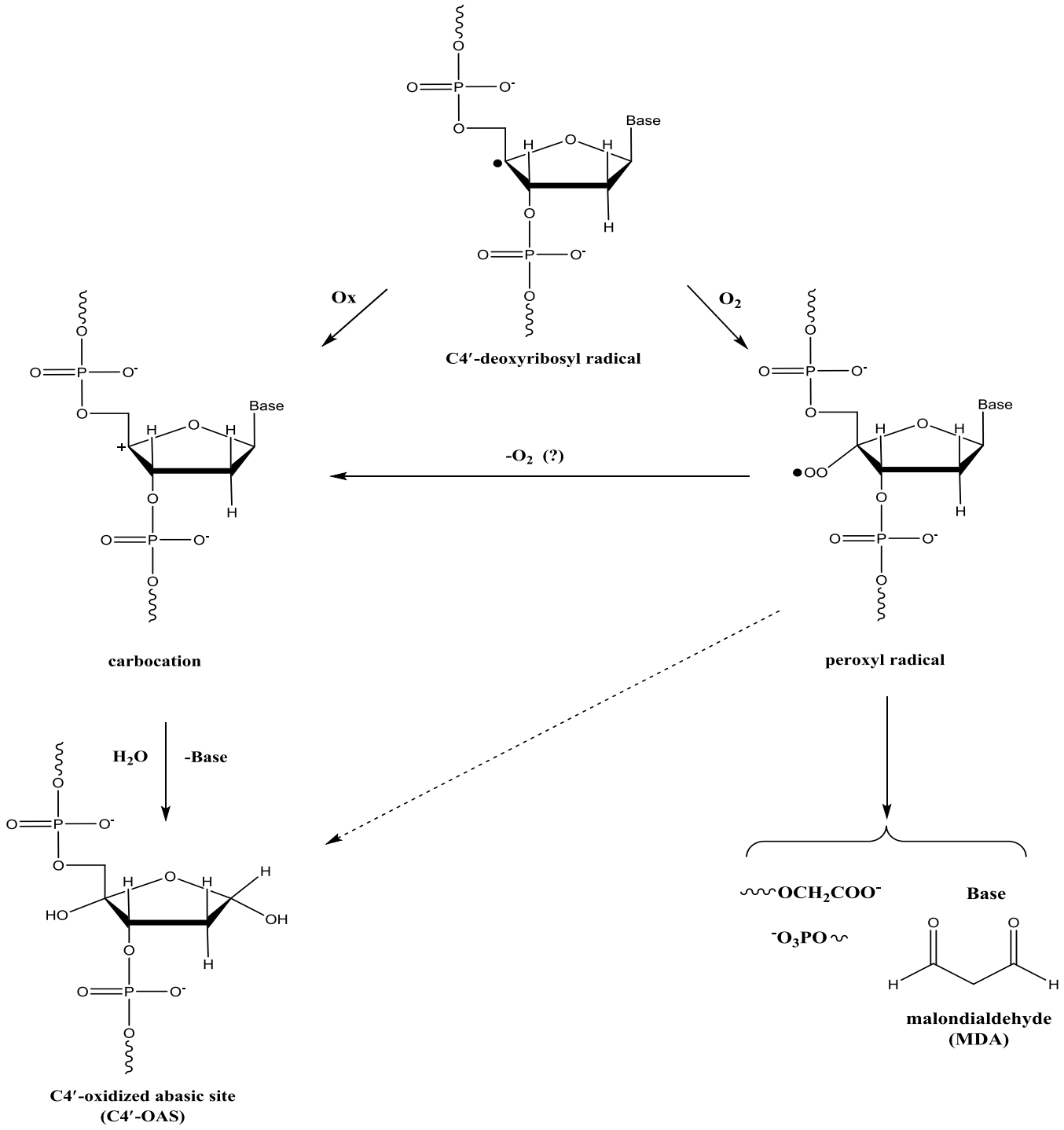

Figure 5: The C4′-pathway chemistry under aerobic and anoxic conditions, leading to the formation of C4′-OAS and MDA sugar damage products. Ox in the left pathway refers to any secondary oxidant. Based on a similar scheme in Roginskaya *et al.*[17]

Malondialdehyde C4′ Chemistry. In oxygenated solutions, a number of products are generated via the C4′-pathway, including 5′-phosphate, 3′-phosphoglycolate, free unaltered base, base propenals and malondialdehyde (MDA)[12,24]. These products, excluding base propenals, are identified in Figure 6, below.

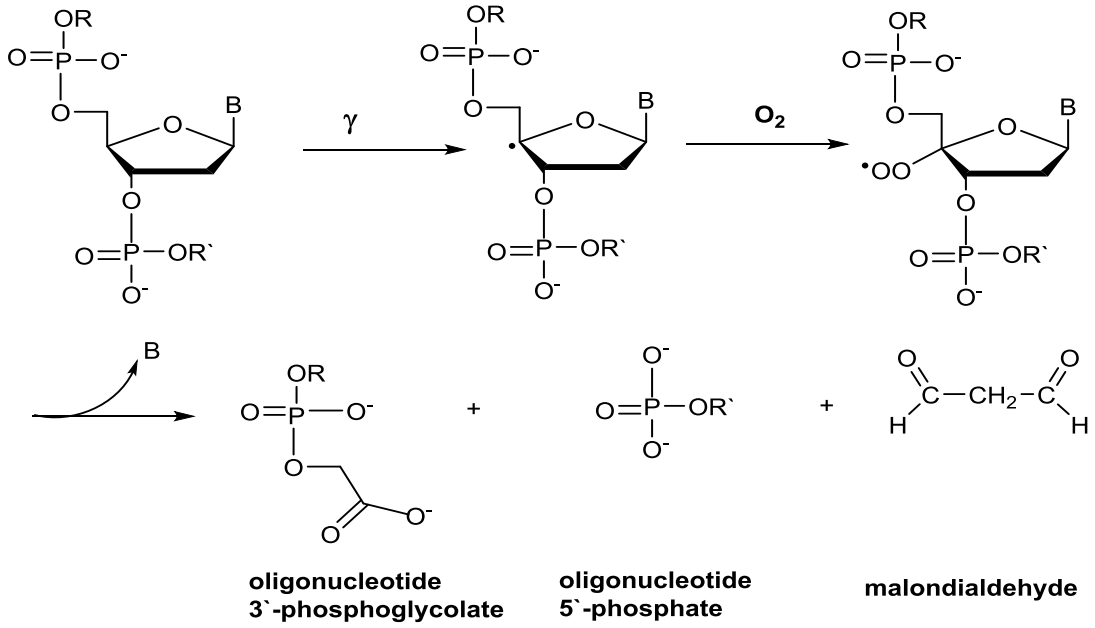

Figure 6: The formation of 3′-phosphoglycolate, 5′-phosphate, and MDA from the C4′-chemistry[18]

The MDA product can be quantified using standard thiobarbituric acid-reactive substances (TBARS) protocol[24]. Two equivalents of 2′-thiobarbituric acid (TBA) react with one equivalent of MDA – produced as a result of oxidative C4′-damage – to yield the MDA-TBA adduct via a condensation reaction[35], as illustrated in Figure 7. The adduct shows absorptions at

532 nm, 305 nm, and 243 nm with extinction coefficients of 1.5 x 10^5 [36], 1.125 x 10^4, and 2.3 x 10^4 M^{-1} cm^{-1}, respectively[37].

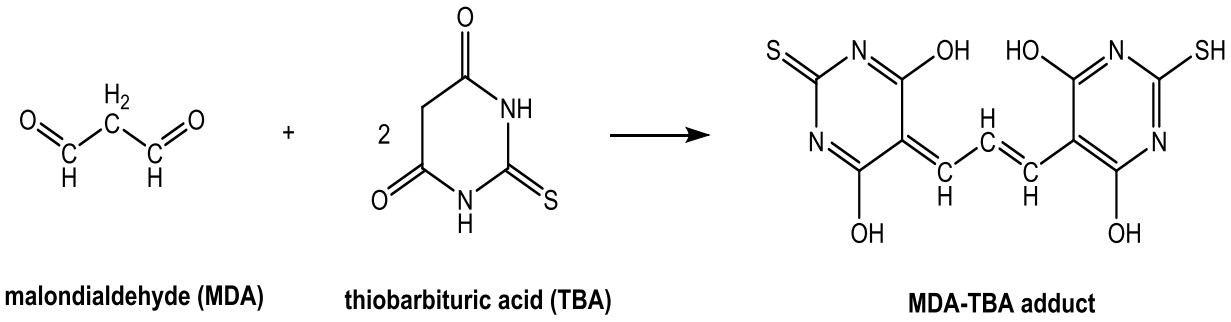

Figure 7: The formation of MDA-TBA adduct from 1 equivalent of MDA and 2 equivalents of TBA. Based on a similar scheme in Giera *et al.*[35]

MDA is produced *in vivo* as an end product of unsaturated lipid peroxidation and as a side product of the biosynthesis of prostaglandin and thromboxane, and as early as the 1980s was known to be toxic, carcinogenic, and mutagenic[38]. MDA is reactive towards nucleic acids, resulting in the loss of template activity, and it has been suggested that this compound also plays a vital role in atherosclerosis[35,39]. MDA also reacts rapidly with amino acids to form 1:1 adducts, as well as initiating nucleobase modifications through cross-linking reactions[40].

The C4′-pathway can also be initiated by other methods than ionizing radiation (e.g. antibiotics such as Fe(II)-bleomycin and neocarzinostatin[18]. In the chemo-initiated systems, versus radio-initiated systems, there is an abundance of base propenals rather than MDA, and

this is indicative of the differing nature between radiation-induced and chemically-induced C4´-pathway chemistry[18].

Base Damage

DNA bases are the primary targets of oxidative damage due to their lower oxidation potentials compared to the DNA sugar-phosphate backbone. The resulting base damage is primarily directed to guanine, due in large part to the fact that the standard reduction potential of guanine (+1.29 V) is considerably lower than the other native DNA nucleobases. Crespo-Hernández *et al.* and Fukuzumi *et al.* reported the oxidation potentials of DNA nucleosides (summarized in Table 1), where E^0 values are reported at pH 7 versus normal hydrogen electrode (NHE)[41,42].

Table 1: The Standard Reduction Potentials for DNA Nucleosides[42]

DNA nucleoside	**E^0, V**
guanosine	1.29
adenosine	1.42
thymidine	1.7
cytidine	1.6

Guanine undergoes a one-electron oxidation to produce the *guanine radical cation* ($Gua^{\bullet+}$or $G^{\bullet+}$). These $G^{\bullet+}$ (pKa = 3.9, experimental and 3.6, calculated[43]) are commonly referred to as DNA holes[44] and are a much stronger acid than the parent G (pKa = 9.5[45]). At physiological pH, $G^{\bullet+}$ quickly ($k \sim 2.0 \times 10^6\ s^{-1}$ [46]) undergoes deprotonation to form $G(N_1\text{-}H)^{\bullet}$ or simply $G^{\bullet}$. The

$G^{\bullet}$ radical has not been detected at room temperature[47], and the $G^{\bullet}$ decays in the 120-230 K range[48]. It is hypothesized that $G^{\bullet}$ undergoes a second one-electron oxidation to form the carbocation $G(N_1\text{-}H)^{+}$ [43,47]. The resulting carbocation can undergo hydrolysis to produce 8-oxo-7,8-dihydroguanine (8oxoG). As an alternative, $G^{\bullet+}$ can be hydrolyzed to form the $G(OH)^{\bullet}$ radical. This $G(OH)^{\bullet}$ radical can proceed down one of two pathways: a second one-electron oxidation to form 8oxoG[49,50], or a one-electron reduction to form 2,6-diamino-4-hydroxy-5-formamidopyrimidine (FapyG)[51,52]. In cellular DNA, oxidatively generated guanine lesions occur with a frequency of approximately one per million guanines[53]. A summary of the oxidation reactions is found in Figure 8.

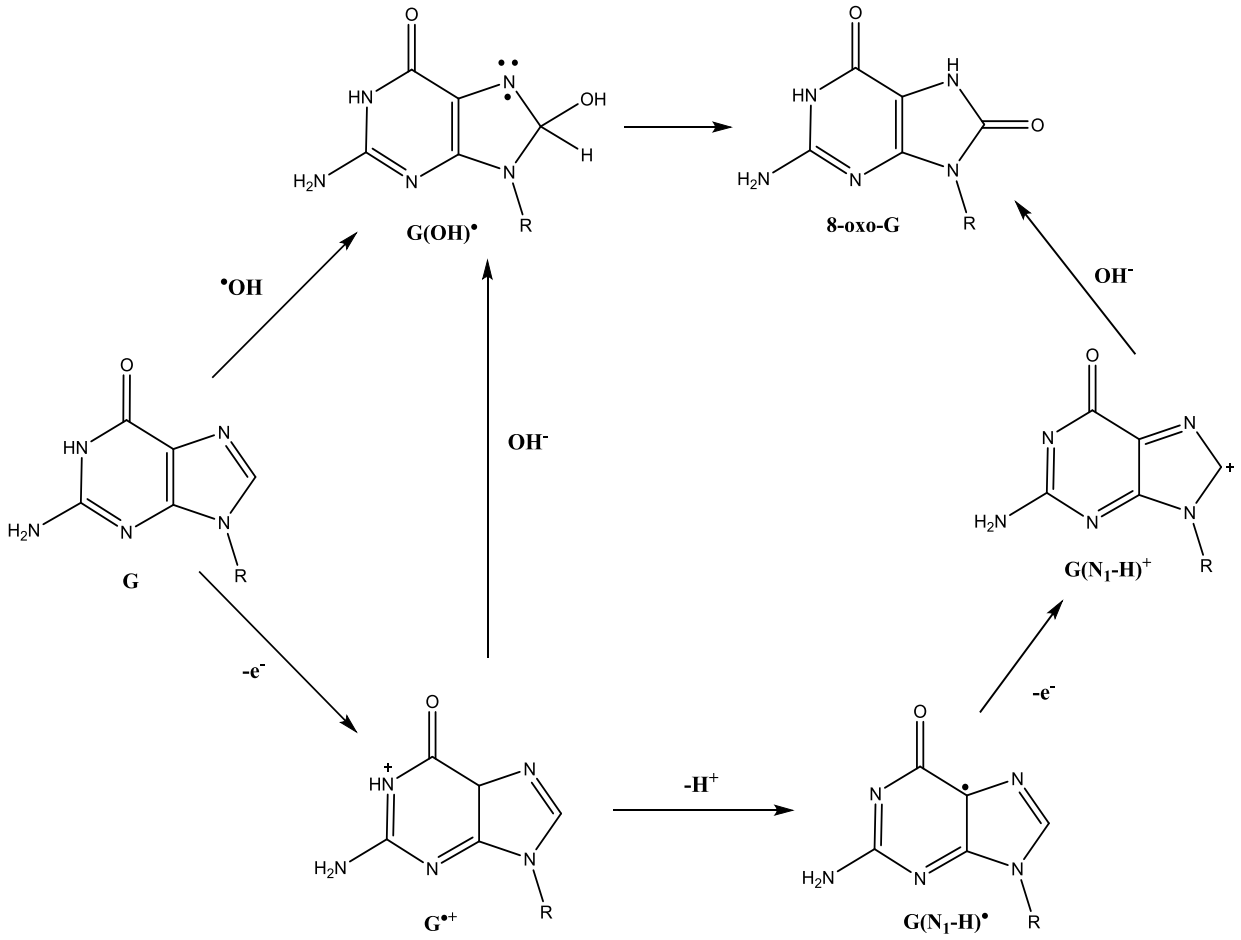

Figure 8: The oxidation products of guanine. The scheme above is based on a similar scheme found in Close *et al.*[47]

8oxoG is known as a biomarker for oxidative stress conditions *in vivo*[54-56]. Elevated levels of 8oxoG have been found in a variety of tissues, including lung tissues[57,58] of individuals living or working in environments with high concentrations of oxidative stressors, including asbestos fibers[59,60], exhaust from diesel engines[61], and environmental pollution[62]. Other oxidative stressors include heavy metals and metalloids[63], polycyclic aromatic hydrocarbons[64-66], and

benzene, styrene, and organoarsenic[61]. Regardless of the nature of these environmental stressors, all were associated with increased levels of 8oxoG due to oxidative stress conditions.

8oxoG can be further oxidized due to its low standard reduction potential (+0.74 V vs. NHE[67]), and multiple research groups have reported that 8oxoG is susceptible to further oxidation using other oxidizers including peroxynitrite, iridium hexachloride anion ($[IrCl_6]^{2-}$), singlet oxygen ($^1O_2$), and the dichromate anion ($[Cr_2O_7]^{2-}$)[68]. The products of these further 2-electron 8oxoG oxidations have been identified *in vitro*[68]. Because of the low reduction potential of 8oxoG, a variety of biologically important oxidizers that are less potent than HO• can also oxidize 8oxoG, including the CR ($E° = +1.59$ V[53]), and organic radicals including the alkylhydroperoxyradical ($E^{\circ} = +0.9$ V). Based on the conditions and oxidant type, 8oxoG can be oxidized to form a number of hyperoxidized products that can also serve as biomarkers for oxidative stress in cells. Guanidinohydantoin (Gh) and iminoallantoin are produced from 8oxoG in oligonucleotides via oxidation by $[IrCl_6]^{2-}$, and are further oxidized to yield parabanic acid and oxaluric acid at neutral pH[69,70]. Two stereoisomers of spiroiminodihydantoin (Sp) were also detected in cellular DNA, and these lesions are indicative of the biological importance of 8oxoG oxidation *in vivo*[68]. Other hyperoxidized products of 8oxoG include imidazalone (2,5-diamino-4H-imidazol-4-one), oxazalone, cyanuric acid[68], and 1,3,5-triazepane-2,4,6,7-tetrone[71,72]. While the *in vivo* 8oxoG lesion is only slightly mutagenic – with < 10% of 8oxoG lesions resulting in G→T transversion – these hyperoxidized products are even more mutagenic than 8oxoG and can result in G-T and/or G-C mutation by transversion both *in vitro* and *in vivo.* Structures for these hyperoxidized guanine products are shown in Figure 9.

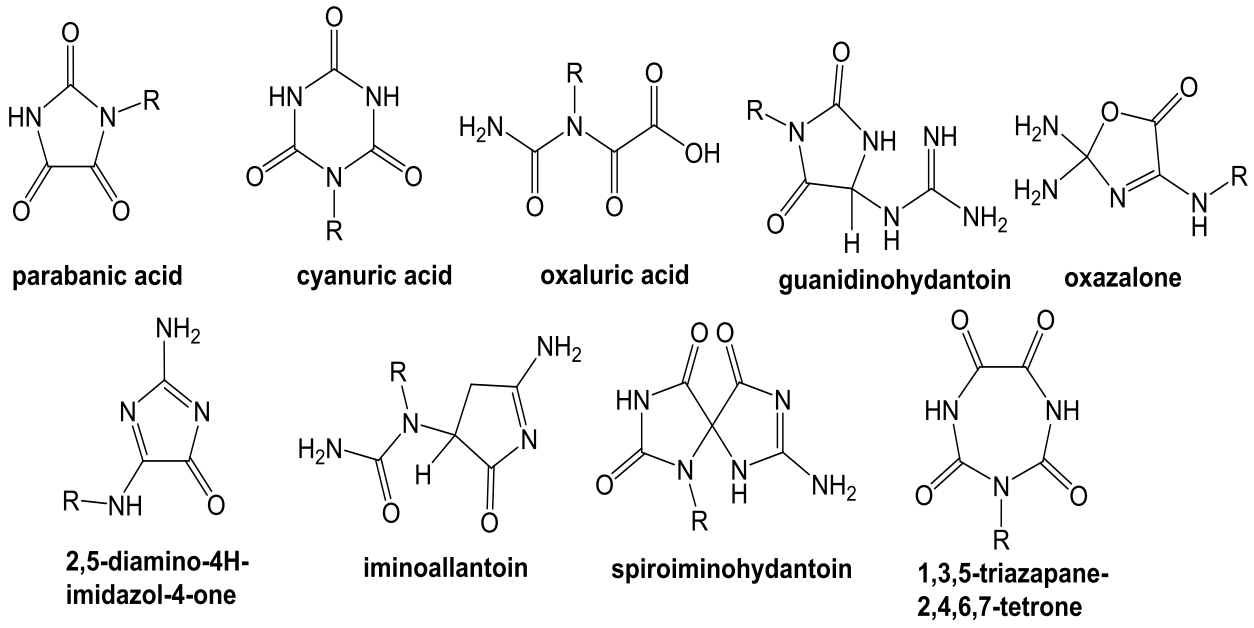

Figure 9: The further oxidation products of 8-oxo-7,8-dihydroguanine (8oxoG)[68,71,72]. The spiroiminodihydantoin (Sp) lesion exists as a pair of stereoisomers[68].

Carbonate Radicals

Until recently, the focus of free radical research has been devoted primarily to a select few biologically important ROS species like HO• (hydroxyl radical), $O_2^{\bullet-}$ (superoxide radical), H_2O_2 (hydrogen peroxide), NO (nitric oxide), and $ONOO^-$ (peroxynitrite). Surprisingly, little attention has been paid to the physiological role of ROS derived from the bicarbonate/carbon dioxide (HCO_3^-/CO_2) pair, despite the prevalence of this buffer in physiological systems. HCO_3^- is abundant in serum and the intracellular medium (25 and 14.4 mM, respectively) and is kept in equilibrium with ~1.3 mM CO_2 to comprise the primary physiological buffer system[73]. Peroxynitrite is formed at nearly diffusion-controlled rates by the reaction of nitric oxide with the

superoxide radical anion (Reaction 1.1)[74]. This peroxynitrite then goes on to further react with the CO_2 (Reaction 1.2) of the bicarbonate buffer to produce the intermediate nitrosoperoxycarbonate anion, which further undergoes homolytic O-O bond cleavage to yield nitric oxide and a carbonate radical (CR, Figure 10). Approximately 35% of peroxynitrite/carbon dioxide interactions result in the products in Reaction 1.2, while the remaining 65% of interactions result in the regeneration of the peroxynitrite and nitric oxide reactants (Reaction 1.3)[73,75].

$$NO^{\bullet} + O_2^{\bullet -} \xrightarrow{k} ONOO^- \ (k = 4.9\ x\ 10^9\ M^{-1}s^{-1}) \quad (1.1)$$

$$ONOO^- + CO_2 \rightarrow [ONO \bullet\bullet OCO_2]^- \rightarrow NO_2^{\bullet} + CO_3^{\bullet -}\ (35\%) \quad (1.2)$$

$$ONOO^- + CO_2 \rightarrow [ONOO \bullet\bullet CO_2]^- \rightarrow ONOO^- + CO_2\ (65\%) \quad (1.3)$$

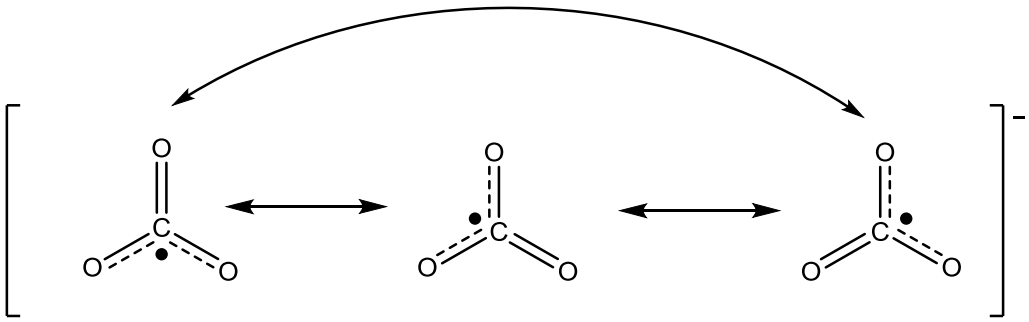

Figure 10: The structure of a carbonate radical anion (CR), indicating the delocalization of the radical electron between two oxygen atoms. The CR structure is composed of three resonance structures, with each resonance structure contributing an equal amount to the hybrid structure.

As early as 1973, the CR was studied via pulse radiolysis by Chan and Hoffman, and it was demonstrated that CR is a strong, one-electron oxidant (E° = + 1.78 V at pH 7.0 for the

carbonate radical/bicarbonate pair[75]) capable of oxidizing many diverse substrates with rate constants over the range of ~10^5 to 10^{10} M^{-1} s^{-1} [76]. CR oxidizes appropriate electron donors via electron transfer mechanisms. The CR exhibits a broad optical absorption in the visible range, with a maximum at 600 nm (ε = 1970 M^{-1} cm^{-1} [77]). It is possible to monitor the formation of CR and the reactions carried out by CR by visible spectroscopy in the 500-700 nm range. CR acts primarily as a one-electron oxidizer and can oxidize many organic and inorganic compounds[78]. CR is negatively charged over the range of physiological pH, including those of acidic pH such as the phagolysosomes of phagocytic cells and ischemic tissues[73]. Recent studies have established that the CR is a very strong acid with a pKa < 0[73,79].

In Vivo and *In Vitro* CR Production

CRs are produced *in vivo* through several channels. As early as 1976, it was proposed that CRs were formed as a byproduct of acetaldehyde oxidation by xanthine oxidase[80]. However, it was not until the 1990s that the role of CR in producing biologically relevant oxidative damage became elucidated. During this time, it was demonstrated by Lymar and Hurst that CR is produced as an intermediate product in the reaction between CO_2 and peroxynitrite ($ONOO^-$)[74]. Later, it was explicitly shown by Bonini *et al.* in continuous-flow EPR studies that CRs are formed as the result of this reaction[81]. Recently, CR has been proposed to be a key mediator of the oxidative damage resulting from peroxynitrite production, xanthine oxidase turnover, and superoxide dismutase (SOD) peroxidase activity[73,75,76]. CRs can also be produced via the reaction between HO• and HCO_3^- (Reaction 1.4, next page)[75,76,82].

$$HCO_3^- + HO^\bullet \xrightarrow{k} H_2O + CO_3^{\bullet -} \ (k = 1.0\ x\ 10^7 M^{-1}s^{-1}) \qquad (1.4)$$

CRs are overproduced at sites of inflammation via the homolytic bond cleavage of nitrosoperoxycarbonate[53], and as such is a biologically important ROS. CRs are especially important in ischemia/reperfusion due to low concentrations of oxygen and high concentrations of CO_2 and NO. Natural formation of oxidants during the initiation of events in ischemia/reperfusion can result in oxidant formation followed by tissue damage[83]. The abundance of NO and endogenously generated $O_2^{\bullet -}$ during these times of oxidative stress can result in the production of peroxynitrite, which coupled with ubiquitous CO_2, can result in the formation of the CR. Liochev and Fridovich[76] also reported recently that CR plays some role in enhancement of the peroxidase activity of SOD. In the presence of CO_2, the oxidant bound to SOD is responsible for attacking a histidine residue in the ligand field of the copper (specifically, CuSOD), which inactivates the enzyme. In the presence of CO_2, a CR is formed as a side product by SOD activity, and the CO_2 present in this system does not protect SOD against inactivation by H_2O_2 since a fraction of the generated CR inactivates the enzyme by oxidizing the histidine residue[76].

Methods of *in vitro* CR generation include the photolysis of carbonato-metal complexes, specifically carbonatotetrammine cobalt(III) and carbonatopentammine cobalt (III)[84] (Reaction 1.5), as well as photolysis of solutions of persulfate and bicarbonate salts, yielding sulfate radicals (SR, Reaction 1.6, $\phi_{308} = 0.55$[85]) which then react with bicarbonate anions to produce CR (Reaction 1.7), and one-electron oxidations of bicarbonate anions by hydroxyl radicals to form CR (Reaction 1.4, above).

$$[Co(NH_3)_nCO_3]^+ + h\nu \rightarrow Co^{2+} + n\,NH_3 + CO_3^{\bullet -} \quad (1.5)$$
$$n = 4\ or\ 5$$

$$S_2O_8^{2-} + h\nu \rightarrow 2SO_4^{\bullet -}\ (\phi_{308} = 0.55) \quad (1.6)$$

$$SO_4^{\bullet -} + HCO_3^- \rightarrow SO_4^{2-} + CO_3^{\bullet -} + H^+ \quad (1.7)$$

Shafirovich and his research group have extensively studied reactions of one-electron oxidation of guanine residues in DNA and model DNA oligos[86] by CR. In most of these works, CRs were generated by flash photolysis of persulfate anions ($S_2O_8^{2-}$) in the presence of bicarbonate anions (HCO_3^-). The persulfate/bicarbonate solutions were subjected to pulses from a XeCl excimer laser (308 nm), which generated sulfate radicals (SRs) through photodissociation (Reaction 1.6). The resulting SR then further reacted with the HCO_3^- to yield sulfate anion and CR (Reaction 1.7), with a rate constant of k = (4.6 ± 0.5) x 10^6 M^{-1} s^{-1} [77]. It was their finding that guanine is the only target of one-electron abstraction reactions by CR[86], and the bimolecular rate constant for guanine oxidation by CR was (1.9 ± 0.2) x 10^7 M^{-1} s^{-1} [46]. Duplexes with single G and contiguous GG and GGG sequences have similar second-order rate constants when oxidized by CR, which differs from other ROS studied. Regardless of the number or distribution of guanine in the duplexes, the G were oxidized by CR at nearly equivalent rate constants over the limited range of 1.5 – 3.0 x 10^7 $M^{-1}s^{-1}$ [77].

The oxidation of G by CR leads to the formation of Sp and Gh lesions, with a preference for the Sp lesion[86]. This Sp lesion is the result of a four-electron site-selective oxidation of G and 8oxoG residues by CR, and the oxidation of guanine to Sp occurs via the formation of 8oxoG lesion intermediates[87]. The Sp lesions are considered as the terminal products of G and 8oxoG oxidation in DNA by CR[87]. In addition to these 8oxoG oxidation products, Shafirovich *et al.*

found that oxidation of the single guanine in model oligos (5′-CCATCGCTACC) yields intrastrand cross-linked oxidation products of 5′-CCAT*CG*CTACC (minor) and 5′-CCATCG*CT*ACC (major) – the latter of which can be referred to as 5′-…G*CT* lesions[86]. The reaction scheme in Figure 11 (p. 40) shows the mechanism for generation of the Sp, Gh, and 5′-…G*CT* lesions proposed by Shafirovich *et al.* Additional studies by Shafirovich *et al.* sought to determine the effect of cytosine base bridging on cross-link formation in a series of 5′-d(GpC_npT) and 5′-d(TpC_npC) with n = 0, 1, 2, and 3, and cross-linking in a 12-mer duplex derived from the self-complementary 5′-d(TTACGTACGTAA) sequence[88]. This research determined that the 5′-d(G*pCpT*) crosslink was the most abundant intrastrand cross-link in these experimental conditions[88].

Recent work by the Shafirovich research group has been dedicated to the investigation of guanine-thymidine cross-links in DNA mediated by the peroxynitrite/carbon dioxide system. *In vitro* experiments by Shafirovich *et al.* have shown that guanine lesions generated by decomposition products of nitrosoperoxycarbonate ($ONOOCO_3$) include not only oxidation products, but nitration products as well[89]. Of the radical species generated by the decomposition of nitrosoperoxycarbonate, only the CR can directly react with guanine in DNA, due to its high reduction potential[89]. The $^{\bullet}NO_2$ radical has a lower reduction potential ($E° = + 1.04$ V vs. NHE[89]), and hence it is a milder oxidant. As a milder oxidant, nitric oxide is unable to react with guanine directly. Further research by Shafirovich *et al.* demonstrated that these cross-links and known guanine oxidation products are also formed in native double-stranded DNA exposed to peroxynitrite in aqueous solutions of carbon dioxide/bicarbonate, and the relative yields of the G*-T* cross-links to other known DNA lesions[89].

Despite extensive research on CR-mediated guanine damage, Shafirovich's research group has never considered the potential reactions between CRs and the 2´-deoxyribose moiety of DNA. The first hypothesis of the present work is that CRs can also damage DNA at the sugar moiety, and that this process is initiated by hydrogen abstraction by CR from 2´-deoxyribose. CRs have been shown to abstract hydrogens from carbohydrates but at a much slower rate than hydroxyl radicals. Extensive chain scission of glycosaminoglycans, long-chain linear polysaccharides, has been observed by both $^{\bullet}OH$ and $CO_3^{\bullet-}$ [90,91]. CR were less efficient in hydrogen abstraction from target polysaccharides than hydroxyl radical and, according to ESR spin trapping experiments with model monosaccharides, show different patterns of hydrogen abstraction than hydroxyl radicals, presumably due to lower hydrogen abstraction ability[90,91]. Chen and Hoffman determined the second-order rate constant of the hydrogen abstraction reaction between CR and glucose to be 7×10^4 M^{-1} s^{-1} [92], indicating that CRs do indeed react with sugars. Carlsson confirmed that CRs react with D-glucose primarily through abstraction of the C1´ hydrogen[93]; this trend can be applied to other sugar groups including 2´-deoxyribose.

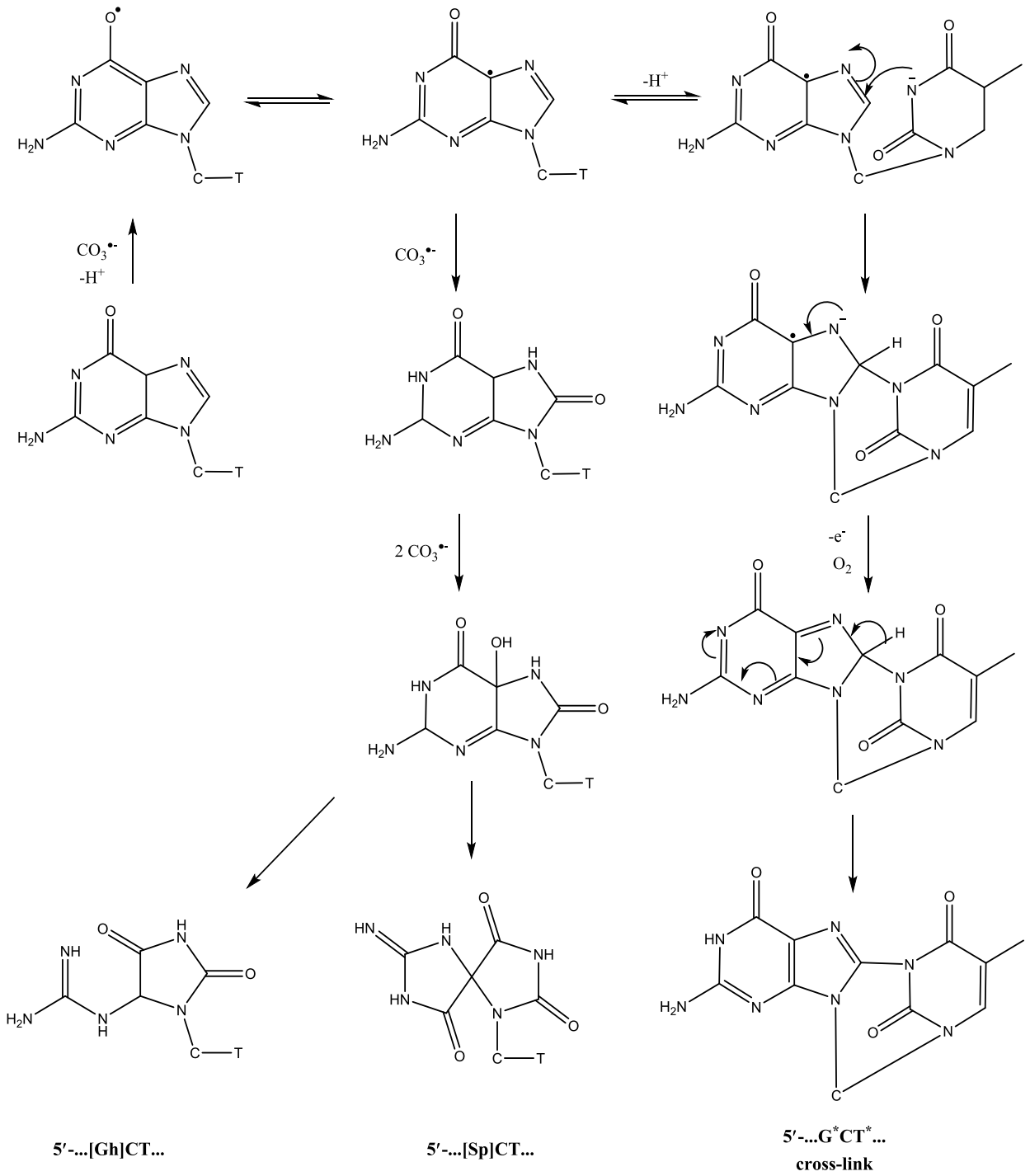

Figure 11: The mechanism of formation of Sp, Gh, and 5´-…G*CT* lesions proposed by Shafirovich *et al.* in DNA oligonucleotide sequence (5´-d(CCATCGCTACC) context[86]

CR vs. Hydroxyl Radicals

While both CR and HO• are considered to be powerful one-electron oxidants, the hydroxyl radical has a much greater standard reduction potential (E° = +2.3 V at pH 7.0[94]) when compared to the CR (E° = + 1.78 V at pH 7.0[75]). As evidenced by the difference in the reduction potentials of these two radical species, both have higher reduction potentials than all of the DNA bases (Table 1). Since hydroxyl radicals react with DNA sugar via a hydrogen abstraction mechanism, it can be assumed that CR behaves in a similar fashion, but with a greater selectivity. This selectivity can be attributed to resonance stability in CR: it has the added benefit of resonance stabilization (Figure 10, p. 34), in stark contrast to HO•, because the unpaired electron can occupy any of the oxygen molecules. Resonance stability in the CR allows for longer lifetimes in aqueous solutions, and allows the CR to diffuse over larger distances. The culmination of all these factors allows CR to be more discriminate in hydrogen abstraction than HO•. Comparison of the rate constants for hydrogen abstraction from glucose for HO• ($k = 1.5 \times 10^9\ M^{-1}\ s^{-1}$ at pH 7.5[95]) and CR ($k = 7 \times 10^4\ M^{-1}\ s^{-1}$ at pH 7.0[92]) further confirms that CR is slower and potentially more discriminate in hydrogen abstraction reactions with sugars. The free radical scavenging reaction with isopropanol illustrates the difference in lifetimes for HO• and CR (Reactions 1.8[96] and 1.9[97], respectively), as evidenced from the respective rate constants (k) in the reactions below. The increased lifetime of CR in solution allows the radical to reach more distal targets in the cell (e.g. DNA) that may have more damaging long-term consequences.

$$HO\bullet + iPrOH \xrightarrow{k} H_2O + iPrO^{\bullet}\ (k = 2.3\ x\ 10^9\ M^{-1}s^{-1}) \qquad (1.8)$$

$$CO_3^{\bullet -} + iPrOH \xrightarrow{k} HCO_3^- + iPrO^{\bullet}\ (k = 4\ x\ 10^4\ M^{-1}\ s^{-1}) \qquad (1.9)$$

The second hypothesis of the present work is based on the comparison of hydrogen abstracting abilities of HO• and CR. CR as slow, selective hydrogen abstractor is expected to show a higher preference for weaker bound hydrogens in DNA sugar (H1´) rather than for more solvent accessible hydrogens (H5´), in contrast to HO• as a fast, indiscriminate hydrogen abstractor. As a result, a higher ratio of the C1´/C5´ products is expected for CR-mediated DNA sugar damage as compared to HO•-mediated damage.

Quantitative Analysis of DNA Sugar and Base Damage Products Using HPLC

The Roginskaya research group has established an HPLC-based method of qualitative and quantitative analysis of DNA sugar damage based on quantitative detection of low-molecular weight products released as the result of DNA sugar damage[14-17]. Our employed methodology makes use of the propensity of oxidized DNA lesions to undergo fragmentation of the 2´-deoxyribose ring by catalytic and/or heat treatment. Typically, such fragmentation produces a strand break, a free DNA base, and a characteristic low-molecular weight product. The products of these catalytic/heat treatments are unique to the precursor 2´-deoxyribose lesion.

C1´and C5´ Pathways

The formation of C1´ and C5´ products from precursor lesions – 5MF from dL (Figure 3, p. 21) and Fur from 5´-Ald (Figure 4, p.23), respectively – is catalyzed by the reaction of the appropriate precursor lesion with a cationic form of polyamine/polypeptide (in this work, spermine or poly-L-lysine (polyL)). The reaction conditions were optimized by the Roginskaya group[14-16] and the results of this optimization indicate that both 5MF and Fur achieve their

kinetic saturation/steady state concentrations at 70 °C within 25-30 minutes of heating in the presence of a polyamine. Ha *et al.* found that spermine, which is present in millimolar concentrations in the cellular nucleus, can function directly as a radical scavenger, among other functions including regulation of gene expression, stabilization of chromatin, prevention of endonuclease-mediated DNA fragmentation, and inhibition of DNA damage[98]. The binding constants of spermine to DNA over a range of ionic strengths were obtained by Braunlin *et al.*, and it was found that as ionic strength in solution increases, there is a significant decrease in the ability of spermine to bind to DNA ($K = (11 \pm 2) \times 10^{-3}\ M^{-1}$ at 71 mM $[Na^+]$ vs. $(0.82 \pm 0.1) \times 10^{-3}\ M^{-1}$ at 154 mM $[Na^+]$)[99]. Braunlin *et al.* also found that the binding of polyamines to DNA is increased with temperature; by holding the ionic strength constant, they were able to discern that increased temperature correlated with increases in the binding of spermine to DNA[99].

Our research group also determined the release of 5MF upon treatment of irradiated DNA with spermine to be quantitative, and the amount of 5MF was found to be a direct measure of the amount of dL precursor lesion present in the irradiated DNA[14-16]. Both 5MF and Fur are released during the heat treatment of DNA in the presence of a DNA-binding catalyst with Lewis acid properties such as spermine or polyL[14-16]. The reaction for formation of 5MF from the precursor lesion (dL) is shown in Figure 12 and the reaction for the formation of Fur from the precursor lesion (5′-Ald) is shown in Figure 13.

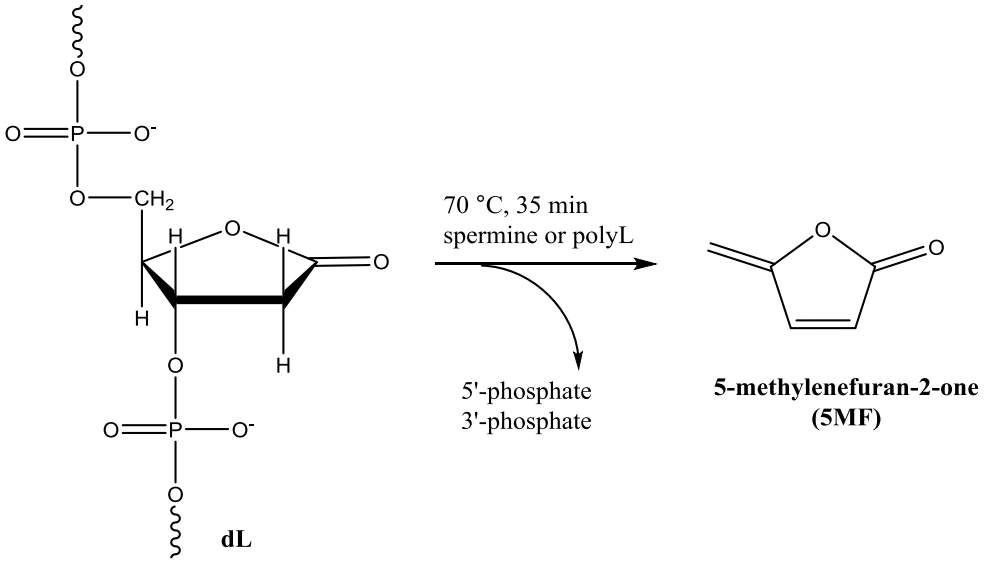

Figure 12: The formation of 5-methylenefuran-2-one (5MF) from the 2´-deoxyribonolactone precursor lesion

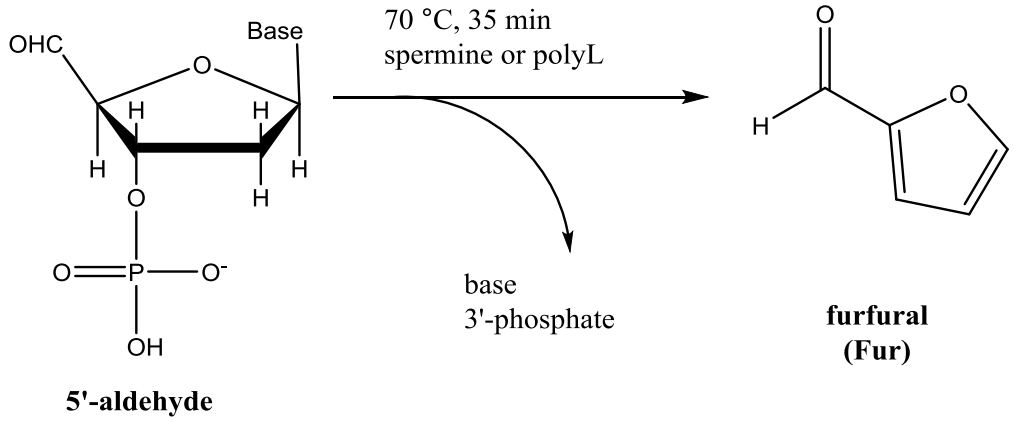

Figure 13. The formation of furfural (Fur) from the 5´-aldehyde precursor lesion

C4´ Pathway

Lac Formation. The C4´-OAS is capable of reacting – under neutral or slightly acidic conditions – with primary amines (RNH_2) to form N-substituted 5-methylene-Δ^3-pyrrolin-2-

ones. The specific product of the reaction is dependent on the structure of the primary amine used to derivatize the C4′-OAS. Yields from these derivatization reactions are nearly quantitative (greater than 75%)[100-102], and the resulting lactams are easily quantified by HPLC with UV detection due to a fairly strong characteristic absorption below 350 nm[100,103]. Whereas traditional fluorimetric[33] and GC/MS methods[34] of determining the yield of C4′-OAS have relied extensively on multiple derivatization steps and calibration with well-characterized authentic oligonucleotides, the cost-prohibitive nature of such oligonucleotides makes the technique difficult to reproduce[17].

Determination of the contribution of the lactam C4′ pathway is facilitated by quantification of the relative yield of 1-N-oxycarbonylmethyl-5-methyleneazacyclopent-3-ene (azalactone, lactam, or Lac) produced from the derivatization of the C4′-OAS by a primary amine[17]; in this work, this primary amine used was specifically glycine (R = CH_2COOH). Choosing glycine as the derivatizing agent for HPLC quantification of C4′-OAS through the formation of Lac was based on several advantages of this reagent over other primary amines previously studied by our research group. Due to glycine's small, hydrophilic, and zwitterionic nature, glycine is not retained under reverse-phase separation conditions, it creates a slightly acidic medium optimal for derivatization, and it does not interfere with subsequent precipitation of DNA by protamine[17]. The derivatization reaction between the C4′-OAS and glycine is shown in Figure 14.

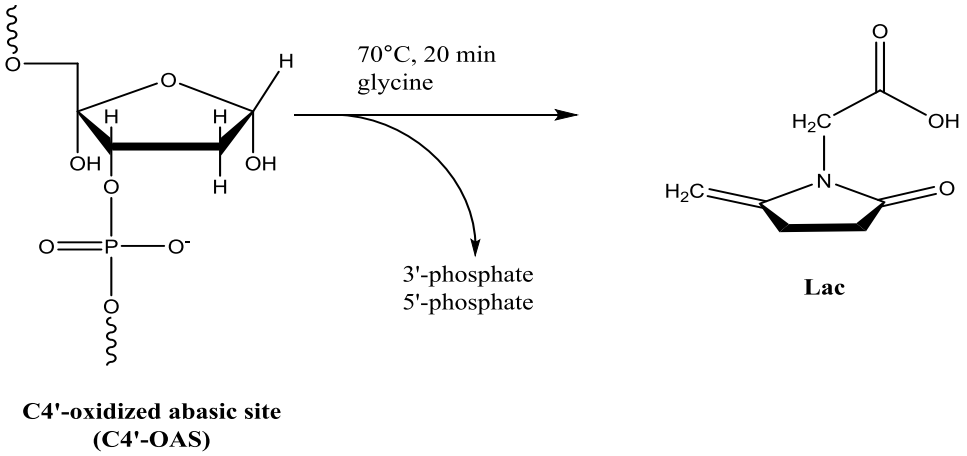

Figure 14. Formation of lactam (Lac) from the C4′-OAS precursor lesion

Lac is formed rapidly at 70 °C in the presence of glycine, and of all the lactam derivatives previously tested by the Roginskaya research group[17] has the highest relative yield based off peak area ratios in HPLC. Lac is also stable at the derivatization temperature, does not co-elute with any significant DNA damage products, and quantification of Lac can easily be performed photometrically due to the known absorption characteristics[17].

Specific Aims

The objective of the current work was to, firstly, determine the optimal method of CR generation in DNA solutions that is suitable for our novel method of HPLC detection. The choice of the optimal method of CR generation is dependent on the requirement of effective minimization of side reactions that can affect the quality of HPLC spectra, especially those reactions which compete with the reactions of interest between the CR and DNA 2′-deoxyribose.

The second goal of the current work was to prove the hypothesis that CR is capable of oxidizing DNA 2′-deoxyribose in a similar manner to the well-studied hydroxyl radical by analysis of the preference of hydrogen abstraction by CR from the 2′-deoxyribose moiety of DNA. The selectivity of these two ROS has been compared to prove that CR is a more discriminate hydrogen abstractor than HO•. In order to prove the above hypothesis, the major products of 2′-deoxyribose oxidation – 5MF, Lac, Fur, and MDA – by CR have been determined for both double-stranded (ds) and single-stranded (ss) DNA, and the relative yields of each product have been compared with those obtained from hydroxyl radical-mediated oxidation of 2′-deoxyribose.

Lastly, the reaction rates of CR with DNA nucleobases – in particular, guanine – have been compared to the reaction rates of the same radical with 2′-deoxyribose in order to determine the ratio of base damage to sugar damage (See Chapter 3).

CHAPTER 2

EXPERIMENTAL METHODS

Instrumentation, Glassware, and Other Materials

Instrumentation

A Shimadzu High Performance Liquid Chromatograph (HPLC), equipped with a degasser, autosampler, column oven, photodiode array (PDA) consisting of a tungsten lamp and deuterium lamp, and an analytical column (Phenomenex Gemini™, C18, reversed phase, 250 mm x 4.6 mm, 5 μm) was used as the primary instrument for data collection. Additionally, a Cary 100 ultraviolet-visible (UV-vis) spectrophotometer from Agilent was used for spectroscopic determination of concentrations of prepared solutions. X-ray radiation was generated via a Phillips X-ray tube with a tungsten anode, courtesy of Dr. David Close (Department of Physics and Astronomy, East Tennessee State University). A high pressure Xe(Hg) lamp from Optical Building Blocks Corporation was used as the primary source of UV light for photolysis experiments. Additional instrumentation used in this research included a laboratory analytical balance, oven, microprocessor-controlled hot water bath, and vortex mixer, all from Fisher Scientific.

Glassware and Other Materials

Additional important glassware and materials, including beakers, graduated cylinders, volumetric flasks, Pasteur pipettes, glass vials, Wheaton ampoules (pre-scored), graduated

pipettes, mechanical pipettes with appropriate pipette tips, graduated plastic vials (1.5 mL), centrifuge tubes (50 mL and 15 mL), and magnetic stirring bars of varying sizes were all used extensively throughout experimentation. HPLC inserts (200 μL) from Fisher were used to reduce the volume of solution needed for HPLC analysis. Matched quartz cuvettes were used in all spectrophotometric measurements.

Reagents

Deoxyribonucleic Acid

The sodium salt of salmon testes deoxyribonucleic acid (DNA) was purchased from Sigma-Aldrich Chemical Company.

Carbonatopentamminecobalt(III) Perchlorate

Carbonatopentamminecobalt(III) perchlorate ($Co(NH_3)_5CO_3]ClO_4$) was synthesized in our research lab according to the procedure published in Basolo and Murmann[104], and its identity was confirmed by IR and UV-vis spectroscopy.

DNA Reagents

Spermine tetrahydrochloride, glycine, protamine sulfate, and poly-L-lysine hydrochloride (polyL) (MW per one lysine hydrochloride = 149.45 g/mol, total MW > 30 000) were purchased from Sigma-Aldrich.

HPLC Solvents

Two distinct mobile phases were used during HPLC separation and analysis; the first was 40 mM aqueous ammonium acetate (prepared from 4 M stock solution of ammonium acetate, ACS reagent grade) in HPLC-grade water (both components of this buffer system were provided by Fisher); the second was an aqueous solution of 80% acetonitrile (CH_3COCN) prepared from HPLC-grade acetonitrile (from VWR) and HPLC-grade water.

4 M ammonium acetate was prepared by dissolving 154 g of ammonium acetate in a small volume of HPLC-grade water contained in a small beaker. After complete dissociation, the solution was transferred to a 500 mL volumetric flask, the solution was diluted to the mark on the volumetric flask, and stirred using a magnetic stirring bar to ensure homogeneity. The 80% (v/v) acetonitrile was prepared by combining 4 volumes of HPLC-grade acetonitrile with 1 volume of HPLC-grade water.

Buffers, Solutions, and Gases

All stock solutions were prepared using HPLC-grade water. 1 M stock solutions of potassium monobasic phosphate (KH_2PO_4) and potassium dibasic phosphate (K_2HPO_4) from Sigma were mixed in equal volumes to make a 1 M phosphate buffer system, pH = 6.9. This stock solution of phosphate buffer was diluted by a factor of 100 to yield 10 mM phosphate buffer with the same pH as the stock solution. This phosphate buffer was used in nearly all experimental protocols to maintain near-physiological pH.

Carbon dioxide gas (100% purity) and molecular oxygen gas (USP) provided by Airgas were used for sample purging.

Preparation of DNA Solutions. DNA solutions were prepared at 10 mM concentration (here and elsewhere in this text, DNA concentration is expressed per DNA nucleotide) by mixing 36 mg ST DNA (average MW per nucleotide = 360 g/mol) sodium salt with 10 mL of 10 mM phosphate buffer, pH 6.9. Following addition of the DNA, the solution was allowed to soak overnight at 4°C, and the following day it was stirred gently for 1 hour to ensure homogeneity.

Other Stock Solutions. The following aqueous stock solutions were prepared in HPLC-grade water and kept at +4°C: 100 mM spermine tetrahydrochloride, 100 mM poly-L-lysine (PolyL) and 2 M glycine 10x stock solutions were used to catalyze the formation of low molecular weight end products of DNA sugar damage. A saturated solution of protamine sulfate from salmon testes (salmine) was prepared for precipitation of DNA. 100 mM potassium persulfate 10x stock solution was used in the generation of CRs via UV photolysis of persulfate in the presence of bicarbonate.

Other Reagents. A saturated solution of 0.67% (w/v) thiobarbituric acid was prepared for MDA analysis. Pure MDA-TBA adduct was synthesized following protocols outlined in von Sonntag *et al.*[36] using 1,1,3,3-tetramethoxypropane and 2´-thiobarbituric acid. The resulting MDA-TBA adduct has a maximum absorption at 532 nm. Solid sodium bicarbonate was used in X-irradiation of bicarbonate solution experiments. Glacial acetic acid liquid was used to neutralize the sodium bicarbonate solutions during X-irradiation of bicarbonate solutions experiments. All reagents above were obtained from Fisher Scientific or Sigma-Aldrich.

Fricke Dosimetry

This method is based on the oxidation of Fe^{2+} to Fe^{3+} by hydroxyl radicals produced by radiolysis aqueous solutions. Fe^{3+} has a characteristic absorption maximum at 303 nm, but absorption by Fe^{2+} may also be observed at this wavelength. It becomes necessary to calculate the difference in the molar absorptivity of the two cations; $\Delta\varepsilon = 2201\ M^{-1}\ cm^{-1}$ [105].

As a consequence of the received dose of ionizing radiation, the ferric ion accumulates linearly with doses in the range from 0 to 400 Gy, and the plot of optical density at 303 nm vs. time ($d[OD_{303}]/dt$) is proportional to the dose rate (dD/dt), where D is the delivered dose to the solution.

A stock Fricke solution containing 1 mM $FeSO_4$ in 0.4 M sulfuric acid was prepared for determination of the dose delivered by the X-ray generator. The X-ray beam was attenuated by using a small copper disk. A small volume of this stock solution (100 μL) was placed into Wheaton ampoules and X-irradiated for 0 (control), 30, 60, 90, 120, 180, and 300 s. The resulting irradiated solutions were analyzed using the Cary 100 UV-vis spectrophotometer, and the OD of the samples was plotted as a function of irradiation time. The resulting regression line was used to calculate the dose via Equation 2.6 (p. 53). The derivation of Equation 2.6 follows below.

Using the Beer-Lambert law, the absorbance of the Fe^{3+} cation can be expressed Equation 2.1, which is then partially differentiated with respect to time in order to yield Equation 2.2,

$$OD_{303} = \varepsilon_{303} * l * \left[Fe^{3+}\right] \tag{2.1}$$

$$\frac{\partial OD_{303}}{\partial t} = \varepsilon_{303} * l * \frac{\partial [Fe^{3+}]}{\partial t} \tag{2.2}$$

where $\frac{\partial OD_{303}}{\partial t}$ is the rate of change in absorbance with respect to time, and can be represented as the slope of the regression line obtained by plotting OD_{303} vs. time, and $\frac{\partial [Fe^{3+}]}{\partial t}$ is the rate of accumulation of Fe^{3+} with time.

The quantity $\frac{\partial [Fe^{3+}]}{\partial t}$ can be expressed as the product of the density of the mixture, the radiation chemical yield of Fe^{3+}, and the partial derivative of dose with respect to time, $\frac{\partial D}{\partial t}$, as expressed in Equation 2.3. The density of a typical Fricke solution can be approximated as 1 kg L^{-1}, approximately the same as water, and the radiation chemical yield of Fe^{3+} is approximately 1.5 x 10^{-6} mol J^{-1} [106] for X-rays in the range of 60 keV. Substitution of Equation 2.3 into Equation 2.2 yields Equation 2.4, which can be rearranged to yield Equation 2.5.

$$\frac{\partial [Fe^{3+}]}{\partial t} = \rho * G\left(Fe^{3+}\right) * \frac{\partial D}{\partial t} \tag{2.3}$$

$$\frac{\partial OD_{303}}{\partial t} = \varepsilon_{303} * l * \rho * G\left(Fe^{3+}\right) * \frac{\partial D}{\partial t} \tag{2.4}$$

$$\frac{\partial D}{\partial t} = \frac{1}{\varepsilon_{303} * l * \rho * G(Fe^{3+})} * \frac{\partial OD_{303}}{\partial t} \tag{2.5}$$

Solving the leading term on the right-hand side of Equation 2.5 yields Equation 2.6.

$$\frac{dD}{dt} = 302.89\ J\ kg^{-1} * \frac{dOD_{303}}{dt} \tag{2.6}$$

where the units J kg^{-1} can be expressed as gray (Gy).

The data from the attenuated X-ray Fricke dosimetry were plotted, and the resulting regression line (OD_{303} = 0.0012t + 0.1709) was used to calculate the attenuated dose rate of the

system using Equation 2.6. The data and plot for OD_{303} vs. time are found in Table 2 and Figure 15, respectively. The unattenuated dose was calculated by the Roginskaya research group in a similar fashion.

Table 2: Optical Density as a Function of Irradiation Time in a Copper Disk Attenuated X-ray Beam.

Irradiation time, s	OD_{303}
0	0.173
30	0.196
60	0.237
90	0.284
120	0.319
180	0.389
300	0.519

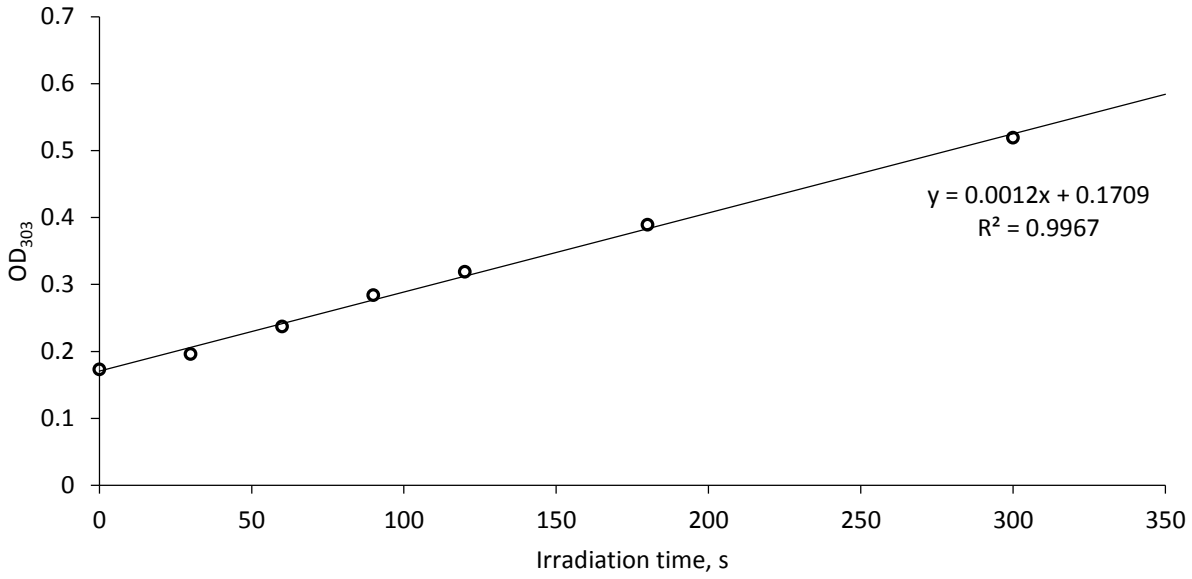

Figure 15: A plot of optical density at 303 nm vs. irradiation time in a copper disk attenuated X-ray beam

Methods of Generation of CR

Generation of CR by X-Irradiation of Bicarbonate Solutions

Preparation of Reaction Solution. A 5 mM solution of DNA was prepared by dilution of stock 10 mM DNA solution in 10 mM phosphate buffer, pH = 6.9. Equal volumes of DNA and phosphate buffer were combined and then were gently inverted to mix. Once prepared, the 5 mM DNA solution was combined with 42 mg solid sodium bicarbonate per 1 mL of 5 mM DNA to yield a solution of 5 mM DNA and 0.5 M $NaHCO_3$. The solid was dissolved via magnetic stirring bar and kept on ice until needed. Reaction solutions containing 1 M sodium bicarbonate were prepared in an identical manner, with the exception of addition of 84 mg solid sodium bicarbonate per 1 mL of 5 mM DNA.

X-Irradiation of Reaction Solution. The resulting reaction solution was divided into 210 μL aliquots and was placed into Wheaton ampoules for X-irradiation. Prior to X-irradiation, each ampoule was bubbled with a ~3:1 mixture of CO_2/O_2 for 10 minutes. The 3:1 mixture of carbon dioxide/oxygen was prepared by bubbling each gas through a round bottomed three-necked flask containing water. The number of bubbles of each gas per 15 s time interval was recorded, and the flow rates were adjusted to yield a ~3:1 mixture of CO_2/O_2. Following the adjustment of the flow rates of each gas, the system was allowed to equilibrate for 10 minutes prior to bubbling of ampoules.

Each ampoule was bubbled individually, and following bubbling with the gaseous mixture ampoules were capped with Parafilm in order to minimize the evolution of CO_2 gas. Samples were then X-irradiated via Phillips X-ray generator (at 10.9 Gy/s dose rate determined

by Fricke dosimetry) for doses of 0 to 1957 Gy. Following irradiation, the samples were treated with glacial acetic acid (7.2 μL) to neutralize the bicarbonate in solution, and the neutralized solution was transferred to labeled plastic centrifuge vials (1.5 mL, graduated). Irradiated solutions were kept on ice until needed. Once all samples were irradiated, each sample was divided into two 100 μL aliquots and transferred to labeled vials for polyL treatment or glycine treatment. Due to the high ionic strength of reaction solutions in this series of experiments because of using high concentrations of bicarbonate, polyL was used to precipitate DNA from solutions instead of spermine.

Generation of CR by Photolysis of Persulfate and Bicarbonate Solutions

Preparation of Reaction Solution. A solution of 5 mM DNA was prepared by mixing equal volumes of 10 mM stock DNA solution with 10 mM phosphate buffer in a 15 mL centrifuge tube. The tube containing the resulting solution was inverted gently several times to ensure adequate mixing of the two solutions, yielding a 5 mM DNA solution. An appropriate amount of solid sodium bicarbonate was added to the centrifuge tube to yield 5 mM DNA + 0.34 M sodium bicarbonate reaction solution. The solution was kept on ice until needed.

Reaction solutions were also prepared with varying concentrations of bicarbonate. The mass of solid bicarbonate and the volume of glacial acetic acid required to neutralize these solutions are summarized in Table 3, below, where the masses of sodium bicarbonate solid are for 800 μL solution volumes prior to neutralization with glacial acetic acid.

Table 3: The Masses of Sodium Bicarbonate and Volumes of Glacial Acetic Acid Used During Varied Ionic Strength Experiments

$[HCO_3^-]$, M	**mass $NaHCO_3$, mg**	**volume glacial acetic acid, µL**
0.3	20.2	13.7
0.5	33.6	22.9
0.8	53.8	36.5
1.0	67.3	45.7

Illumination of Reaction Solution. The resulting solution was divided into 540 µL aliquots, and each aliquot was transferred to a glass vial. The glass vials were capped with a plastic cap containing a septum, and the cap was left loose in order to allow the sample to be bubbled with a ~3:1 mixture of CO_2/O_2. Samples were bubbled individually for 10 minutes with the gaseous mixture of carbon dioxide and oxygen, and after bubbling the cap was closed tightly to minimize exchange of CO_2 with the atmosphere. Immediately prior to illumination, 10% of final volume of stock 100 mM potassium persulfate solution (10 mM final concentration) was added to each vial by injecting the persulfate stock solution through the septum, and samples were illuminated via Xe lamp equipped with water IR filter from 0 (control, no illumination) up to 5 minutes. Samples were immediately treated with an equimolar amount of glacial acetic acid to neutralize the bicarbonate in solution. Samples were divided into two 100 µL aliquots each, and were treated with glycine or polyL (see Post-Irradiation/Post-Illumination Sample Treatments, p. 60).

Generation of CR by Photolysis of Carbonatopentamminecobalt(III) Perchlorate

Preparation of Carbonatopentamminecobalt(III) Perchlorate Solution. A small amount of the carbonatopentamminecobalt(III) perchlorate complex was dissolved in ~3.0 mL of 10 mM phosphate buffer, pH 6.9 and was briefly vortexed. Once completely dissolved, the concentration of the resulting solution was determined spectrophotometrically using a UV-visible spectrophotometer. The absorbance of the complex at 506 nm was determined using the Beer-Lambert Law (Equation 2.7):

$$A = \varepsilon l c \tag{2.7}$$

where A is absorbance, ε is the molar absorptivity coefficient, l is the path length, and c is the concentration. Rearrangement of Equation 2.7 yields Equation 2.8:

$$c = \frac{A}{\varepsilon l} \tag{2.8}$$

For the carbonatopentamminecobalt(III) perchlorate complex, ε = 70 M^{-1} cm^{-1} [84], and the path length of the cuvette was 1 cm.

Preparation of the Reaction Solution. A reaction solution consisting of 5 mM DNA, 2 mM $[Co(NH_3)_5CO_3]ClO_4$, and 10 mM phosphate buffer to dilute to the appropriate concentrations of each component was prepared. Since the stock solution of DNA was 10 mM in bases, a 2-fold dilution was required for the DNA. The total volume of the DNA (V_{DNA}) was determined by use of Equation 2.9, where V_T is the total volume of the original solution.

$$V_{DNA} = \frac{V_T}{2} \tag{2.9}$$

Once the concentration of the cobalt complex was determined, the dilution factor was calculated using Equation 2.10, and the resulting dilution factor was then substituted into Equation 2.11, where V_{Co} is the volume of the cobalt complex:

$$f_{dil} = \frac{c_i}{c_f} = \frac{c_i}{2.00\ mM} \tag{2.10}$$

$$V_{Co} = \frac{V_T}{f_{dil}} \tag{2.11}$$

Once V_{DNA} and V_{Co} were calculated, the volume of 10 mM phosphate buffer (V_P) was calculated using Equation 2.12:

$$V_P = V_M - (V_{DNA} + V_{Co}) \tag{2.12}$$

Illumination of Reaction Solution. The reaction solution was divided into 800 μL aliquots, placed into a glass vial with a flea stirring bar, and illuminated via high pressure Xe(Hg) lamp or Xe lamp to photolyze the cobalt complex and generate CR. The lamp apparatus was operated at a power of ~ 65 W (12.2 V, 5.42 A, direct current (DC)), and was supplied with a water IR filter to avoid overheating of the reaction solution. The beam of light entering the illumination chamber was attenuated using a 3 mm slit. Samples were illuminated with constant stirring for 0 (control, no illumination) and up to 8 min, and were kept on ice following illumination until needed.

Post-Irradiation/Post-Illumination Sample Treatments

Each of the following treatments catalyzes the formation of HPLC-detectable low-molecular weight sugar damage products (SDP) in CR-damaged DNA. Spermine treatment was utilized to quantify the conversion of C1′ deoxyribosyl radicals to 5-methylenefuran-2-one (5MF) and C5′ deoxyribosyl radicals to furfural (Fur), as well as to quantify free, unaltered base release (FBR). Glycine treatment was utilized to quantify the conversion of C4′ deoxyribosyl radicals to 1-N-(oxycarbonylmethyl)-5-methyleneazacyclopent-3-ene (lactam, or Lac). In solutions with high ionic strength, the binding of spermine to DNA is disrupted, and poly-L-lysine (polyL) was utilized in place of spermine for C1′ and C5′ analysis.

Heat Treatment with Spermine. Following illumination or irradiation, an aliquot from each sample was placed into a labeled plastic tube for treatment with 10 mM spermine (final concentration). 10% of the total volume of the stock solution of 100 mM spermine + 20 or 40 μM uracil (as an HPLC internal standard) was added, vortexed for 15 s to precipitate DNA, briefly centrifuged, and was then placed into a water bath at 70°C. Samples were heated in the bath for 35 min, and following the heat treatment were cooled on ice for 1 min. After cooling, 10 μL of saturated protamine stock solution was added to each sample to precipitate any DNA remaining in solution, and the samples were allowed to cool on ice for an additional 10 min to allow for full precipitation of DNA. Following complete precipitation of DNA, samples were centrifuged for 2 min to pelletize DNA, and the supernatant (typically, 200 μL) was transferred to HPLC vials with plastic inserts for the 5MF, Fur, and FBR analysis.

Heat Treatment with Glycine. Following illumination, an aliquot from each sample was placed into a labeled plastic vial for treatment with glycine and combined with 10% of final volume the stock solution of 2 M glycine + 20 or 40 μM uracil, vortexed for 15 s, briefly centrifuged, and was then placed into a water bath, set to 70°C. Samples were heated in the bath for 20 minutes, and following the heat treatment were cooled on ice for 1 min. After cooling, 30 μL of saturated protamine stock solution was added to each sample to precipitate DNA remaining in solution, and the samples were allowed to cool on ice for an additional 10 min to allow for full precipitation of DNA. Following complete precipitation of DNA, samples were centrifuged for 2 min to pelletize DNA, and typically 200 μL of the supernatant was transferred to HPLC vials with plastic inserts for the Lac analysis.

Heat Treatment with PolyL. 10% of the solution volume of a 100 mM stock polyL solution was added to 100 μL of X-irradiated or UV-vis illuminated samples to yield a final concentration of 10 mM polyL. Samples were vortexed briefly, and precipitation of DNA was observed. The solutions were allowed to remain on ice for 10 minutes to completely precipitate DNA. Following precipitation, the samples were centrifuged for 2 minutes, and the supernatant was discarded. The precipitate was washed twice with 10 mM phosphate buffer to remove any unbound polyL from the precipitate. After each wash, the samples were vortexed briefly and were centrifuged to separate the precipitate from the supernatant. The supernatant resulting from each wash was discarded.

Following washing, 110 μL of 4 μM uracil in 10 mM phosphate buffer, pH 6.9 was added to each sample, and the samples were heated in a 70°C water bath for 35 minutes as with spermine. After heating, each sample was cooled on ice for 2 minutes. The samples were

centrifuged to separate DNA precipitate, and ~80 µL of supernatant was transferred to HPLC vials with plastic inserts for 5MF and Fur analysis.

Malondialdehyde (MDA) Analysis

HPLC Calibration for MDA Detection. A 100-fold dilution of MDA-TBA stock solution was prepared by mixing 10 µL of the stock MDA-TBA adduct with 990 µL of HPLC-grade water. The concentration of the diluted solution was determined spectrophotometrically. A series of dilutions of authentic MDA-TBA adduct (0.25, 0.50, 1.0, 2.0, 5.0, 8.0, 12, and 15 µM) were prepared by diluting the original MDA-TBA adduct in HPLC-grade water, and the resulting solutions were analyzed via HPLC (MDA gradient elution, 20 µL injection). The resulting calibration curve is found in Figure 16 below, where the y-intercept was forced through zero.

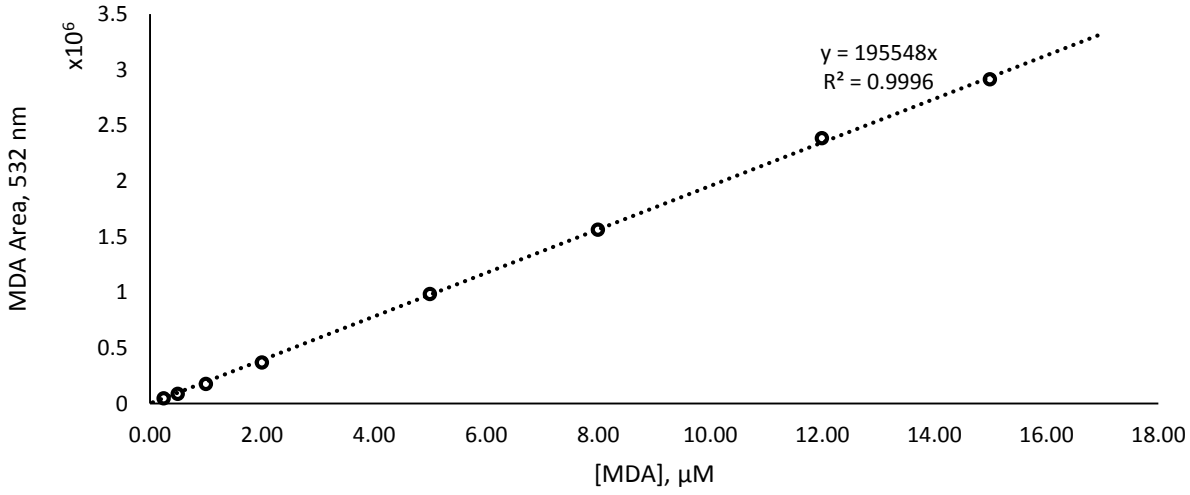

Figure 16: The initial MDA calibration curve

After a series of experiments, it was determined that the actual yield of MDA-TBA adduct was outside of the range of this calibration curve, and a new calibration curve was prepared using similar methodology with lower concentrations of the adduct (0.01, 0.05, 0.08, 0.10, 0.20, and 0.40 μM). The revised calibration curve is found below (Figure 17). Areas obtained via HPLC for all calibration curves were determined at 532 nm. The two calibration curves agree with each other reasonably well. Data were then recalculated using the revised calibration curve regression line.

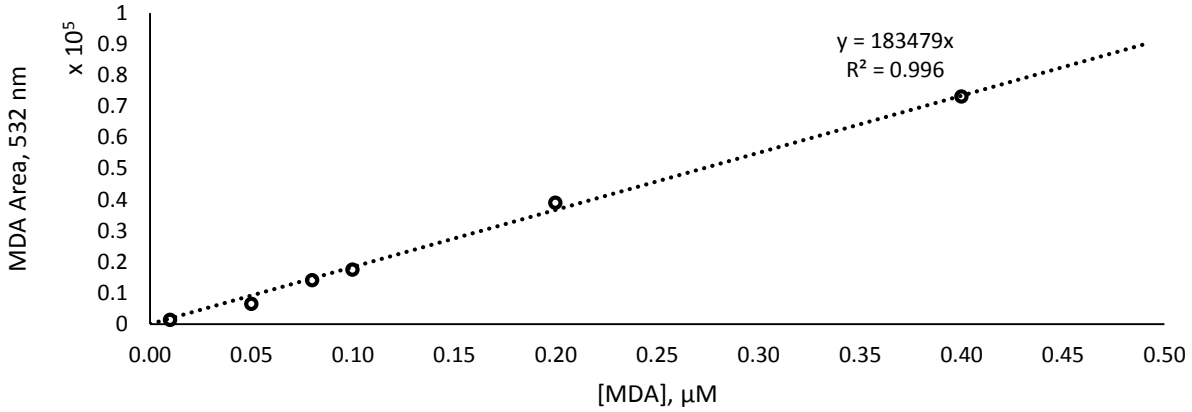

Figure 17: The revised MDA calibration curve

HPLC Detection of MDA. Reaction solutions were analyzed for MDA using a standard thiobarbituric acid (TBA) reactive substances (TBARS) protocol[107], which has been modified in our research lab to accommodate our systems[17]. Following illumination or X-irradiation, 100 μL of the solution was transferred to a labeled plastic vial, and one tenth by volume (10 μL) of saturated protamine sulfate stock solution was added to each sample to precipitate DNA. Samples were vortexed for 15 s to allow for DNA precipitation. After vortexing, samples were cooled on ice for 10 min to fully precipitate DNA.

Once the DNA was fully precipitated, samples were centrifuged and 80 μL of the supernatant was transferred to a fresh plastic vial, and 80 μL of saturated (0.67% w/v) thiobarbituric acid (TBA) was added. One tenth of the original volume of supernatant (8 μL) of 1 M HCl was added, and the samples were vortexed to mix thoroughly. Samples were then heated in a 90°C water bath for 15 minutes to form the MDA-TBA adduct.

Following heating, samples were cooled on ice for 5 minutes, and 80 μL of the resulting solution was transferred to HPLC vials for analysis. The extinction coefficient of the MDA-TBA adduct is $1.56 \times 10^5\ M^{-1}\ cm^{-1}$ at 532 nm[108], and chromatograms were analyzed at this wavelength.

Extraction of MDA with N-Butanol. After irradiation or illumination, 200 μL of DNA solution was heated in a 70°C water bath to maximize the release of MDA from DNA into the solution. The heated DNA solution was chilled on ice for 1 minute, and 10% of the original volume of saturated protamine solution (20 μL) was added to each sample to precipitate DNA. The samples were allowed to chill on ice for 15 minutes to fully precipitate DNA. The resulting solution was centrifuged to pelletize the DNA. Equal volumes of the resulting supernatant and saturated solution of TBA were combined in a clear centrifuge tube. To this solution was added 1/10 volume of 1 M HCl, and the solution was vortexed to ensure homogeneity. The reaction solution was then heated for 15 minutes in a 90°C water bath. Following heating, the solution was chilled on ice for 2 minutes.

200 μL of n-butanol was added to each centrifuge tube, and the mixture was vortexed vigorously for 30 s. The MDA-TBA adduct is extracted nearly quantitatively by n-butanol. Following extraction, the mixture was centrifuged for 1 min. 130-150 μL of each layer (aqueous

and organic) were transferred into a quartz cuvette, and the UV-vis spectra of the organic and aqueous layers were recorded.

Determination of the MDA-TBA Extinction Coefficient in n-Butanol. MDA-TBA adduct standards of varying concentrations were prepared from pure MDA-TBA adduct with OD_{532} of approximately 0.2, 0.4, 0.6, 0.8, and 1.0. After spectrophotometric determination of the OD in water for the given concentration, a 200 μL (1 volume) aliquot was combined with 1 volume of n-butanol and 1/10 volume (20 μL) of 1 M HCl, and the samples were vortexed vigorously for 30 s. The resulting samples were centrifuged for 2 minutes to extract the MDA-TBA adduct into the organic phase. Both the organic layer and the aqueous layer were measured spectrophotometrically.

The OD_{532} from the larger aliquot was used to determine the concentration of MDA-TBA adduct present prior to n-butanol extraction. Following the extraction by n-butanol, the OD_{532} of the post-extraction aqueous layer was measured, and the concentration of the MDA-TBA adduct remaining in the aqueous layer was calculated. The difference between the pre- and post- n-butanol extraction concentrations was calculated by subtraction, and the resulting concentration was used as the concentration of the adduct present in the organic layer. The OD_{532} in organic layer was measured, and the concentration of MDA-TBA adduct was plotted versus the OD_{532} of the organic layer. Least-squares linear regression of the plot yielded a line with a slope equal to the extinction coefficient of MDA-TBA in n-butanol at 532 nm, 1.71×10^5 M^{-1} cm^{-1}.

DNA Denaturation

For preparation of single-stranded DNA solutions, approximately 3 mL of previously prepared double-stranded DNA solution in 10 mM phosphate buffer, pH 6.9, was thermally denatured in a 90°C water bath for 15 minutes. After this, the DNA solution was allowed to cool gently to room temperature for 1 h. Following equilibration to room temperature, the single-stranded DNA solution was placed on ice until needed.

HPLC Analysis

For all HPLC analysis programs, a two-solvent system was used: 40 mM aqueous ammonium acetate buffer (solvent A) and 80% v/v aqueous acetonitrile (solvent B). Linear acetonitrile gradients were applied to elute the products. The flow rate was 1 mL/min, the column temperature was maintained at 30^{o}C, and samples in the autosampler tray were kept at 4^{o}C. Optical measurements were performed by a two-lamp photodiode array (PDA), composed of a deuterium lamp (D) for the UV wavelength range, and a tungsten filament lamp (W) for visible wavelengths.

HPLC Analysis of Lac, 5MF, Fur, and FBR. Typically, 100-200 μL of each sample was transferred into a labeled HPLC vial containing a 200 μL plastic insert. Injection volumes were typically 50-100 μL. The column was equilibrated for a minimum of 30 min with 100% Solvent A. Equilibration was followed by a conditioning run (no sample injection).

All the low-molecular products mentioned in this section were eluted by a linear gradient of Solvent B from 0% to 20% over 15 min, which corresponds to the linear increase of acetonitrile from 0 to 16%. After 20 min from the beginning of the run the PDA detection was stopped, and the concentration of acetonitrile was increased to 40% B to wash the column with a

higher concentration of the organic solvent (solvent B) for 2 min and then the system was returned to the original condition of 100% solvent A and was equilibrated for 20 min until the next injection. The gradient is represented by Figure 18, below.

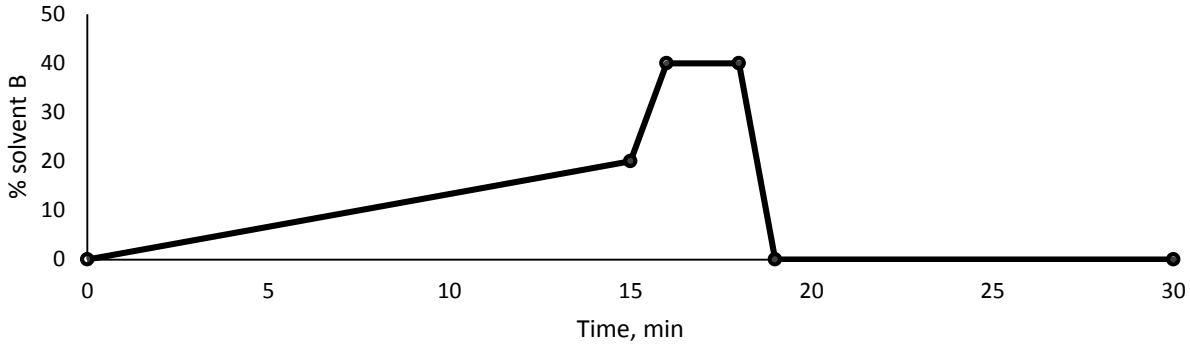

Figure 18: A graphical representation of the SDP/FBR gradient elution method. Solvent B composition is plotted as a function of time.

Products were identified based on comparisons of retention times with authentic samples and UV spectra (D/W lamps) and were typically quantified at 254 nm. All low-molecular weight products of HPLC damage studied in this work with the exception of MDA were analyzed using this HPLC gradient program.

Gradient Elution of MDA-TBA Adduct. Typically, 80 µL of each sample was transferred to a labeled HPLC vial containing a 200 µL plastic insert. Injection volumes of MDA-TBA adduct samples were typically 20 µL. The column was equilibrated for 30 min with 15% solvent B. Equilibration was followed by a conditioning run (no sample injection).

The HPLC program used for detection of MDA-TBA consisted of a linear gradient from 15% to 30% Solvent B (12% to 24% pure acetonitrile) over 15 min, after which PDA detection was stopped and concentration of solvent B was increased to 50% B (40% acetonitrile) over 2

min. After this increase to 50% B, the solvent ratio was held constant for 2 minutes, then reduced back to 15% B over 1 min, and then the column was equilibrated for 15 min. The gradient is represented by Figure 19, below.

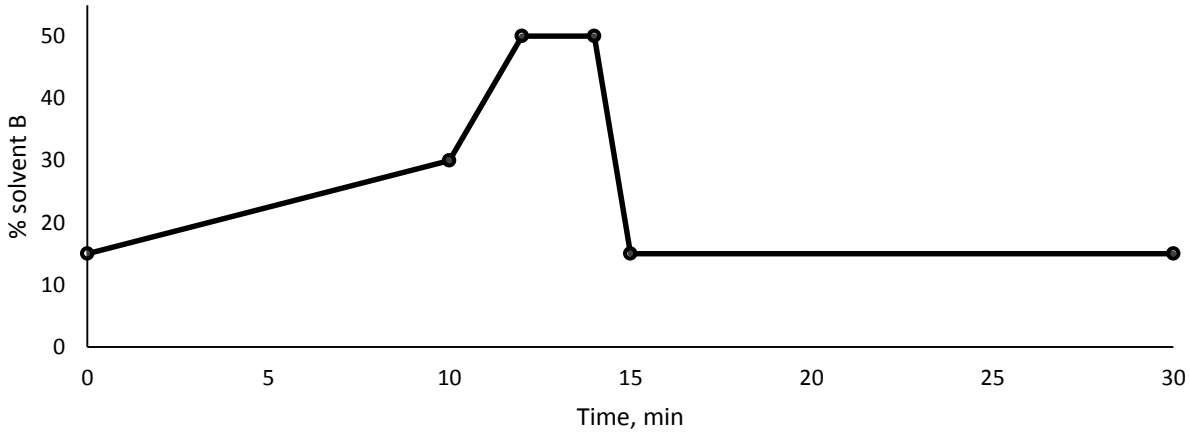

Figure 19: A graphical representation of the MDA gradient elution method. Solvent B composition is plotted as a function of time.

The MDA-TBA adduct product was identified based on comparison of retention times with authentic MDA-TBA adduct and quantified at 532 nm.

Quantification of HPLC Chromatograms. Uracil was selected as an internal standard for the quantification of SDP and FBR low molecular weight end products due to its absence in native DNA. Using the known concentration of uracil present in each reaction solution, the concentration of respective SDPs and FBR could be calculated using Equation 2.13, derived from the Beer-Lambert Law:

$$\frac{A_X}{A_U} = \frac{\varepsilon_{X,254\ nm} * l * [X]}{\varepsilon_{U,254\ nm} * l * [U]} = \frac{\varepsilon_{X,254\ nm}}{\varepsilon_{U,254\ nm}} * \frac{[X]}{[U]} \qquad (2.13)$$

where A_X is area under the assigned chromatographic peak of compound X and ε is the molar extinction coefficient. Rearrangement of Equation 2.13 results in Equation 2.14, which can be solved for the concentration of the SDP or free base of interest.

$$[X] = [U] * \frac{A_X}{A_U} * \frac{\varepsilon_{U,254\,nm}}{\varepsilon_{X,254\,nm}} \quad (2.14)$$

Use of Equation 2.14 requires that the molar extinction coefficients of each of the SDP and free base be known, and these extinction coefficients were determined by the Roginskaya research group in 40 mM ammonium acetate, pH 6.9. The results of these calculations are summarized in Tables 4 and 5, respectively.

Table 4: The Molar Extinction Coefficients for SDP in 40 mM Ammonium Acetate, pH 6.9

SDP	molar extinction coefficient (ε) at 254 nm, $M^{-1}cm^{-1}$
5MF	10830
Lactam	8700
Fur	5500

Table 5: The Molar Extinction Coefficients for Uracil and Native DNA Bases in 40 mM Ammonium Acetate, pH 6.9

Base	molar extinction coefficient (ε) at 254 nm, $M^{-1}cm^{-1}$
Uracil	7950
Cytosine	5070
Guanine	9280
Adenine	11990
Thymine	6690

CHAPTER 3

RESULTS AND DISCUSSION

Generation of CR by X-Irradiation of Bicarbonate Solutions

Hydroxyl radicals can react with bicarbonate anions to form water and the CR, as shown in Reaction 1.8 (page 42). The reaction follows second-order kinetics, and the rate constant was reported by Buxton *et al.* to be 1.0×10^7 M^{-1} s^{-1} [82]. Udovicic *et al.* reported that HO• reacts with DNA with a second-order rate constant of 2.5×10^8 M^{-1} s^{-1} [109], and the greater rate constant for the reaction of HO• and DNA is indicative for the preference of HO• to react with DNA itself rather than form CR. The working hypothesis of the experiments described in this section is that with a less than one order of magnitude difference in rate constants, bicarbonate anions at sufficiently high concentrations can successfully compete with DNA for the hydroxyl radical, so the reaction may be redirected to follow the reaction pathway between HO• and HCO_3^-.

Solutions of 5 mM DNA and 0.5 M HCO_3^- were prepared following protocols described in Chapter 2. These solutions were X-irradiated at the 10.9 Gy/s dose rate for doses over the range from 0 to ~ 2 kGy. Following irradiation, samples were divided into two aliquots, and one was heat treated in the presence of polyL to catalyze the formation of 5MF and Fur (Figures 12 and 13, respectively, p. 44). The other aliquot was heat treated in the presence of glycine to derivatize the C4′-OAS to Lac. Following heat treatment, all samples were analyzed by reverse phase HPLC to quantify the yield of each respective sugar damage product (SDP). Representative chromatograms for all post-irradiation treatments under these experimental

conditions are presented in Figure 20 (see next page). Each post-irradiation treatment chromatogram is labeled with the 4 native DNA nucleobases, uracil (used as an internal standard), and the SDP that are formed via catalytic/heat treatment with the appropriate reagent. Control chromatograms (no irradiation) display only the chromatographic peak for uracil.

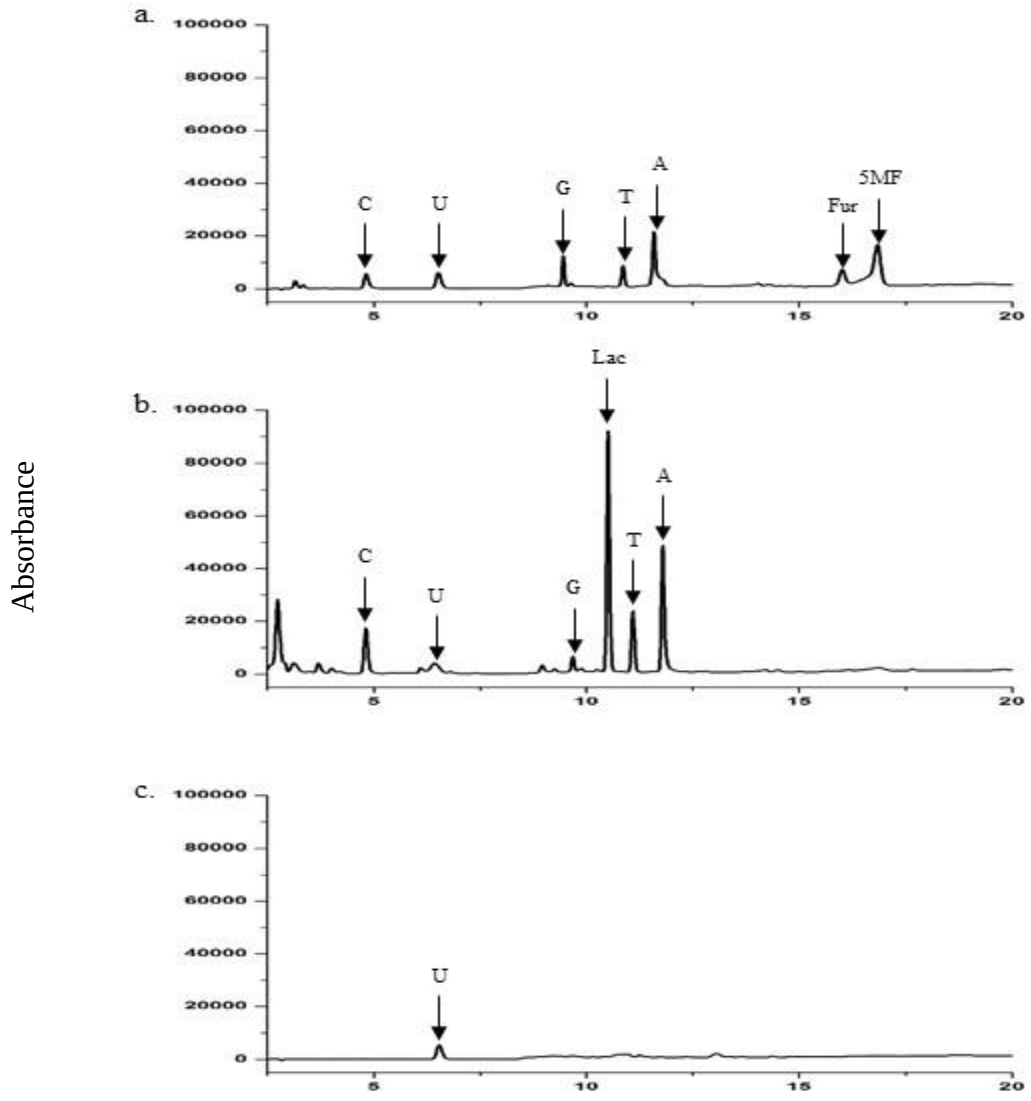

Figure 20: The representative chromatograms obtained from X-irradiation of 5 mM dsDNA + 0.5 M HCO_3^- solutions: a) polyL treatment after 180 s X-irradiation, b) glycine treatment after 180 s X-irradiation, and c) polyL treatment after 0 s X-irradiation (control). HPLC conditions: reversed phase, C18 analytical column, linear acetonitrile gradient from 0 to 16% acetonitrile over 15 minutes at a flow rate of 1 mL/min. The column was equilibrated with 40 mM ammonium acetate buffer.

Chromatographic peaks were integrated in accordance with methodology previously discussed (Chapter 2, page 68). Several replicate (typically, triplicate) experiments using the same conditions were performed to quantify the individual and total SDP, as well as the individual and total free base release (FBR). The resulting data from each experiment were statistically analyzed, and the resulting graph of the average yields individual SDP, of the total SDP calculated as a sum of yields of Lac, 5MF, and Fur, of and the total FBR vs. radiation dose is presented in Figure 21.

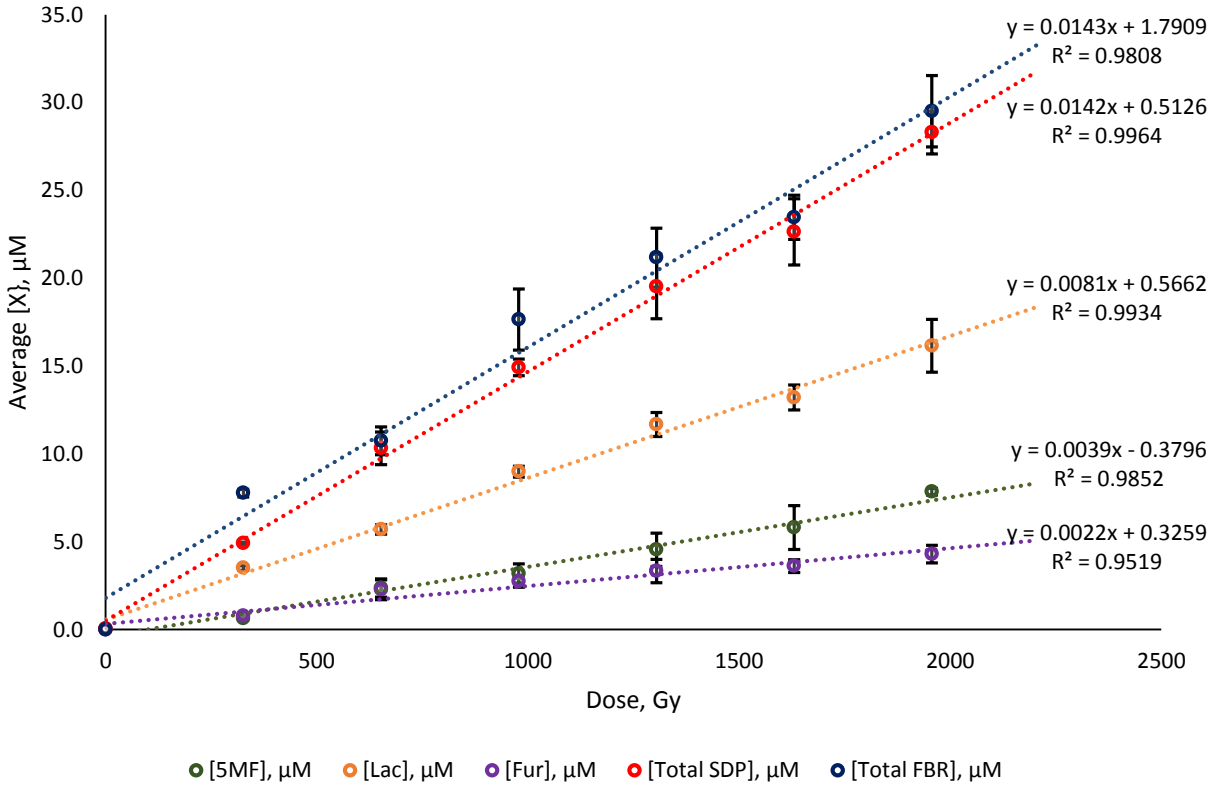

Figure 21: The average yields of individual SDP, total SDP, and total FBR as a function of radiation dose (Gy)

Radiation chemical yields (in nmol J^{-1}) were calculated from the slopes of the regression lines, assuming that the density of the solutions was near that of water (1 g/mL). The ratio of the slope for the product of interest and for the total FBR slope gives a relative yield of each sugar damage pathway (C1′, C4′, and C5′). The slopes, radiation chemical yields, and relative yields of each SDP are summarized in Table 6. The value of the slope for total FBR is normalized to 100%, and the relative yields of the product of interest are expressed as the ratio between the slope values of this product and the total FBR. There is a very good agreement between the total SDP and total FBR slopes, and the R^2 values for all linear regression lines are > 95%. It should be noted, however, that MDA, the product of the second pathway of C4`-OAS, was not quantified in these experiments due to use of a different gradient for elution of the MDA-TBA adduct.

Table 6: The Linear Regression Data and Radiation Chemical Yields (G) from the Plot of Individual SDP, Total SDP, and Total FBR as a Function of Dose

Product	Slope (μM/Gy)	G (nmol J^{-1})	Relative % Yield
5MF	0.0039	3.9	27%
Lac	0.0081	8.1	57%
Fur	0.0022	2.2	15%
Total SDP	0.0142	14.2	99%
Total FBR	0.0143	14.3	100%

‡Ratio of the G values for each species to the G value of Total FBR

Comparison of SDP with FBR was used in a manner consistent with previous studies authored by our research group[14-17]. The choice of FBR as the internal benchmark for irradiated DNA solutions is a reasonable one due to the majority of free-radical initiated damage to the DNA sugar-phosphate backbone being capable of destabilization of the glycosidic bond[12] and

releasing a free, unaltered base in conjunction with formation of a deoxyribosyl radical[17]. Base propenals, which have been shown to be an exception to this rule, are not significant contributors to radiation-induced DNA damage[110,111]. Because other 2′-deoxyribose lesions are FBR generators (including abstraction of C5′-hydrogen to form the 1, 4-dioxobutane lesion[112] and C3′-hydrogen abstraction resulting in the formation of 2-methylenefuran-3-one)[113,114], the total yield of FBR must be greater than or equal to the combined yield of all SDP and MDA, and any deviation from this trend would be characteristic of a 2′-deoxyribose lesion not accounted for in the present work.

In these experiments, MDA was not measured, but yields of this type of lesion can be estimated as ½ of the yield of Lac as an upper limit[17]. This estimate is the upper limit for MDA concentration, and in subsequent experiments the yield of MDA produced by CR-initiated DNA sugar damage was found to be very low.

Relative yields of the three SDP indicate that the preferential locus of hydrogen abstraction in this system is C4′ > C1′ > C5′. This mirrors the trend for the reaction of X-ray-generated hydroxyl radicals with DNA sugar described in our recent work[17], though the radiation yields of products are lower (the yields of FBR are ~3.5-fold lower in the present experiment than in Roginskaya *et al.*[17]). Furthermore, the ratios of relative yields of Lac, 5MF, and Fur obtained in this work (Lac: 5MF: Fur = 2.1 : 1 : 0.56) match rather closely the same ratios obtained in our recent work[17] under analogous conditions for the damage of DNA sugar by hydroxyl radicals (Lac: 5MF: Fur = 1.9 : 1 : 0.74). While it is possible that CRs generated in our system via Reaction 1.4 (see page 37) react with DNA sugar with selectivity similar to that of hydroxyl radicals, it cannot be excluded from these data comparisons that bicarbonate anions

function mostly as hydroxyl radical scavengers in the bulk. The result of this radical scavenging is to confer partial protection to DNA from the hydroxyl radical attack, instead of the intended function of switching the role of a major oxidizer from HO• to CR. If this is the case then it means that though Reaction 1.4 (p. 36) between HCO_3^- and HO• is efficient, resultant CRs might not be able to compete for DNA sugar with remaining hydroxyl radicals. Further increase of the concentration of bicarbonate would solve this problem, but it is not realistic since even at 0.5 M of bicarbonate electrostatic interactions between DNA and positively charged DNA-binding polyamines are significantly impaired, so that spermine can no longer be used as a catalyst of 5MF/Fur release due to its decreased DNA affinity observed as the absence of DNA precipitation. Higher ionic strengths will likely cause disruption of DNA interaction for even such as strong DNA binder as polyL.

To summarize, it is impossible to determine if the sugar damage observed in this system is the result of the reaction with CRs or with HO•. This indicates that this system is not quite suitable for studying the reactions of CR with DNA sugar.

Generation of CR by Photolysis of Persulfate + Bicarbonate Solutions

In most of their studies described in Chapter 1, Shafirovich *et al.* used the method of CR generation based on photolysis of solutions of persulfate anions with a large excess of bicarbonate anions (Reaction 1.6, p. 37). This research group compared the rate constant between their model oligonucleotides and sulfate radicals ($(3.2 \pm 0.3) \times 10^9\ M^{-1}\ s^{-1}$ [87]) to the rate constant for the reaction between the sulfate radical and the bicarbonate anion ($(4.6 \pm 0.5) \times 10^6$ [46]) in order to determine the optimal reaction conditions to reduce the oxidation

of DNA by $SO_4^{\bullet-}$. The results of these optimization experiments by Shafirovich *et al.* determined the optimal concentration of HCO_3^- to be 0.3 M, and this concentration was used in the present work to determine the suitability of this persulfate/bicarbonate system for determining the ratio of H-abstraction preference in CR attack of 2′-deoxyribose. It is worth noting that the use of oligonucleotides results in essentially homogenous solutions of DNA, but in the current work polymerized DNA was used, which results in solutions that are highly viscous.

Exposure of persulfate anions to UV light (308 nm) results in the generation of sulfate radicals (SR). This reaction (Reaction 1.6, page 38) follows second-order kinetics, and the rate constant for the photolysis of persulfate was reported by Huie and Clifton as 2.8×10^6 M^{-1} s^{-1} (as ionic strength $\rightarrow 0$)[115]. The quantum yield for this reaction at 308 nm is 0.55, as reported by Ivanov *et al.*[85]. Once formed in the presence of HCO_3^-, SR can proceed down one of two pathways: a SR can recombine with another SR in a second-order reaction to re-form the initial persulfate anion with a second-order rate constant of 1.6×10^8 M^{-1} s^{-1}, reported by Herrmann *et al.*[116], or SR can react with HCO_3^- to generate a CR with a second-order rate constant of 2.8×10^6 M^{-1} s^{-1} [115]; this rate constant is in agreement with the one reported by Shafirovich *et al.* ($(4.6 \pm 0.5) \times 10^6$ [46]). Because the CR-forming reaction occurs at a slower rate than the recombination reaction, large concentrations of HCO_3^- can drive the reaction towards the CR-forming reaction. However as ionic strength of the reaction solution increases, product yields of SDP decrease (see Figure 24, p. 84). In order to optimize yield of SDP, 0.3 M solutions of bicarbonate were used in these reactions.

Photolysis of Persulfate + 0.3 M Bicarbonate Solutions

Using the method adapted from the Shafirovich research group, solutions of 0.3 M HCO_3^- and 10 mM $S_2O_8^{2-}$ were illuminated with Xe lamp in the presence of 5 mM DNA (all final concentrations). Following illumination, samples were neutralized with an equimolar amount of glacial acetic acid and the resulting reaction solutions were analyzed via HPLC for individual Lac, 5MF, Fur, and DNA free bases. As reported by Braunlin *et al.*, the binding of small polyamines like spermine, spermidine, and putrescine to DNA is disrupted in solutions where the ionic strength is increased[99]. Due to the high ionic strength of these reaction solutions, a stronger DNA precipitating agent (polyL) was used in order to facilitate removal of DNA from solution before HPLC analysis of C1′ and C5′ products.

Representative chromatograms for all post-illumination treatments under these experimental conditions are shown in Figure 22. Each post-illumination treatment chromatogram is labeled with the four native DNA nucleobases, uracil, and the sugar damage products that are formed via catalytic/heat treatment with the appropriate reagent. Control chromatogram (no irradiation) displays only the chromatographic peak for uracil. The chromatographic peaks were integrated in line with previously described methods (see Quantification of HPLC Chromatograms, p. 68).

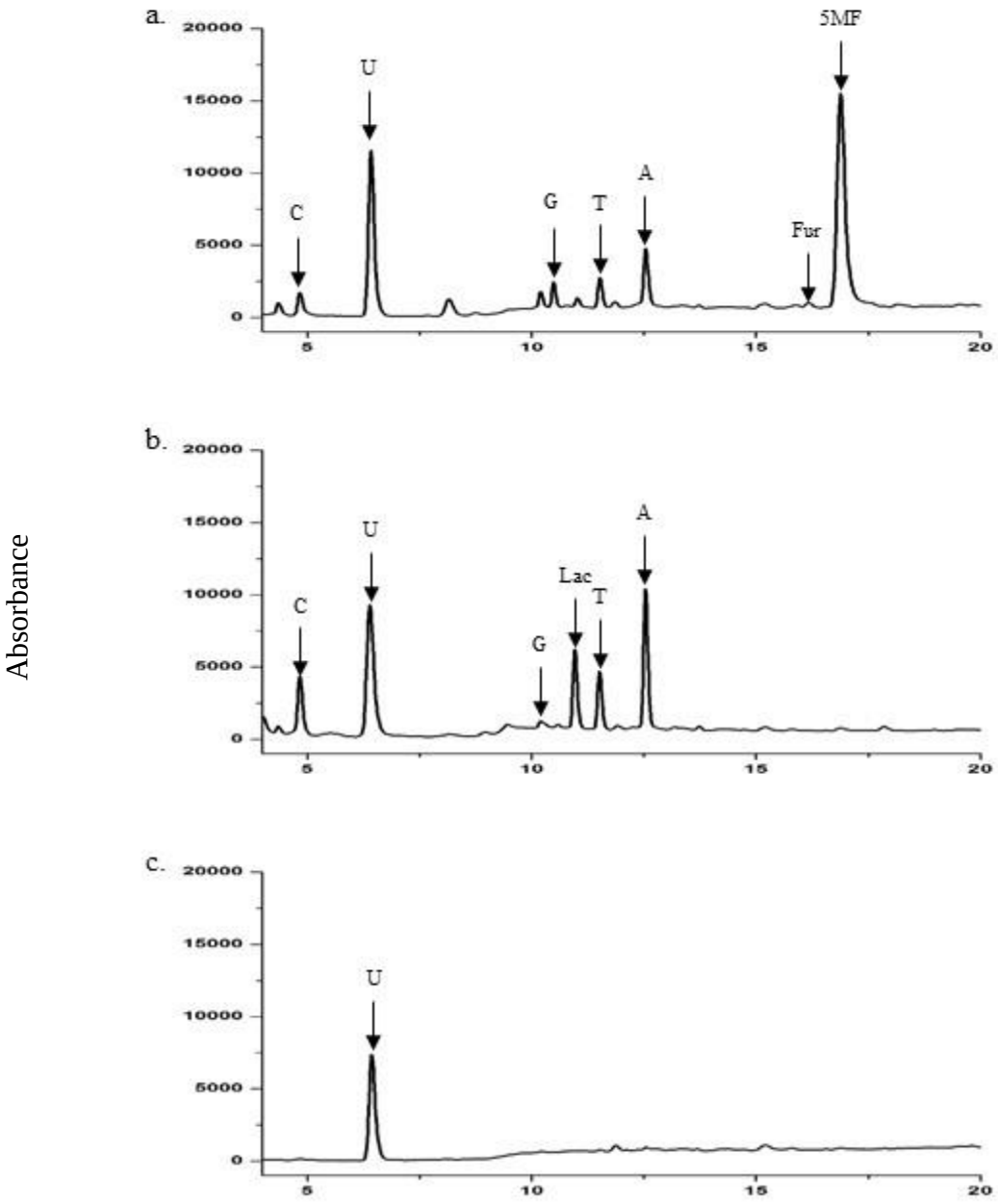

Figure 22: The representative chromatograms obtained from the photolysis of persulfate solutions (10 mM) in the presence of 5 mM DNA (in bases) and 0.3 M HCO_3^-: a) polyL treatment following 300 s of illumination with Xe lamp; b) glycine treatment following 300 s of illumination with Xe lamp; c) polyL treatment, no illumination (control).

Once chromatographic peaks were integrated, the resulting areas were converted to concentrations of individual SDP, total SDP, and total FBR. The plot for these data is found in Figure 23. The results found in Figure 23 are from a singular pilot experiment, and no error bars are associated with the data.

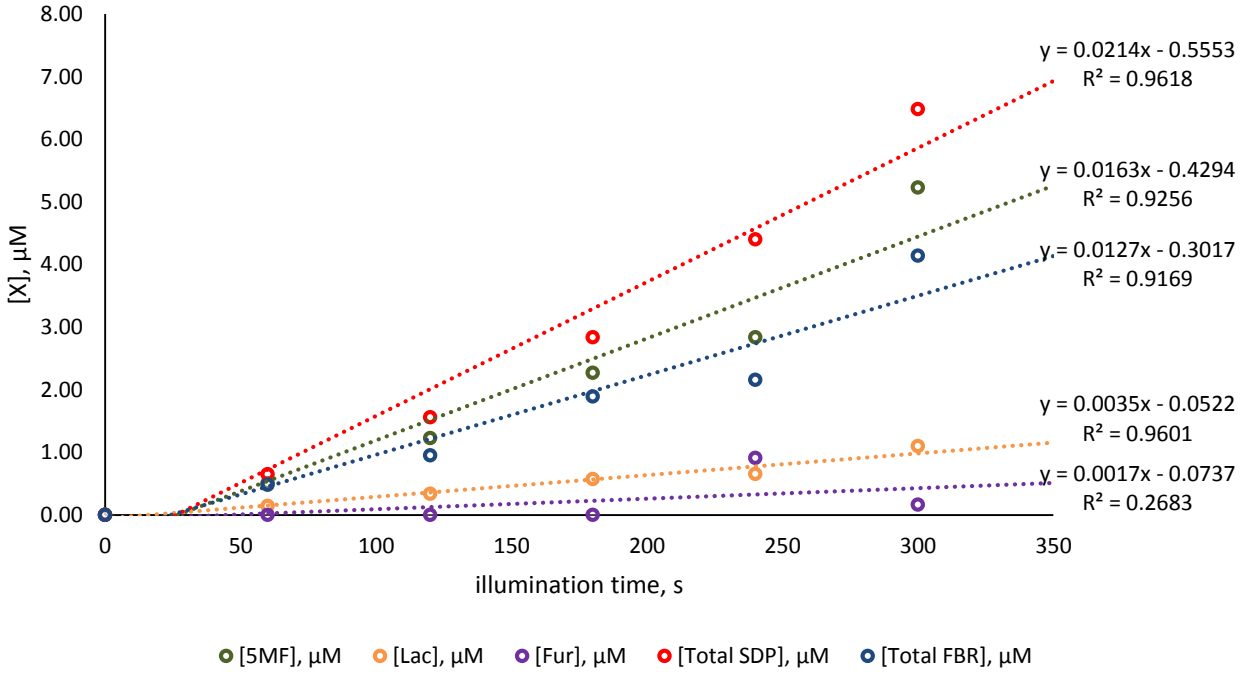

Figure 23: A plot of the yields of individual SDP, total SDP, and total FBR as a function of illumination time (s) in persulfate/bicarbonate systems.

The resulting plot (Figure 23) was analyzed using linear regression, and the values for the slopes (in µM s^{-1}) were compared for each individual SDP, the total SDP, and total FBR. The value of the slope for total FBR is normalized to 100%, and the relative yield of the product of interest is expressed as the ratio between the slope values of this product and the total FBR. The data are summarized in Table 7.

Table 7: The Linear Regression Data and Relative Product Yields from the Plot of Individual SDP, Total SDP, and Total FBR as a Function of Illumination Time for the Persulfate/ Bicarbonate System

Product	Slope (μM/s)	Relative % Yield‡
5MF	0.0163	128%
Lac	0.0035	28%
Fur	0.0017	13%
Total SDP	0.0214	169%
Total FBR	0.0127	100%

‡Ratio of rate of accumulation of each species to the rate of accumulation of FBR

It is obvious from comparing Figures 21 (p. 74) and 23 (p. 81), and Tables 6 (p. 75) and 7 that the relative yields of products of DNA sugar damage in the experiment with X-irradiation of bicarbonate and photolysis of solutions of persulfate and bicarbonate are in sharp contrast. For the method of X-irradiation of bicarbonate, the C4` pathway prevails, with the C1` pathway contributing nearly one half of the yield of the C4` pathway. In the meantime, the C1` pathway is absolutely dominant in the experiment with photolysis of solutions of persulfate and bicarbonate, so that other pathways of DNA sugar damage are suppressed. Additionally, there is a substantial disagreement between total SDP and total FBR in these experiments; the yield of 5MF alone surpasses the yield of FBR.

In almost all of the post-illumination samples, no detectable levels of guanine were found. This can be explained by fast oxidation of guanine by the persulfate anion and and/or resulting sulfate radicals (SR), both of which are strong oxidizers and can oxidize guanine in DNA or free guanine released into the bulk of the solution. Also, it is noteworthy that the levels of Fur were very low.

There are two potential reasons for the unexpected product yields observed in this experiment: 1) aforementioned high oxidizing ability of the parent persulfate anion and the generated sulfate radical anion and 2) high ionic strength associated with high concentrations of bicarbonate required for the experimental conditions. Each factor individually, or a combination of both, can contribute to the occurrence of undesired side reactions, which can seriously alter the product yields. For example, released bases in the solution can be oxidized by persulfate and/or by sulfate radical anion. Also, it is not clear if 0.3 M of bicarbonate is a sufficient concentration in our system for the reaction of bicarbonate with sulfate radical anion (Reaction 1.7, p. 37) to successfully compete with the reaction of sulfate radical anion with DNA. Shafirovich and co-workers used an essentially lower concentration of DNA oligonucleotides (~100 μM in bases) in their experiments[87].

Photolysis of Persulfate in the Presence of Varied Concentrations of HCO_3^-

This set of experiments was designed to study the effect of $[HCO_3^-]$/ionic strength on the product yields and to examine whether the increase of $[HCO_3^-]$ can modify the spectrum of the product yields.

Reaction solutions were prepared with varying $[HCO_3^-]$ to investigate the effect of bicarbonate concentration/ionic strength of the reaction solution on the formation of SDP. DNA solutions containing 0.3, 0.5, 0.8, and 1.0 mM bicarbonate were prepared and illuminated for 5 minutes under similar conditions from the fixed bicarbonate concentration. Following illumination, samples were treated with polyL and glycine, and analyzed by HPLC as described before. The results of this pilot experiment are found in Figure 24, below.

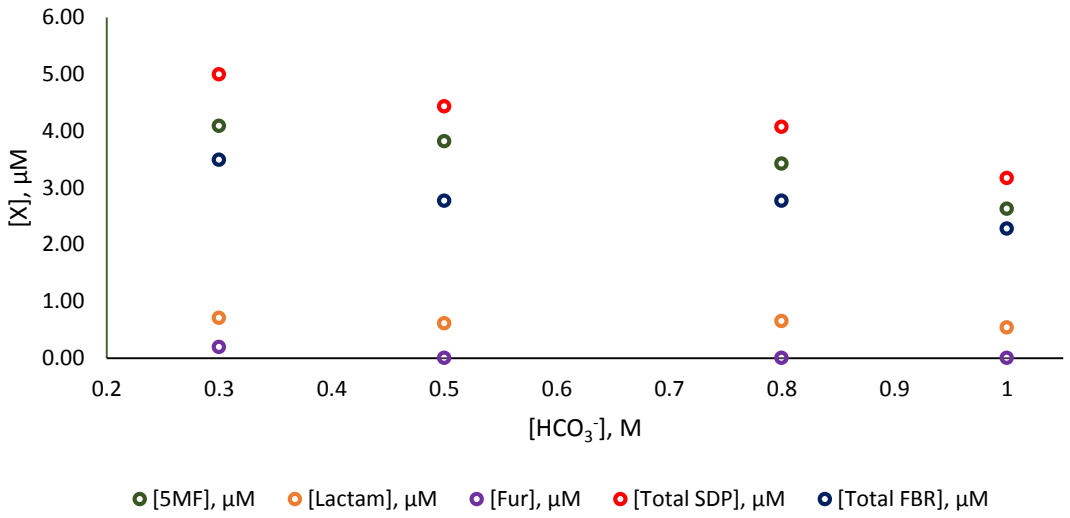

Figure 24: A plot of the yields of individual SDP, total SDP, and total FBR in photolyzed persulfate solutions vs. the concentration of bicarbonate. All samples were illuminated for 5 min. All other conditions are the same as indicated in Figure 23 (p. 81).

The plot indicates an approximately linear inverse relationship between the SDP yield and $[HCO_3^-]$/ionic strength of the reaction solution. However, the general trend in the SDP ratio still remains the same: 5MF still is a major product even at 1 M of bicarbonate, and the imbalance between SDP and FBR still remains. These results indicate that while the increase of $[HCO_3^-]$ up to 1 M does not change the spectrum of DNA SDP, so that the competition between SRs and bicarbonate is most likely not an issue even at 0.3 M of bicarbonate, high ionic strength of reaction solutions might result in unexpected distortions of reaction mechanism, which is reflected by the decrease in all product yields with $[HCO_3^-]$, *i.e.* with the increase of ionic strength.

Logically, the next clarifying experiment would be the one on DNA concentration dependence. However, at this point it was decided that this method of generation of CRs appears to be inappropriate for the goal of HPLC detection of DNA SDP generated by CRs. Most likely, much lower concentrations of DNA would be required to suppress the reaction of DNA with SR, which cannot be afforded due to the limited HPLC sensitivity. High ionic strength is associated with a decreased binding of DNA with other reagents, which causes an additional problem. Finally, this experiment is overly labor-intensive. With all these considerations, further experiments on this method were halted.

Generation of CR by Photolysis of the Carbonatopentaaminecobalt(III) Complex

As it was concluded in the first two sections of this chapter, the previous two methods of CR generation are not suitable for our goal. The major problem with these methods is that in both of them the formation of competing ROS, hydroxyl radical in the first method and sulfate radical in the second method, does not allow for dissection of reactions of CRs with DNA sugar based on HPLC product analysis. The deficiencies of the previous two methods of CR generation are alleviated by the use of the method of photolysis of carbonatopentamminecobalt(III) perchlorate solution. As illustrated by Busset *et al.*[84], no other ROS are formed as the result of UV photolysis of carbonato-metal complexes except for the CR (Reaction 1.5, page 38). When exposed to light with wavelengths in the range of the charge transfer band ($\lambda < 350$ nm), the carbonato-cobalt complexes undergo inner sphere charge transfer from the bound carbonate ligand group to Co^{3+}, which is immediately followed by the formation of a free CR (Reaction 1.5, page 38).

Two carbonato-cobalt complexes were synthesized by our research group: carbonatotetramminecobalt(III) and carbonatopentamminecobalt(III) perchlorates. These carbonato-cobalt complexes were selected as the method of CR generation for the current work for a number of reasons: unpublished data of our research group shows that both of these complexes are suitably stable in phosphate buffered solutions of DNA (pH ~ 7) towards ligand exchange at room temperature over the time course needed to perform the experiments. Additionally, UV-Vis spectra show that binding between DNA and both of these complex cations is not observed and this substantiates the assumption that CR generated by these precursors are formed in the bulk of the solution and not in the vicinity of DNA. Both of these complexes demonstrate sufficiently strong absorption bands in the range of wavelengths from 300 nm to 350 nm when the complex is present in millimolar (~1-2 mM) concentrations. The absorption of light by DNA in this region is negligible, and this allows for selective production of CR via UV light, even in the presence of relatively high concentrations of DNA needed to increase the efficacy of CR trapping by the target. Lastly, the photodissociation of these carbonato-cobalt complexes has a great enough quantum yield to produce sufficient amounts of the desired DNA damage products for HPLC analysis after several minutes of illumination times with a 75 W Xe lamp. We used only the pentammine complex in our experiments of generation CRs.

The UV-Vis spectra of the pentammine complex in Figure 25 show the spectral changes observed from exposure of these carbonato-cobalt complexes to UV light in the presence of 5 mM DNA. The disappearance of the peak maximum at 510 nm, shows the time course of dissociation of the complex during illumination up to 12 min.

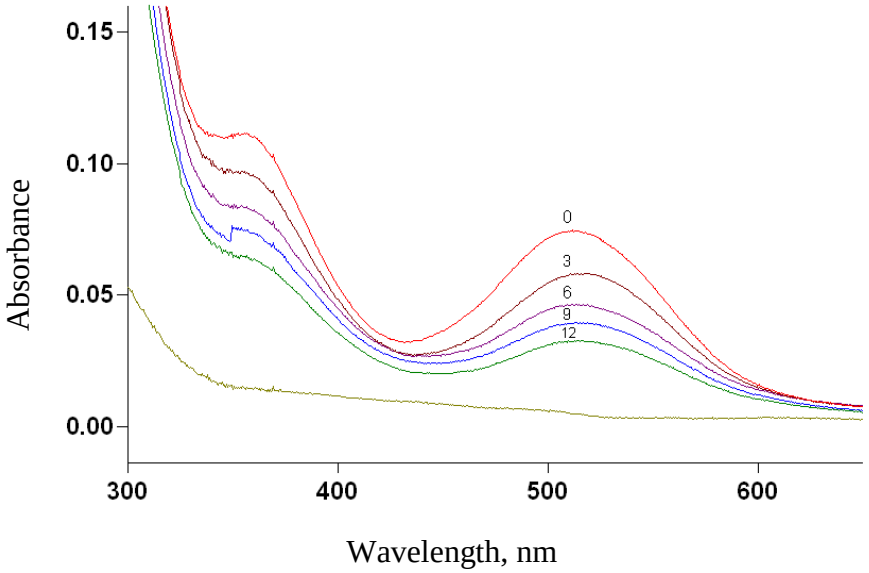

Figure 25: The absorption changes induced in the UV-Vis spectrum of $Co(NH_3)_5CO_3^+$ by photolysis in presence of 5 mM DNA. Numbers shown in the Figure are the exposure times in min.

Double-Stranded DNA

5MF, Fur, Lac, and FBR Analysis. 5 mM dsDNA solutions were prepared with 2 mM $[Co(NH_3)_5CO_3]^+ ClO_4^-$ in 10 mM phosphate buffer, pH 6.9 (all final concentrations). The resulting solutions were subjected to UV illumination via high-pressure Hg(Xe) lamp, and the resulting solutions were divided and treated with either 10 mM spermine or 200 mM glycine (final concentrations) in a 70 °C water bath. Post-illumination solutions were analyzed by the HPLC method previously discussed, and the areas of the resulting chromatographic peaks were integrated manually.

Representative chromatograms for all post-illumination treatments under these experimental conditions are shown in Figure 26 (next page). Each post-illumination treatment chromatogram is labeled with the four native DNA nucleobases, uracil (used as an internal standard), and the SDP that are formed via catalytic/heat treatment with the appropriate reagent. Control chromatograms (no illumination) display mostly the chromatographic peak for uracil.

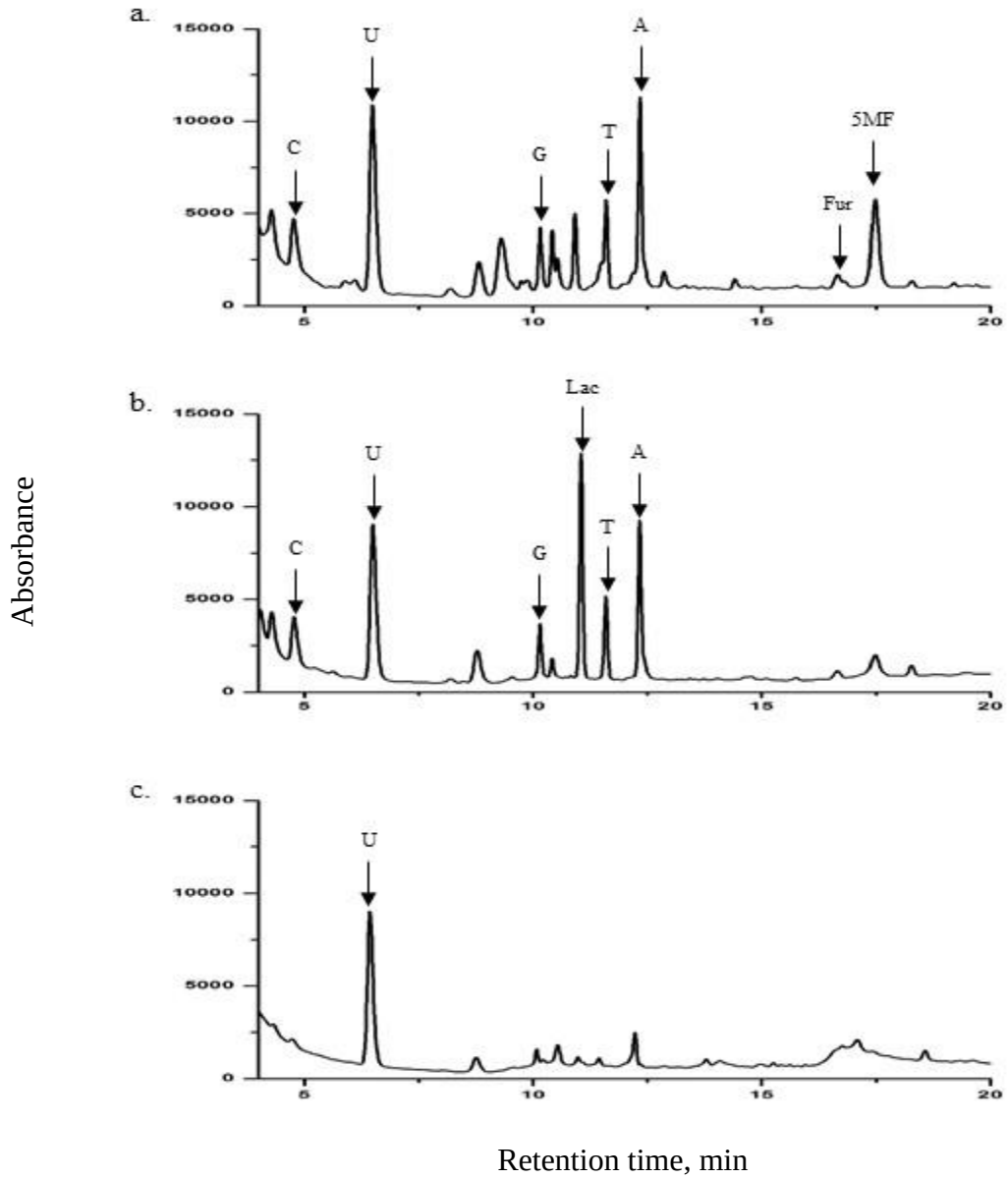

Figure 26: The representative chromatograms obtained from the photolysis of carbonatopentamminecobalt(III) perchlorate in the presence of 5 mM DNA: a) spermine treatment following 8 min illumination with Hg(Xe) lamp; b) glycine treatment following 8 min illumination with Hg(Xe) lamp; c) glycine treatment, no illumination (control). HPLC conditions: reversed phase, C18, equilibrated with 40 mM ammonium acetate, and application of a linear acetonitrile gradient from 0 to 16% acetonitrile over 15 min, flow rate 1 mL/min.

The areas obtained from integration were used to quantify the relative yields of each individual SDP, the total SDP, and individual and total FBR for the reaction solutions. Replicate experimental data (data of 3 or 4 independent experiments) were statistically analyzed, and the plots of the statistical analysis and linear regression data are shown in Figure 27, below, and Table 8 (p. 95), respectively.

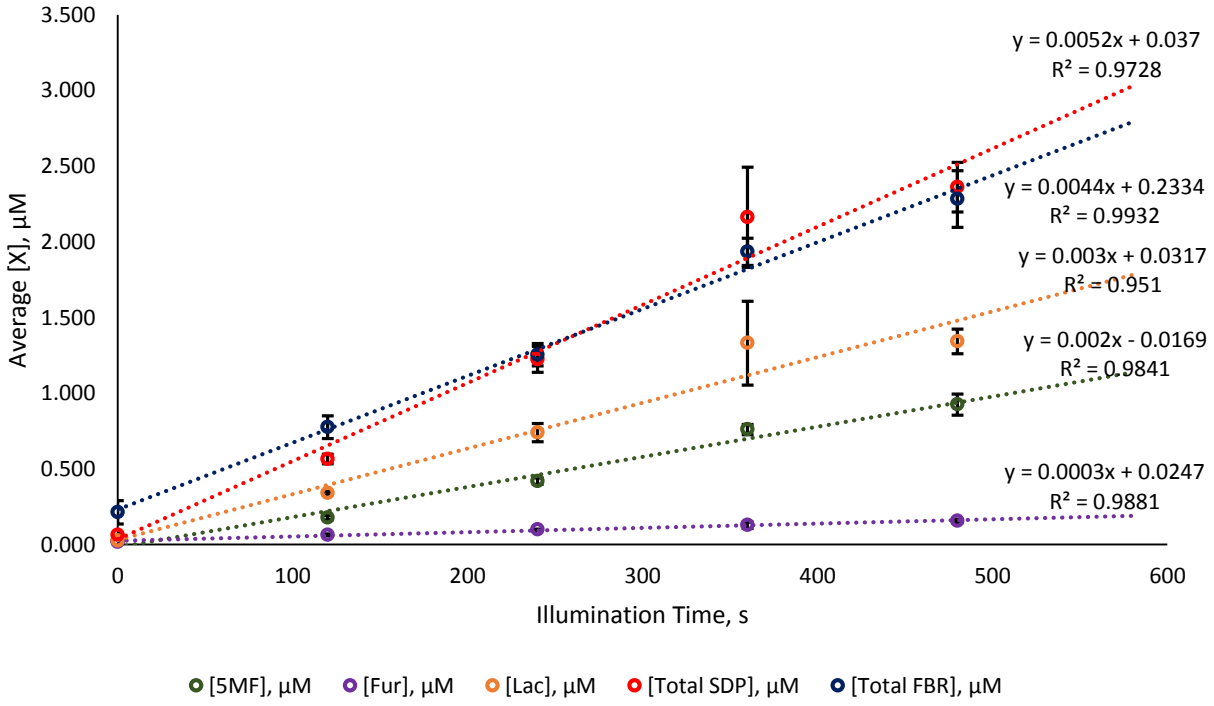

Figure 27. A plot of average product yields of individual SDP, total SDP, and total FBR obtained from photolysis of carbonatopentamminecobalt(III) perchlorate complex in the presence of 5 mM DNA as a function of illumination time.

dsDNA MDA HPLC Analysis. Separate MDA analysis was carried out to determine the contribution of MDA formation to the overall yield of SDP. Solutions of 5 mM DNA, 2 mM carbonatopentamminecobalt(III) perchlorate, in 10 mM phosphate buffer (pH 6.9) were prepared in accordance with previously discussed methodology, and the resulting samples were illuminated over a time course from 0 to 8 minutes. The resulting reaction mixtures were treated with an equal volume of saturated (0.67% w/v) solution of 2-thiobarbituric acid (TBA) and one tenth volume of 1 M HCl – in accordance with TBARS protocol – and the solutions were heated at 90°C for 15 minutes to generate the MDA-TBA adduct. Following heating, the reaction solutions were analyzed by HPLC to determine the yield of MDA.

Representative chromatograms for the MDA gradient elution are shown in Figure 28, below. Chromatograms were detected at 532 nm (the maximum absorbance of the MDA-TBA adduct) by two-lamp PDA, and integrated manually. Inspection of Figure 28 shows that MDA was present in the control (no illumination) samples. This is potentially due to the mildly oxidizing capacity of the Co^{3+} cation that can be generated in solution without photolysis of the carbonato-cobalt complex.

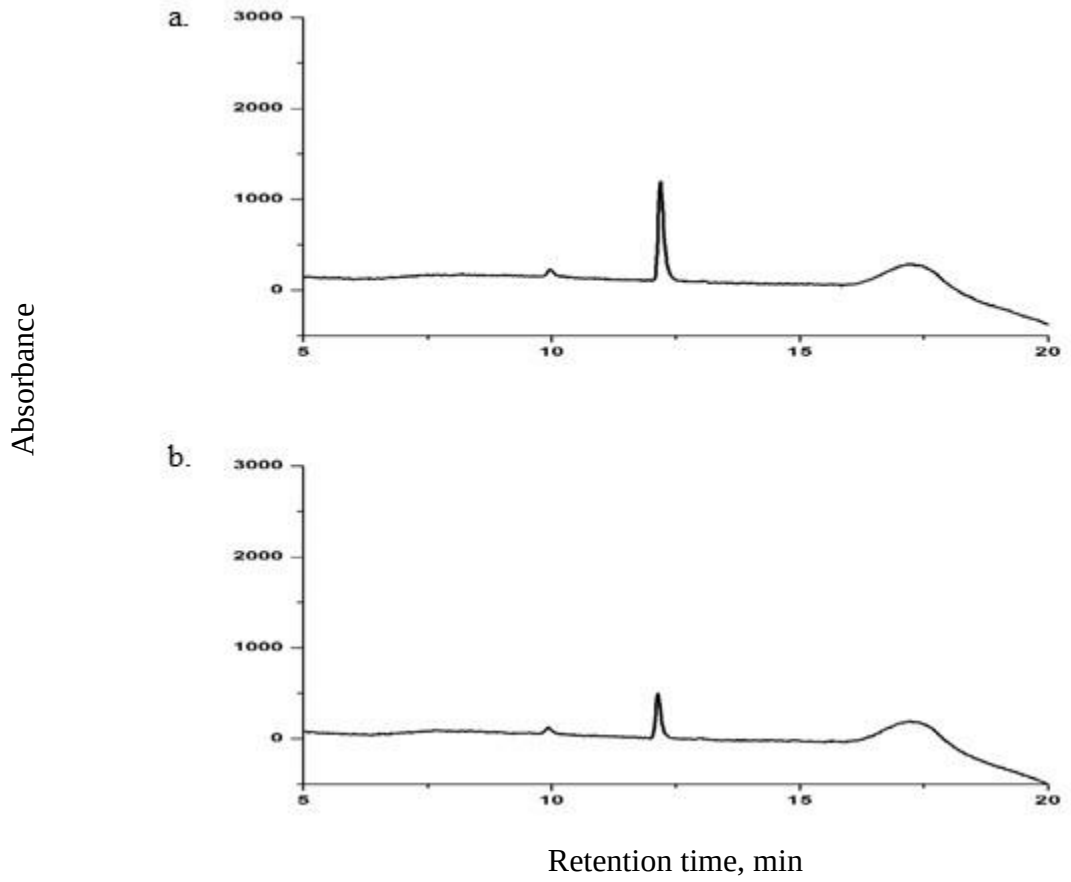

Figure 28: The representative chromatograms obtained from MDA analysis of dsDNA solutions; a) 240 s illumination; b) control (no illumination). HPLC conditions: reversed phase, C18 analytical column, equilibrated with 40 mM ammonium acetate, with a linear gradient from 12 to 24% acetonitrile over 10 min and a flow rate of 1 mL/min.

Multiple sets of data were statistically analyzed, and the resulting plot is found in Figure 29. Figure 29 is the result of two differing time courses for illumination, as the first few experimental data sets showed saturation in the upper time limits. An abbreviated time course was performed, and the slopes of the extended and abbreviated time courses agreed reasonably

well with each other. The resulting data were plotted on one graph, and error bars for replicate measurements have been included.

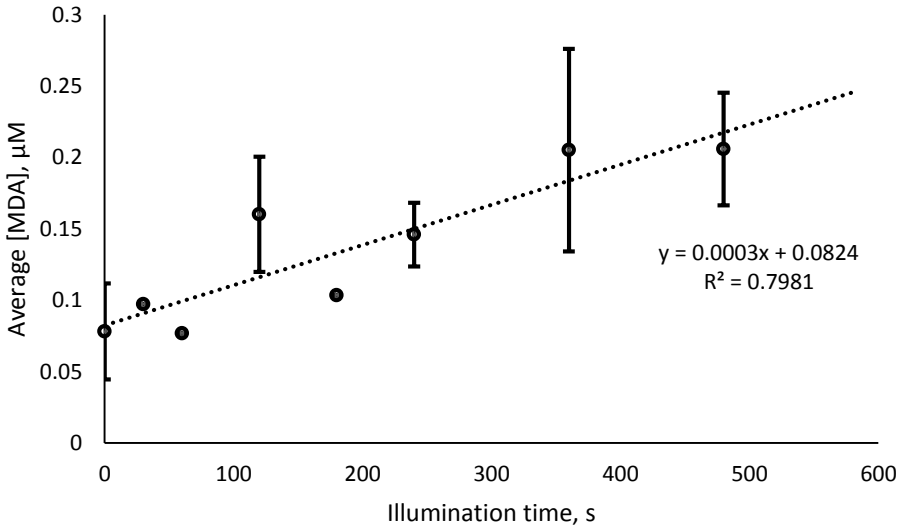

Figure 29: A plot of MDA concentration as a function of illumination time in solutions of 5 mM dsDNA and 2 mM $[Co(NH_3)_5CO_3]^+ClO_4^-$ in 10 mM phosphate buffer, pH 6.9

MDA Analysis Using N-Butanol Extraction. The MDA pathway has been estimated to contribute as much as one-third of all C4´ damage by hydroxyl radicals in DNA solutions[17], but the determined yields in these experiments were exceptionally low. In order to confirm the magnitude of these yields, a liquid-liquid extraction of MDA with n-butanol was performed as a confirmatory test. In order to spectroscopically determine the concentration of MDA present, the molar absorptivity coefficient in n-butanol was calculated using a series of standards of known concentration. The quantity of MDA-TBA adduct was determined in an aqueous solution using the previously determined molar absorptivity coefficient for the adduct in water (1.56×10^5 M^{-1}

cm^{-1})[108], and then the samples of known concentration were extracted into n-butanol. The resulting aqueous and organic layers were measured using Cary 100 UV-vis spectrophotometer, and the molar absorptivity coefficient of the MDA-TBA adduct in n-butanol was calculated by the difference between the known concentrations and the resulting aqueous and organic layers. The resulting slope of the regression line (Figure 30) was taken to be the new n-butanol molar absorptivity coefficient, or 1.78 x 10^5 M^{-1} cm^{-1}.

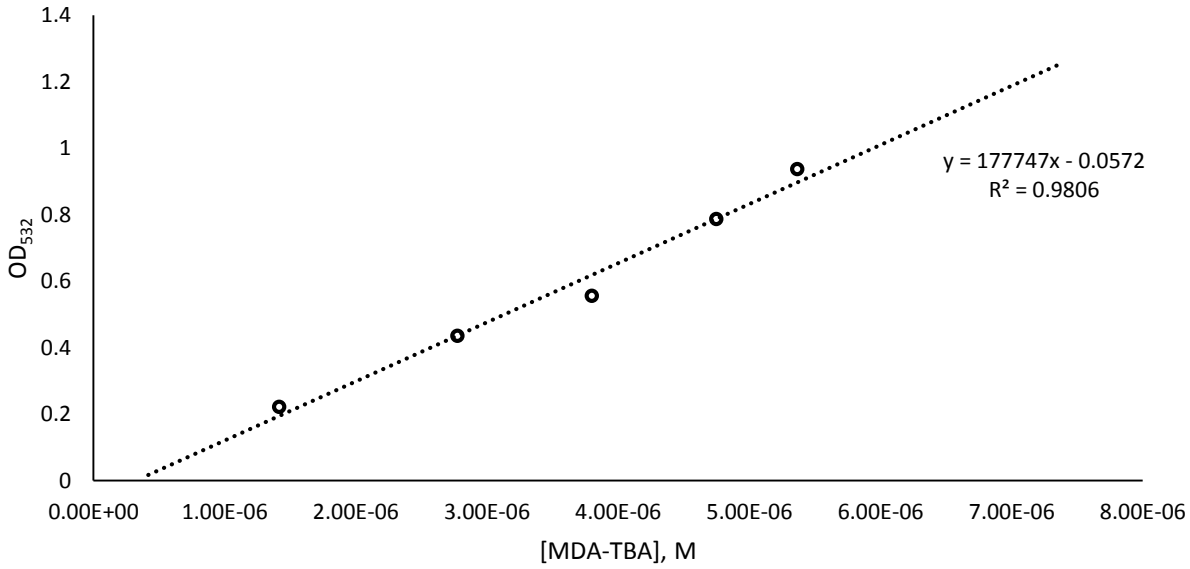

Figure 30: The determination of the molar absorptivity coefficient of the MDA-TBA adduct in n-butanol

Once this value was calculated, a confirmatory set of samples of double-stranded DNA and carbonatopentamminecobalt(III) perchlorate were prepared, and the MDA-TBA adduct concentration was determined for each sample following 0, 30, and 180 s illuminations. The resulting [MDA-TBA] was on the order of 0.06-0.11 μM in these samples, in agreement with the

data in Figure 29 (p. 93). Therefore, the low yield of MDA produced in the reaction of DNA with CRs has been confirmed.

Discussion of Results. All the data sets for SDP, MDA, and FBR were compiled, and the results of these experiments are summarized in Table 8, below. The values for slopes are equivalent to the rates of accumulation of the specified SDP (in units of $\mu M\ s^{-1}$), and the relative yield of each SDP is calculated as the ratio of the rate of accumulation of the product of interest to the rate of accumulation of total FBR, where total FBR is assumed to be 100%.

Linear regression analysis was applied to the resulting mean data in the Figure 27 plot (p. 90), and the ratios of the slopes of individual SDPs and total SDP to the slopes of the total FBR were calculated to determine relative product yields for all individual SDPs and total SDP.

Table 8: The Relative Yields of Individual SDP, Total SDP, and Total FBR in the Carbonatopentamminecobalt(III) Perchlorate System for dsDNA

SDP	Slope (μM/s)	Relative % Yield‡
5MF	0.0020	45%
Lac	0.0030	68%
Fur	0.0003	7%
MDA	0.0003	7%
Total SDP	0.0056	127%
Total FBR	0.0044	100%

‡Ratio of the rate of accumulation of the SDP to the total FBR

These data show an overall C4′preference (of which Lac and MDA are characteristic products) in the photolyzed carbonatopentamminecobalt(III) perchlorate system, and the trend follows C4′ > C1′ >> C5′. The preferential order for hydrogen abstraction by CR matches that for HO•. However, the actual yields of the products – and thus the contribution of each pathway – are quite different than reported by our research group for HO•[17]. The ratio of the contribution of the C4′ pathway (as measured by Lac + MDA) to the C1′ pathway (as measured by 5MF) the decreases from ~1.9 for the HO• damage[17] to ~1.7 for the CR damage (present work). This decrease may be explained by a greater selectivity of CR as a hydrogen abstractor and hence by a more significant contribution of the thermodynamic control to the hydrogen abstraction kinetic process. This results in a preferential formation of a more stable C1′ radical in the case of CR chemistry (thermodynamic control) rather than preferential abstraction of more surface accessible C4′ and C5′ hydrogen in the case of the HO• chemistry (kinetic control). This model also explains very low yields of Fur (the C5′ chemistry product) in the reaction of CR with DNA as compared to the reaction of HO•.

Interestingly, very low yields of MDA were observed in the present experiments. The yield of MDA in the present work comprises only 10% of the yield of Lac, while in the reaction of HO• with DNA sugar the contribution of MDA was much more significant: ~1/2 of the yield of Lac. At first glance, this is a paradox since both products are believed to stem from the same parent intermediate, C4′-OAS (see Figure 5, page 26). In this case, one should not expect any difference in the Lac-to-MDA ratio between the carbonate and hydroxyl radicals, since different hydrogen abstracting selectivity of these two ROS would affect only the yield of C4′-OAS but not its further transformations. A likely explanation for the low relative yield of MDA in the carbonatopentamminecobalt(III) solution is that cobalt(III) in the complex is a mild oxidant

capable of oxidizing a C4′ radical into a carbocation (the left part of the scheme in Figure 5). As a result, the pathway culminating in the C4′-OAS formation dominates (the left part in Figure 5) over the MDA pathway (the right part in Figure 5).

There is an appreciable imbalance between the FBR and total SDP yields, which leads to an inflated value for total SDP of an unrealistic 127% in Table 8 (p. 95). This is most probably the result of base modification reactions occurring in the reaction solution. Since the methodology relies heavily on free unaltered base release to quantify the product yields, the oxidation of these bases (most likely guanine to 8oxoG and its further oxidation products) can artificially deflate the total amount of FBR present in the solution, and the combinative effect on total SDP is that the yield of sugar damage products is greater than 100%.

It is very important to compare the rate of reactions of CRs with guanine reported by Shafirovich with the cumulative rate of reactions of these species with DNA sugar. While base damage by CRs have been extensively studied by the Shafirovich research group, this is the first time that DNA sugar damage by CRs has been analyzed, and the comparison of rates is necessary for further understanding of the mechanistic effect of CR-mediated oxidative damage to DNA.

The Roginskaya research group (Roginskaya M, Ampadu-Boateng, D, and Razskazovskiy, Y, unpublished data) has estimated the initial rate (during the first 10 s) of accumulation of 8oxoG, a key indicator of guanine damage, to be ~ 4.5 μM/s (Figure 31). The determination of 8oxoG yields was accomplished using the method of complete DNA hydrolysis in hot (150°C) 88% formic acid for 90 min following lyophilization and reconstitution of the precipitate in an HPLC buffer[117]. It can be seen from Figure 31 that the kinetics of 8oxoG

reaches the steady-state regime very fast, after ~ 20 s of beginning of the reaction. The sigmoid shape of 8oxoG accumulation as a result of one-electron oxidation of guanine in native DNA is in agreement with the findings of Derrick Ampadu-Boateng[117]. Further discussions about these findings are beyond the scope of the present work.

The rate of accumulation for all SDP was found to be ~ 5.6 nM/s (this work). It can be estimated from comparison of the rates of formation of 8oxoG and total SDP (as a sum of all major SDP) that guanine damage is the most predominant oxidative insult to DNA by CRs. The ratio of ~ 800 indicates that CR has a ~ 3 orders of magnitude greater preference to oxidize guanine than to abstract hydrogen from DNA sugar. This trend is in agreement with the property of CR as a potent oxidant and a weak, selective hydrogen abstractor.

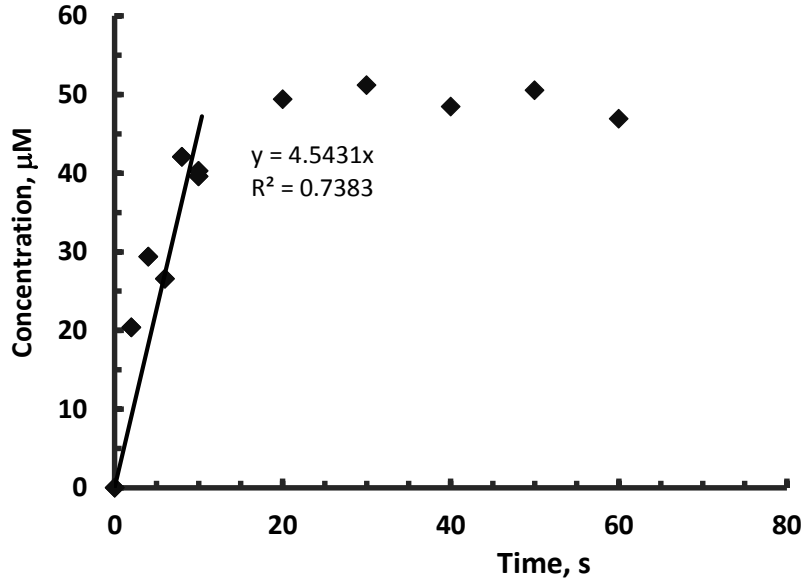

Figure 31: The initial rate of accumulation of 8oxoG formed by CR attack as a function of illumination time

Single-Stranded DNA

The rationale for studying the product yields of DNA sugar damage by CRs in solutions of ssDNA (also known as denatured DNA) is based on the idea that once the DNA double helix is thermally denatured, there is a drastic increase of solvent accessibility to previously inaccessible sites – such as the C1′ site which is deeply buried in the minor groove of dsDNA (B-form). As a result, the relative yield of 5MF, the staple product of the C1′ pathway is expected to increase significantly. This approach has already been successfully used by our research group for DNA sugar damage by hydroxyl radicals[14,17].

DNA (10 mM in bases in 10 mM phosphate buffer, pH 6.9),was thermally denatured as described in Chapter 2 and then used instead of 10 mM dsDNA stock solutions for preparing the reaction mixture containing 5 mM ssDNA and 2 mM carbonatopentamminecobalt(III) perchlorate. Illumination of samples, subsequent post-illumination treatment, and HPLC analysis were conducted in the same way as with dsDNA.

Representative chromatograms for all post-illumination treatments under these experimental conditions are shown in Figure 32. Each chromatogram is labeled with the four native DNA nucleobases, uracil, and the SDP that are formed via catalytic/heat treatment with the appropriate reagent. Control chromatogram (no illumination) displays only the chromatographic peak for uracil.

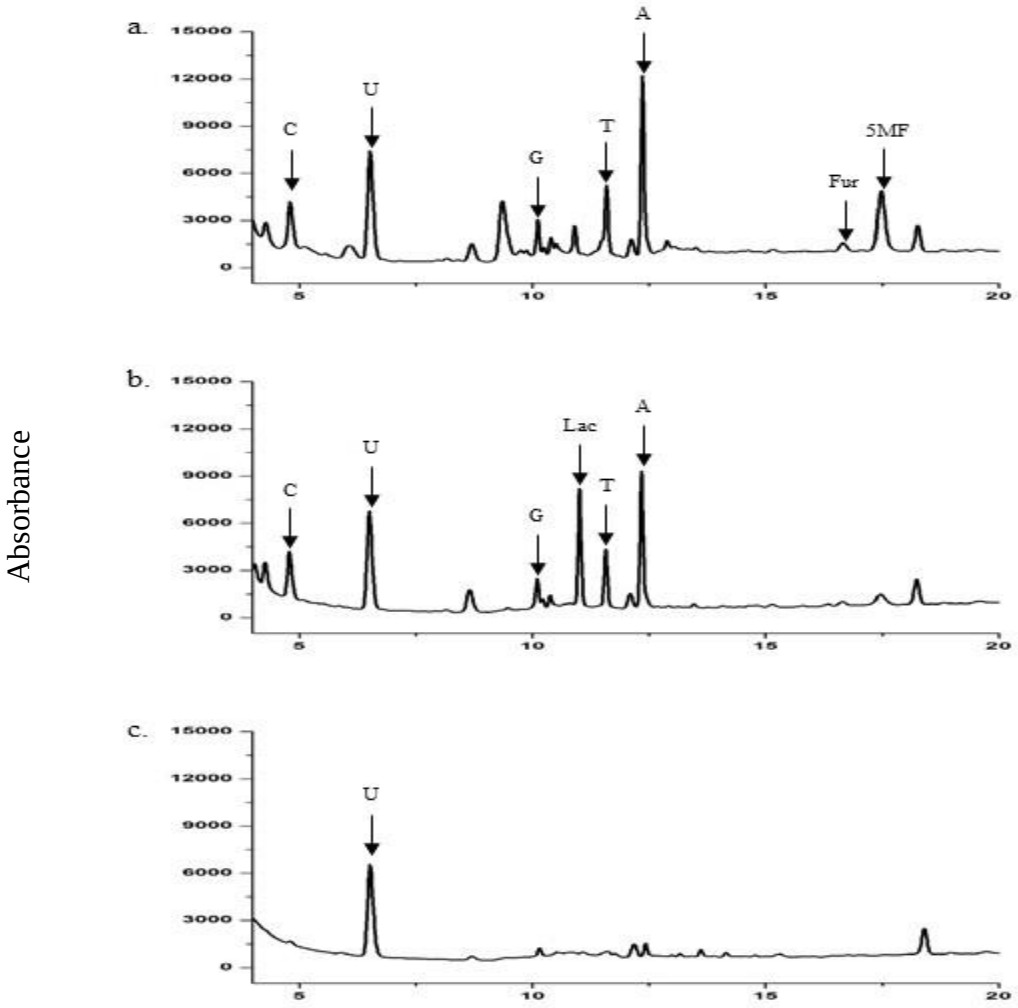

Figure 32: The representative chromatograms obtained from the photolysis of carbonatopentamminecobalt(III) perchlorate in the presence of 5 mM ssDNA: a) spermine treatment following 8 min of illumination with Hg(Xe) lamp; b) glycine treatment following 8 min of illumination with Hg(Xe) lamp; c) glycine treatment, no illumination (control).

Chromatographic peaks were integrated manually to yield areas, and the resulting areas were converted into product concentrations using previously described methods. Replicate sets of experiments (3 or 6 sets of experiments) were conducted, and the resulting data were statistically analyzed to yield the plot shown in Figure 33.

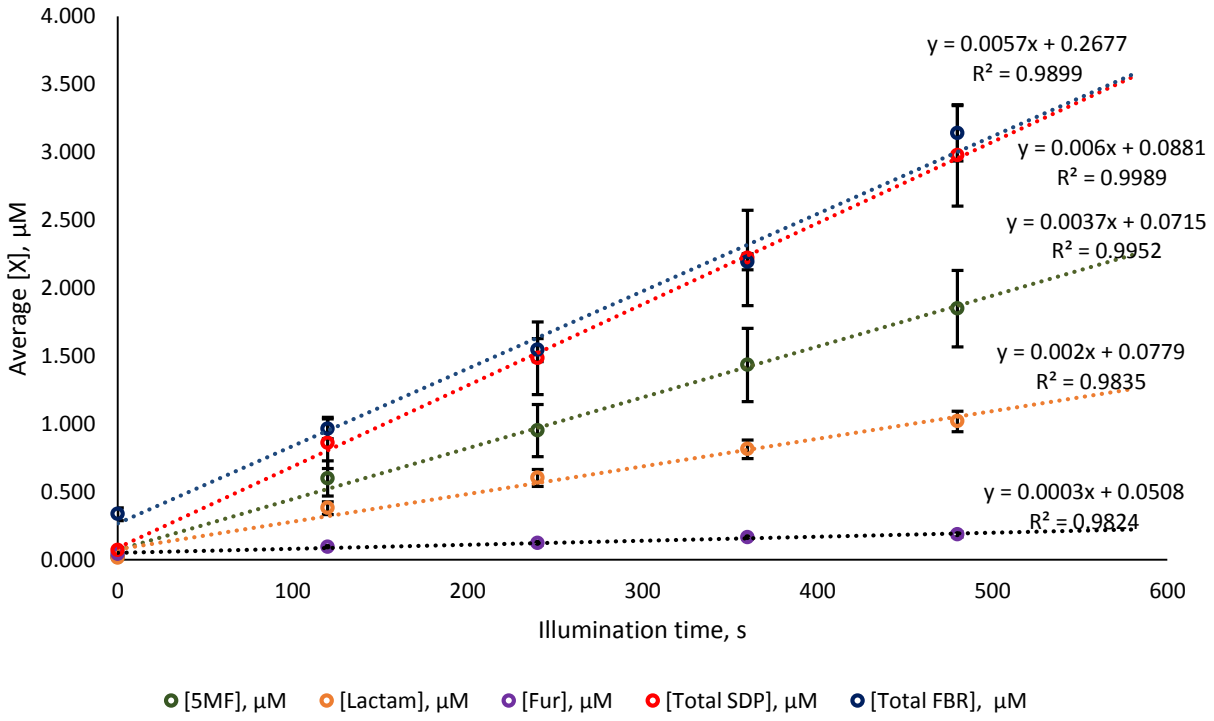

Figure 33: A plot of average product yields of individual SDP, total SDP, and total FBR obtained through photolysis of carbonatopentamminecobalt(III) perchlorate complex in the presence of 5 mM ssDNA as a function of illumination time

Comparison of Figures 27 (p. 90) and 33 shows that, contrary to dsDNA, in ssDNA the production of 5MF by CRs significantly surpasses the production of Lac. The same pattern was

observed earlier for hydroxyl radicals[17]. Linear regression analysis was applied to the resulting average data in the Figure 33 plot, and the ratios of the slopes of individual SDPs and total SDP to the slopes of the total FBR were calculated to determine relative product yields for all individual SDPs and total SDP. These data are presented in Table 9.

ssDNA MDA HPLC Analysis. Separate MDA analysis was carried out to determine the contribution of MDA formation to the overall yield of SDP. Solutions of 5 mM ssDNA, 2 mM carbonatopentamminecobalt(III) perchlorate in 10 mM phosphate buffer, pH 6.9 were prepared in accordance with previously discussed methodology, and the resulting reaction mixtures were analyzed by HPLC to determine the yield of MDA.

The peak for adduct was detected at 532 nm by two-lamp PDA, and integrated manually. Chromatograms obtained for the MDA-TBA adduct in the ssDNA system closely match those obtained using dsDNA shown in Figure 28 (p. 92). Replicate sets of data were analyzed statistically, and the resulting plot of these repeated measurements is found in Figure 34.

Table 9: The Relative Yields of Individual SDP, Total SDP, and Total FBR in the Carbonatopentamminecobalt(III) Perchlorate System for ssDNA

SDP	Slope (μM/s)	Relative % Yield‡
5MF	0.0037	65%
Lac	0.0020	35%
Fur	0.0003	5%
MDA	0.0002	4%
Total SDP	0.0062	109%
Total FBR	0.0057	100%

‡Ratio of the rates of accumulation for each SDP compared to Total FBR

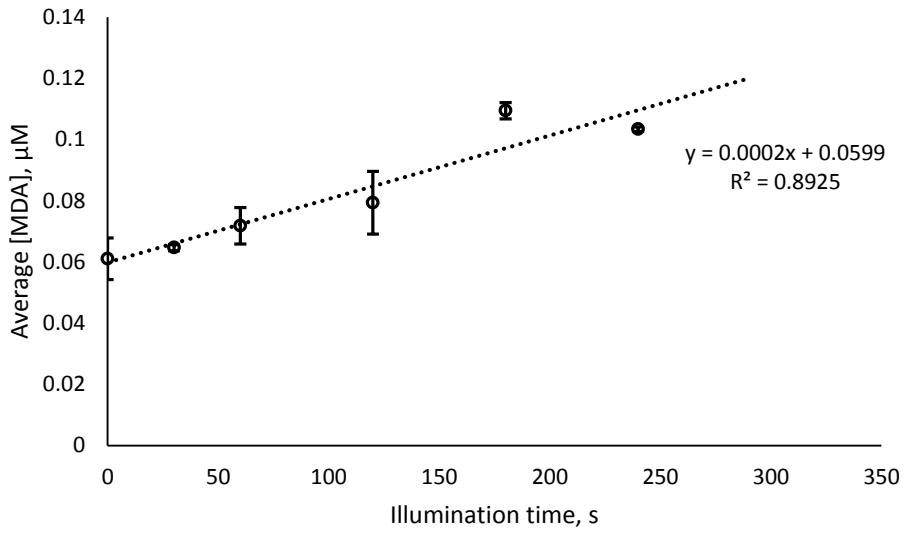

Figure 34: The concentration of MDA as a function of illumination time in solutions of 5 mM ssDNA, 2 mM $[Co(NH_5)_3CO_3]^+ClO_4^-$ in 10 mM phosphate buffer, pH 6.9

ssDNA Results. All the data sets for SDP, MDA, and FBR were compiled, and the results of these experiments are summarized in Table 9, above. The values for slopes are equivalent to the rates of accumulation of the specified SDP (in units of µM s^{-1}), and the relative yield of each SDP is calculated as the ratio of the rate of accumulation of the product of interest to the rate of accumulation of total FBR, where total FBR is assumed to be 100%.

The hydrogen abstraction preferential order in ssDNA solutions follows the trend C1′ > C4′ >> C5′. The increased dominance of the C1′-pathway at the expense of the C4′-pathway is attributed to the increase in solvent accessibility of the C1′-hydrogen in thermally denatured DNA. For ssDNA, there is a closer balance between total SDP and total FBR (127% of SDP for

dsDNA and 109% of SDP for ssDNA). Interestingly, for hydroxyl radical-mediated damage of DNA sugar, denaturation of DNA also resulted in a close to 100% balance between SDP and FBR[17]. This likely indicates that elimination of steric hindrances in ssDNA allows all DNA sites to exhibit their 'true' reactivity towards a given ROS.

CHAPTER 4

CONCLUSIONS

Interest in the CR as an emerging ROS in biology and chemistry of oxidative stress has been recently dramatically increased due to numerous findings during the last 10-15 years which shed light on the great significance of this free radical oxidizing intermediate in physiological processes and, in particular, in DNA damage during oxidative stress. While the reactions between CR and DNA nucleobases have been extensively studied, the reactivity of this ROS toward DNA 2′-deoxyribose has never been reported. From the experimental data collection described in Chapter 3, the following conclusions have been made:

1. The present work has demonstrated for the first time that CRs abstract hydrogens from DNA 2′-deoxyribose. These reactions have never been reported before, though they could be predicted based on analogous reactions of CRs with other sugars such as glucose[92,93,95] and glycosaminoglycans[90,91], with the bimolecular reaction rate constants in the order of $10^4 – 10^5\ M^{-1}\ s^1$ [92,95].

2. While the general trend for CR-mediated hydrogen abstraction from DNA 2′-deoxyribose mirrors the observed trend for HO$^\bullet$ (C4′ > C1′ > C5′), the actual ratios of product yields differ for CR as compared to HO$^\bullet$, which is indicative of a difference in hydrogen abstracting selectivity between these two ROS. The relative contribution of pathways of

hydrogen abstraction from DNA 2′-deoxyribose for CRs is: C1′, 36%; C4′, 59%, and C5′, 5% (present work), while for HO• it is C1′, 22%; C4′, 62%; and C5′, 16% [17]. So, while there is no essential difference in the relative contribution of the C4′ pathway, in CR-mediated DNA sugar damage there is a pronounced increase of the C1′ pathway by the expense of the C5′ pathway as compared to the HO•-mediated damage. Because of the lack of resonance stabilization in HO•, the hydroxyl radical is a more indiscriminate hydrogen abstractor, while CR is a more selective hydrogen abstractor due to resonance stabilization. As a result, CR tends to abstract hydrogen from the weakest C-H bond of DNA 2′-deoxyribose (at C1′), so that the most stable 2′-deoxyribosyl radical is formed, as opposed to the tendency of HO• to abstract hydrogen from the most solvent-accessible position in 2′-deoxyribose (at C5′). Thus in CR-mediated DNA 2′-deoxyribose damage, the C5′ pathway is suppressed, and the C1′ pathway is stimulated because accessibility is no longer the most important factor while the stability of a 2′-deoxyribosyl radical becomes more significant.

3. Three techniques of CR generation have been tested in the present work to find the most adequate system for use in our HPLC-based methods of analysis of low-molecular products of DNA damage: X-irradiation of bicarbonate solutions, photolysis of persulfate/bicarbonate solutions, and photolysis of carbonatopentamminecobalt(III) complexes. Of the three techniques evaluated only in the latter method no ROS capable of competing with CR were produced, which provided unequivocal certainty that observed DNA sugar damage is inferred by CRs. Therefore, photolysis of

carbonatopentamminecobalt(III) complexes has been chosen as the optimal method of CR generation in the present work.

4. It has been found that in the reaction of CR with DNA, the initial rate of accumulation of 8oxoG, a key product of guanine oxidation, exceeds the rate of accumulation of total sugar damage products by a factor of ~ 800. Since 8oxoG is one of the major, but not the only product of guanine oxidation, this ratio can be interpreted as a lower limit of the branching ratio of two competing processes in the reaction of CR with DNA: a one-electron oxidation of guanines and hydrogen abstraction from DNA sugar. This ~ 800-fold preference of CR for guanines in DNA over DNA sugar as compared to only 2-fold preference of hydroxyl radicals[11] is not surprising taking into account an essential difference in the rate constants of the hydrogen abstraction reactions of CR and HO•.

To summarize, it has been demonstrated for the first time that CRs react with 2′-deoxyribose via hydrogen abstraction reactions at the C1′, C4′, and C5′ positions. The ratio of rates of accumulation of 8oxoG and rates of accumulation of products of damage to 2′-deoxyribose has been estimated as ~800. These finding are in line with the hypothesis that CR is a potent one-electron oxidant and a weak, selective hydrogen abstractor.

REFERENCES

1. Valko, M. M., H.; Cronin, M. T. D. *Curr. Med. Chem.* **2005**, *12*, 1161-1208.
2. Cadet, J. D., T.; Pouget, J. P.; Ravanat, J. L.; Sauvaigo, S. *Curr. Probl. Dermatol.* **2001**, *29*, 62-73.
3. Cook, J. A.; Gius, D.; Wink, D. A.; Krishna, M. C.; Russo, A.; Mitchell, J. B. *Semin. Radiat. Oncol.* **2004**, *14*, 259-266.
4. Schmidt-Ullrich, R. K.; Dent, P.; Grant, S.; Mikkelsen, R. B.; Valerie, K. *Radiat. Res.* **2000**, *153*, 245-257.
5. Shirley, R. O., E. N. J.; Work, L. *Antioxidants* **2014**, *3*, 472-501.
6. Toyokuni, S. O., K.; Yodoi, J.; Hiai, H. *FEBS Lett.* **1995**, *358*, 1-3.
7. Gil-Mohapel, J.; Brocardo, P. S.; Christie, B. R. *Curr. Drug Targets* **2014**, *15*, 454-468.
8. Xing, S. S., D.; Chen, C.; Wang, J.; Yu, Z. *Mol. Med. Rep.* **2014**, *10*, 599-604.
9. Aoshiba, K. Z., F.; Tsuji, T.; Nagai, A. *Eur. Respir. J.* **2012**, *39*, 1368-1376.
10. Ishii, T.; Yasuda, K.; Akatsuka, A.; Hino, O.; Hartman, P. S.; Ishii, N. *Cancer Res.* **2005**, *65*, 203-209.
11. Xu, Y. J.; Kim, E. Y.; Demple, B. *J. Biol. Chem.* **1998**, *273*, 28837-28844.
12. Pogozelski, W. K.; Tullius, T. D. *Chem. Rev.* **1998**, *98*, 1089-1107.
13. Colson, A.-O.; Sevilla, M. D. *J. Phys. Chem.* **1995**, *99*, 3867-74.
14. Price, C. S.; Razskazovskiy, Y.; Bernhard, W. A. *Radiat. Res.* **2010**, *174*, 645-649.
15. Roginskaya, M.; Razskazovskiy, Y.; Bernhard, W. A. *Angew. Chem. Int. Ed. (English)* **2005**, *44*, 6210-6213.

16. Roginskaya, M.; Bernhard, W. A.; Marion, R. T.; Razskazovskiy, Y. *Radiat. Res.* **2005**, *163*, 85-89.

17. Roginskaya, M.; Mohseni, R.; Moore, T. J.; Bernhard, W. A.; Razskazovskiy, Y. *Radiat. Res.* **2014**, *181*, 131-137.

18. Roginskaya, M. *Oxidative Damage to DNA by Ionizing Radiation: Chemical Pathways and Radioprotection*; Ph. D. Dissertation, University of Rochester: Rochester, NY, 2006, pp 231.

19. Miaskiewicz, K.; Osman, R. *J. Am. Chem. Soc.* **1994**, *116*, 232-238.

20. von Sonntag, C.; Hagen, U.; Schon-Bopp, A.; Schulte-Frohlinde, D. *Adv. in Rad. Biol.* **1981**, *9*, 109-142.

21. Stelter, L.; von Sonntag, C.; Schulte-Frohlinde, D. *Int. J. Radiat. Biol.* **1974**, *25*, 515.

22. Behrens, G.; Koltzenburg, G.; Ritler, A. *Int. J. Radiat. Biol.* **1978**, *33*, 163.

23. Giese, B.; Burger, J.; Kang, T. W.; Kesselheim, C.; Wittmer, T. *J. Am. Chem. Soc.* **1992**, *114*.

24. von Sonntag, C. *The Chemical Basis of Radiation Biology*; Taylor & Francis: London–New York–Philadelphia, 1987.

25. Balasubramanian, B.; Pogozelski, W. K.; Tullius, T. D. *Proc. Natl. Acad. Sci. U.S.A.* **1998**, *95(17)*, 9738-43.

26. Dizdaroglu, M.; von Sonntag, C.; Schulte-Frohlinde, D. *J. Am. Chem. Soc.* **1975**, *97*, 2277-2228.

27. Dizdaroglu, M.; von Sonntag, C.; Schulte-Frohlinde, D. *Z. Naturforsch C* **1975**, *30*, 826-828.

28. Regulus, P.; Duroux, B.; Bayle, P. A.; Favier, A.; Cadet, J.; Ravanat, J. L. *Proc. Natl. Acad. Sci. U.S.A.* **2007**, *104*, 14037-14037.

29. Sczepanski, J. T.; Jacobs, A. C.; Majumdar, A.; Greenberg, M. M. *J. Am. Chem. Soc.* **2009**, *131*.

30. Sczepanski, J. T.; Hiemstra, C. N.; Greenberg, M. M. *Bioorg. Med. Chem.* **2011**, *19*.

31. Greenberg, M. M.; Weledji, Y. N.; Kim, J.; Bales, B. C. *Biochemistry* **2004**, *43*, 8178-8183.

32. Jacobs, A. C.; Kreller, C. R. *Biochemistry* **2011**, *50*, 136-143.

33. Dhar, S.; Kodama, T.; Greenberg, M. M. *J. Am. Chem. Soc.* **2007**, *129*, 8702-8703.

34. Chen, B.; Zhou, X.; Taghizadeh, K.; Chen, J.; Strubbe, J. A.; Dedon, P. C. *Chem. Res. Toxicol.* **2007**, *20*, 1701-1708.

35. Giera, M.; Lingeman, H.; Niessen, W. M. A. *Chromatographia* **2012**, *75*, 433-440.

36. von Sonntag, C.; Rashid, R.; Langfinder, D.; Wagner, R.; Schuchmann, H.-P. *Int. J. Radiat. Biol.* **1999**, *75*, 101-109.

37. Nair, V.; Turner, G. A. *Lipids* **1984**, *19*, 804-805.

38. Marnett, L. J.; Niedernhofer, L. J.; Daniels, J. S.; Rouzer, C. A.; Greene, R. E. *J. Biol. Chem.* **2003**, *278*, 31426-31433.

39. Del Rio, D.; Stewart, A. J.; Pellegrini, N. *Nutr. Metab. Cardiovasc. Dis.* **2005**, *15*, 316-328.

40. Nair, V.; Cooper, C. S.; Vietti, D. E.; Turner, G. A. *Lipids* **1986**, *21*, 6-10.

41. Crespo-Hernandez, C. E.; Close, D. M.; Gorb, L.; Leszczynski, J. *J. Phys. Chem.* **2007**, *111*, 5386-5395.

42. Fukuzumi, K.; Miyao, H.; Ohkubo, K.; Suenobu, T. *J. Phys. Chem. A.* **2005**, *109*, 3285-3294.

43. Steenken, S. *Free Radic. Res. Commun.* **1992**, *16*, 349-379.

44. Reynisson, J.; Steenken, S. *Phys. Chem. Chem. Phys.* **2002**, *4*, 5346-5352.

45. Close, D. M. *J. Phys. Chem. A* **2013**, *117*, 473-480.

46. Shafirovich, V.; Dourandin, A.; Huang, W.; Geacintov, N. E. *J. Biol. Chem.* **2001**, *276*, 24261-24626.

47. Close, D. M.; Nelson, W. H.; Bernhard, W. A. *J. Phys. Chem. A* **2013**, *117*, 12608-12615.

48. Wang, W.; Razskazovskii, Y.; Sevilla, M. D. *Int. J. Radiat. Biol.* **1997**, *71*, 387-399.

49. Cai, Z.; Sevilla, M. D. *Radiat. Res.* **2003**, *159*, 411-419.

50. Saito, I.; Nakamura, T.; Nakatani, K.; Yoshioka, Y.; Yamaguchi, K.; Sugiyama, H. *J. Am. Chem. Soc.* **1998**, *120*, 12686-12687.

51. Cadet, J.; Douki, T.; Gasparutto, D.; J-L., R. *Mutat. Res.* **2003**, *531*.

52. Douki, T.; Martini, R.; Ravanat, J.-L.; Turesky, R. J.; Cadet, J. *Carcinogenesis* **1997**, *18*, 2385-2391.

53. Rokhlenko, Y.; Geacintov, N. E.; Shafirovich, V. *J. Am. Chem. Soc.* **2012**, *134*, 4955-4962.

54. Burrows, C. J.; Muller, J. G. *Chem. Rev.* **1998**, *98*, 1109-1151.

55. Cullis, P. M.; Malone, M. E.; Merson-Davies, L. A. *J. Am. Chem. Soc.* **1996**, *118*, 2775-2781.

56. Doddridge, A. Z.; Cullis, P. M.; Jones, G. D. D.; Malone, M. E. *J. Am. Chem. Soc.* **1998**, *120*, 10998-10999.

57. Asami, S.; Hirano, T.; Yamaguchi, R.; Tomioka, Y.; Itoh, H.; Kasai, H. *Cancer Res.* **1996**, *56*, 2546-2549.

58. Kiyosawa, H.; Suko, M.; Okudiara, H.; Murata , K.; Miyamoto, T.; Chung, M. H.; Kasai, H.; Nishimura, S. *Free Radic. Res. Commun.* **1990**, *11*, 23-27.

59. Jackson, J. H.; Schraufstatter, I. U.; Hyslop, P. A.; Vosbeck, K.; Sauerheber, R.; Weitzman, S. A.; Cochrane, C. G. *J. Clin. Invest.* **1987**, *80*, 1090-1095.

60. Chen, Q.; Marsh, J.; Ames, B.; Mossman, B. *Carcinogenesis* **1996**, *17*, 2525-2527.

61. Valavandis, A.; Vlachogianni, T. *J. Environ. Sci. Health., Part C.* **2009**, *27*, 120-139.

62. Pope III, C. A.; Burnett, R. T.; Thun, M. J.; Calle, E. E.; Krewski, D.; Ito, K.; Thurston, G. D. *JAMA-J. Am. Med. Assoc.* **2002**, *287*, 1132-1141.

63. Kasprzak, K. S. *Free Radic. Biol. Med.* **2002**, *32*, 958-967.

64. Marczynski, B.; Preuss, R.; Mensing, T.; Angerer, J.; Seidel, A.; El Mourabit, A.; Wilhem, M.; Bruning, T. *Int. Arch. Occup. Environ. Health* **2005**, *78*, 97-108.

65. Marczynski, B.; Rihs, H.-P.; Rossbach, B.; Holzer, J.; Angerer, J.; Scherenberg, M.; Hoffman, G.; Bruning, T.; Wilhelm, M. *Carcinogenesis* **2002**, *23*, 273-281.

66. Toraason, M.; Hayden, C.; Marlow, D.; Rinehart, R.; Mathias, P.; Werren, D.; Olsen, L. D.; Neumeister, C. E.; Mathews, E. S.; Cheever, K. L.; Marlow, K. L.; Debord, D. G.; Reid, T. M. *Int. Arch. Occup. Environ. Health* **2001**, *74*, 396-404.

67. Steenken, S.; Jovanovic, S. V.; Bietti, M.; Berhard, K. *J. Am. Chem. Soc.* **2000**, *112*, 2373-2374.

68. Delaney, S.; Neeley, W. L.; Delaney, J. C.; Essigmann, J. M. *Biochemistry* **2007**, *46*, 1448-1455.

69. Luo, W.; Muller, J. M.; Rachlin, E. M.; Burrow, C. J. *Chem. Res. Toxicol.* **2001**, *14*, 927-938.

70. Duarte, V.; Muller, J. G.; Burrows, C. J. *Nucleic Acids Res.* **1999**, *27*, 496-502.

71. Sheu, C.; Foote, C. S. *J. Am. Chem. Soc.* **1995**, *117*, 474-477.

72. Sheu, C.; Foote, C. S. *J. Am. Chem. Soc.* **1995**, *117*, 6439-6442.

73. Medinas, D. B.; Cerchiaro, G.; Trindade, D. F.; Augusto, O. *IUBMB Life* **2007**, *59*, 255-262.

74. Lymar, S. V.; Hurst, J. K. *J. Am. Chem. Soc.* **1995**, *117*, 8867-8868.

75. Augusto, O.; Bonini, M. G.; Amanso, A. M.; Linares, E.; Santos, C. C. X.; De Menezes, S. L. *Free Radic. Biol. Med.* **2002**, *32*, 841-859.

76. Liochev, S. I.; Fridovich, I. *Free Radic. Biol. Med.* **2010**, *48*, 1565-1569.

77. Shafirovich, V.; Young, A. L.; Durandin, A.; Dedon, P. C.; Geacintov, N. E. *J. Phys. Chem. B.* **2008**, *112*, 1834-1844.

78. Neta, P.; Huie, R. E.; Ross, A. B. *J. Phys. Chem. Ref. Data* **1988**, *17*, 1027-1284.

79. Czapski, G.; Lymar, S. V.; Schwarz, H. A. *J. Phys. Chem. A* **1999**, *103*.

80. Hodgson, E. K.; Fridovich, I. *Arch. Biochem. Biophys.* **1976**, *172*, 202-205.

81. Bonini, M. G.; Radi, R.; Ferrer-Sueta, G.; Ferreira, A. M. D. C.; Augusto, O. *J. Biol. Chem.* **1999**, *274*, 10802-10806.

82. Buxton, G. V.; Wood, N. D.; Dyster, S. *J. Chem. Soc., Faraday Trans. 1* **1988**, *84*, 1113-1121.

83. Warner, D. S.; Sheng, H.; Batinic-Haberle, I. *J. Exp. Biol.* **2004**, *207*, 3221-3231.

84. Busset, C. M., P; Sarakha, M.; De Laat, J. *J. Photoch. Photobio. A.* **2007**, *185*, 127-132.

85. Ivanov, K. L.; Glebov, E. M.; Plyusnin, V. F.; Ivanov, Y. V.; Grivnin, V. P.; Bazhin, N. M. *J. Photochem. Photobiol. A.* **2000**, *133*.

86. Shafirovich, V.; Crean, C.; Lee, Y. A.; Yun, B. H.; Geacintov, N. E. *ChemBioChem* **2008**, *9*.

87. Joffe, A.; Geacintov, N. E.; Shafirovich, V. *Chem. Res. Toxicol.* **2003**, ***16***, 1528-1538.

88. Crean, C.; Uvaydov, Y.; Geacintov, N. E.; Shafirovich, V. *Nucleic Acids Res.* **2008**, *36*, 742-755.

89. Yun, B. H.; Geacintov, N. E.; Shafirovich, V. *Chem. Res. Toxicol.* **2011**, *24*, 1144-1152.

90. Al-Assaf, S.; Navaratnam, S.; Parsons, B. J.; Phillips, G. O. *Free Radic. Biol. Med.* **2006**, *40*, 2018-2027.

91. Kennett, E. C.; Davies, M. J. *Free Radic. Biol. Med.* **2009**, *47*, 389-400.

92. Chen, S.; Hoffman, M. Z. *Radiat. Res.* **1973**, *56*, 40-47.

93. Carlsson, M. *The Inter- and Intramolecular Selectivity of the Carbonate Radical Anion in its Reaction with Lignin and Carbohydrates*; Ph.D. Dissertation Kungliga Tekniska Högskolan: Stockholm, 2005, pp 62.

94. Wardman, P. *J. Phys. Chem. Ref* **1989**, *Data 18*, 1637-755.

95. Motohashi, N.; Saito, Y. *Chem. Pharm. Bull.* **1993**, *41*, 1842-1845.

96. Elliot, A. J.; Simsons, A. S. *Radiat. Phys. Chem.* **1984**, *24*, 229-231.

97. Chen, S.; Cope, V. W.; Hoffman, Z. *J. Phys. Chem.* **1972**, *77*, 1111-1116.

98. Ha, H. C.; Sirisoma, N. S.; Kuppusamy, P.; Zweier, J. L.; Woster, P. M.; Casero Jr., R. A. *Proc. Natl. Acad. Sci. U.S.A.* **1998**, *95*, 11140-11145.

99. Braunlin, W. H.; Strick, T. J.; Record Jr., M. T. *Biopolymers* **1982**, *21*, 1301-1314.

100. Aso, M.; Kondo, M.; Suemune, H.; Hecht, S. M. *J. Am. Chem. Soc.* **1999**, *121*, 9023-9033.

101. Aso, M.; Usui, K.; Fukuda, M.; Kakihara, Y.; Goromaru, T.; Suemune, H. *Org. Lett.* **2006**, *8*, 3183-3186.

102. Usui, K.; Aso, M.; Fukuda, M.; Suemune, H. *J. Org. Chem.* **2008**, *73*, 241-248.

103. Scheffold, R.; Dubs, P. *Helv. Chim. Acta* **1967**, *50*, 798-808.

104. Basolo, F.; Murmann, R. K. *Inorg. Synthesis* **1953**, ***4***, 173.

105. Allen, A. O. *The Radiation Chemistry of Water and Aqueous Solutions*; Van Nostrand: Princeton, N.J., 1961.

106. Greenling, J. R. *Fundamentals of Radiation Dosimetry*; 2nd ed.; Taylor & Francis Group: New York, 1985.

107. Kinter, M. *J Chromatogr B* **1995**, *671*, 223-236.

108. Uslu, C.; Taysi, S.; Bakan, N. *Ann. Clin. Lab. Sci.* **2003**, *33*, 18-22.

109. Udovicic, L.; Mark, F.; Bothe, E. *Radiat. Res.* **1994**, *140*, 166-171.

110. von Sonntag, C. *Free-Radical-Induced DNA Damage and its Repair: A Chemical Perspective.*; Springer-Verlag: Berlin, 2006.

111. Breen, A.; Murphy, J. *Free Radic. Biol. Med.* **1995**, *18*, 1033-1077.

112. Chen, B.; Bohnert, T.; Zhou, X.; Dedon, P. C. *Chem. Res. Toxicol.* **2004**, ***17***, 1406-1413.

113. Lahoud, G. A.; Hitt, A. L.; Bryant-Friedrich, A. C. *Chem. Res. Toxicol.* **2006**, *19*, 1630-1636.

114. Chan, W.; Chen, B.; Wang, L.; Taghizadeh, K.; Demott, M. S.; Dedon, P. C. *J. Am. Chem. Soc.* **2010**, ***132***, 6145-6153.

115. Huie, R. E.; Clifton, C. L. *J. Phys. Chem.* **1990**, *94*, 8561-8567.

116. Herrmann, H.; Reese, A.; Zellner, R. *J. Mol. Struct.* **1995**, *348*, 183-186.

117. Ampadu-Boateng, D. A. *Kinetics of Formation and Oxidation of 8-oxo-7,8-dihydroguanine (8oxoG)*; Master's Thesis.; East Tennessee State University: Johnson City, TN, 2014, pp 105.

APPENDIX

Plotting Data and Statistical Analyses

Table A.1: SDP Data for X-Irradiated Bicarbonate Solutions (dsDNA)

Dose, Gy	[5MF], μM			Mean	SD	SEM
0	ND	ND	ND	0	0	0
326.1	0.470	0.629	0.810	0.636	0.170	0.0983
652.2	3.38	1.69	2.02	2.36	0.895	0.5169
978.3	4.04	2.18	3.35	3.19	0.938	0.5415
1304.4	6.28	3.03	4.30	4.54	1.64	0.9455
1630.5	7.67	3.44	6.31	5.81	2.16	1.2449
1956.6	8.22	7.70	7.61	7.84	0.327	0.1887

Dose, Gy	[Lac], μM			Mean	SD	SEM
0	ND	0.131	ND	0.0436	0.0756	0.0436
326.1	3.65	3.62	3.24	3.50	0.233	0.134
652.2	6.10	5.20	5.76	5.69	0.454	0.262
978.3	8.50	9.57	8.90	8.99	0.545	0.314
1304.4	12.9	10.6	11.5	11.7	1.18	0.684
1630.5	14.6	12.8	12.2	13.2	1.22	0.705
1956.6	18.5	16.6	13.4	16.2	2.59	1.50

Dose, Gy	[Fur], μM			Mean	SD	SEM
0	ND	ND	ND	0	0	0
326.1	0.681	0.648	0.979	0.769	0.182	0.105
652.2	1.85	1.57	3.38	2.27	0.973	0.562
978.3	2.57	2.27	3.39	2.74	0.583	0.337
1304.4	2.95	2.40	4.61	3.32	1.15	0.664
1630.5	3.55	3.03	4.28	3.62	0.632	0.365
1956.6	3.75	3.86	5.28	4.30	0.857	0.495

Dose, Gy	[Total SDP], μM			Mean	SD	SEM
0	ND	0.131	ND	0.0436	0.0756	0.0436
326.1	4.80	4.90	5.02	4.91	0.111	0.0642
652.2	11.3	8.5	11.2	10.3	1.61	0.930
978.3	15.1	14.0	15.6	14.9	0.821	0.474
1304.4	22.2	16.0	20.5	19.5	3.18	1.84
1630.5	25.8	19.3	22.8	22.6	3.26	1.88
1956.6	30.5	28.1	26.3	28.3	2.11	1.22

Table A.2: FBR Data for X-Irradiated Bicarbonate Solutions (dsDNA)

Dose, Gy	[C], μM			Mean	SD	SEM
0	ND	ND	ND	0	0	0
326.1	2.33	2.24	1.99	2.18	0.176	0.101
652.2	3.96	3.01	3.21	3.39	0.502	0.290
978.3	5.20	5.81	8.23	6.41	1.60	0.925
1304.4	8.14	6.38	6.97	7.16	0.893	0.516
1630.5	8.89	7.81	7.68	8.13	0.664	0.384
1956.6	11.1	10.6	8.22	9.98	1.54	0.891

Dose, Gy	[G], μM			Mean	SD	SEM
0	ND	ND	ND	0	0	0
326.1	1.16	1.15	0.89	1.07	0.150	0.0864
652.2	1.34	0.90	1.37	1.20	0.262	0.151
978.3	1.31	1.26	1.14	1.24	0.0900	0.0520
1304.4	1.61	1.12	1.03	1.25	0.310	0.179
1630.5	1.53	1.21	1.03	1.25	0.253	0.146
1956.6	1.65	1.32	1.27	1.41	0.206	0.119

Dose, Gy	[T], μM			Mean	SD	SEM
0	ND	ND	ND	0	0	0
326.1	2.21	2.24	1.94	2.13	0.165	0.0952
652.2	3.67	2.98	2.99	3.21	0.394	0.227
978.3	4.49	5.40	5.06	4.98	0.459	0.265
1304.4	7.38	5.82	6.28	6.49	0.801	0.463
1630.5	7.87	7.02	6.63	7.17	0.634	0.366
1956.6	9.41	8.72	7.05	8.39	1.21	0.701

Dose, Gy	[A], μM			Mean	SD	SEM
0	ND	ND	ND	0	0	0
326.1	1.65	2.25	3.25	2.38	0.807	0.466
652.2	3.32	2.72	2.77	2.93	0.333	0.192
978.3	3.94	4.66	6.46	5.02	1.30	0.749
1304.4	7.31	5.54	5.99	6.28	0.920	0.531
1630.5	7.49	7.12	6.14	6.92	0.695	0.401
1956.6	10.1	10.1	8.98	9.73	0.644	0.372

Table A.2 (continued). FBR Data for X-Irradiated Bicarbonate Solutions (dsDNA)

Dose, Gy	[Total FBR], μM			Mean	SD	SEM
0	ND	ND	ND	0	0	0
326.1	7.35	7.87	8.07	7.77	0.376	0.749
652.2	12.3	9.6	10.3	10.7	1.38	0.861
978.3	14.9	17.1	20.9	17.7	3.00	1.990
1304.4	24.4	18.9	20.3	21.2	2.90	1.689
1630.5	25.8	23.2	21.5	23.5	2.16	1.297
1956.6	32.2	30.8	25.5	29.5	3.53	2.083

Table A.3: SDP data for Photolyzed Persulfate/Bicarbonate Solutions (dsDNA)

Illumination time, s	[5MF], μM	[Lac], μM	[Fur], μM	[Total SDP], μM
0	ND	ND	ND	0
60	0.507	0.141	ND	0.648
120	1.23	0.333	ND	1.56
180	2.26	0.569	ND	2.83
240	2.83	0.654	0.910	4.40
300	5.22	1.09	0.160	6.48

Table A.4: FBR Data for Photolyzed Persulfate/Bicarbonate Solutions (dsDNA)

Illumination time, s	[C], μM	[G], μM	[T], μM	[A], μM	[Total FBR], μM
0	ND	ND	ND	ND	0
60	0.0840	ND	0.150	0.245	0.479
120	0.180	ND	0.317	0.453	0.950
180	0.676	ND	0.520	0.694	1.89
240	0.653	ND	0.619	0.881	2.15
300	1.69	ND	1.05	1.39	4.14

Table A.5: SDP Data for Photolyzed $[Co(NH_3)_5CO_3]^+ClO_4^-$ Solutions (dsDNA)

Illumination time, s	[5MF], μM			Mean	SD	SEM
0	0.0141	0.0289	0.0240	0.0224	0.00753	0.00435
120	0.150	0.195	0.187	0.177	0.0241	0.0139
240	0.460	0.391	0.405	0.419	0.0365	0.0211
360	0.827	0.712	0.744	0.761	0.0591	0.0341
480	1.039	0.941	0.796	0.925	0.1220	0.0704

Illumination time, s	[Lac], μM			Mean	SD	SEM
0	0.0241	0.0186	0.0360	0.0262	0.00893	0.00516
120	0.322	0.361	0.340	0.341	0.0199	0.0115
240	0.861	0.694	0.665	0.740	0.106	0.0611
360	1.88	1.04	1.07	1.33	0.479	0.277
480	1.50	1.28	1.24	1.34	0.140	0.0811

Illumination time, s	[Fur], μM			Mean	SD	SEM
0	0.0179	0.0126	0.0221	0.0175	0.00475	0.00275
120	0.0527	0.0725	0.0676	0.0643	0.0103	0.00596
240	0.0925	0.0985	0.105	0.0987	0.00626	0.00362
360	0.0894	0.137	0.157	0.128	0.0349	0.0201
480	0.173	0.163	0.133	0.156	0.0207	0.0119

Illumination time, s	[Total SDP], μM			Mean	SD	SEM
0	0.0561	0.0601	0.0751	0.0638	0.00999	0.0122
120	0.524	0.629	0.544	0.566	0.0558	0.0314
240	1.41	1.18	1.07	1.224	0.173	0.0858
360	2.80	1.89	1.80	2.164	0.553	0.331
480	2.71	2.38	1.99	2.362	0.364	0.163

Table A.6. FBR data for photolyzed $[Co(NH_3)_5CO_3]^+ClO_4^-$ solutions (dsDNA).

Illumination time, s	[C], μM			Mean	SD	SEM
0	0.0203	0.0302	0.0721	0.0408	0.0275	0.0159
120	0.180	0.301	0.238	0.239	0.0607	0.0351
240	0.419	0.380	0.426	0.408	0.0249	0.0144
360	0.632	0.683	0.652	0.656	0.0255	0.0147
480	0.873	0.885	0.701	0.819	0.103	0.0596

Illumination time, s	[G], μM			Mean	SD	SEM
0	0.0428	0.0499	0.0794	0.0573	0.0194	0.0112
120	0.128	0.124	0.134	0.128	0.00503	0.0029
240	0.227	0.143	0.225	0.198	0.0479	0.0277
360	0.326	0.191	0.290	0.269	0.0700	0.0404
480	0.347	0.246	0.289	0.294	0.0508	0.0293

Illumination time, s	[T], μM			Mean	SD	SEM
0	0.00477	0.0257	0.0149	0.0151	0.0105	0.00604
120	0.119	0.173	0.156	0.149	0.0277	0.0160
240	0.294	0.249	0.244	0.262	0.0277	0.0160
360	0.453	0.405	0.355	0.404	0.0490	0.0283
480	0.589	0.501	0.374	0.488	0.108	0.0625

Illumination time, s	[A], μM			Mean	SD	SEM
0	0.0568	0.0572	0.189	0.101	0.0765	0.0441
120	0.225	0.295	0.256	0.259	0.0351	0.0203
240	0.416	0.361	0.382	0.386	0.0281	0.0162
360	0.592	0.613	0.611	0.605	0.0118	0.00684
480	0.750	0.668	0.628	0.682	0.0621	0.0359

Illumination time, s	[Total FBR], μM			Mean	SD	SEM
0	0.125	0.163	0.356	0.214	0.124	0.0773
120	0.652	0.893	0.783	0.776	0.121	0.0743
240	1.36	1.13	1.28	1.25	0.114	0.0742
360	2.00	1.89	1.91	1.93	0.0599	0.0903
480	2.56	2.30	1.99	2.28	0.284	0.187

Table A.7. SDP data for photolyzed $[Co(NH_3)_5CO_3]^+ClO_4^-$ solutions (SSDNA).

Illumination time, s	[5MF], μM						Mean	SD	SEM
0	0.0183	0.0199	0.0204	0.0293	0.0110	0.0147	0.0189	0.00618	0.00252
120	0.207	0.534	0.681	0.394	0.629	1.15	0.599	0.319	0.130
240	0.394	0.966	1.21	0.506	0.956	1.68	0.952	0.470	0.192
360	0.722	1.10	1.96	0.786	1.71	2.33	1.43	0.661	0.270
480	1.04	2.30	2.19	0.925	2.10	2.54	1.85	0.688	0.281

Illumination time, s	[Lac], μM						Mean	SD	SEM
0	0.00258	0.0320	0.0118	0.0264	0.00695	0.00941	0.0149	0.0117	0.00476
120	0.332	0.335	0.275	0.460	0.300	0.579	0.380	0.116	0.0475
240	0.593	0.587	0.508	0.509	0.516	0.907	0.603	0.154	0.0628
360	0.949	0.819	0.649	0.731	0.667	1.07	0.814	0.168	0.0684
480	1.18	1.21	0.759	0.902	0.922	1.14	1.02	0.183	0.0747

Illumination time, s	[Fur], μM						Mean	SD	SEM
0	0.0723	0.0403	0.0824	0.0385	ND	0.0234	0.0428	0.0306	0.0125
120	0.100	0.0701	0.121	0.121	0.0890	0.0674	0.0948	0.0237	0.00966
240	0.125	0.177	0.117	0.123	0.0877	0.102	0.122	0.0305	0.0125
360	0.211	0.125	0.164	0.192	0.143	0.149	0.164	0.0320	0.0131
480	0.264	0.219	0.161	0.165	0.157	0.150	0.186	0.0457	0.0186

Illumination time, s	[Total SDP], μM						Mean	SD	SEM
0	0.0932	0.0922	0.115	0.0601	0.0179	0.0476	0.0709	0.0356	0.0198
120	0.639	0.938	1.08	0.629	1.02	1.79	0.860	0.426	0.188
240	1.11	1.73	1.83	1.18	1.56	2.69	1.48	0.570	0.267
360	1.88	2.05	2.77	1.89	2.52	3.55	2.22	0.650	0.351
480	2.49	3.72	3.11	2.38	3.18	3.83	2.98	0.602	0.374

Table A.8. FBR data for photolyzed $[Co(NH_3)_5CO_3]^+ClO_4^-$ solutions (ssDNA).

Illumination time, s	[C], μM			Mean	SD	SEM
0	0.0653	0.0582	0.0471	0.0569	0.00921	0.00532
120	0.233	0.301	0.329	0.288	0.0490	0.0283
240	0.505	0.575	0.450	0.510	0.0628	0.0363
360	0.715	0.729	0.646	0.697	0.0446	0.0257
480	1.20	1.30	0.888	1.131	0.217	0.125

Illumination time, s	[G], μM			Mean	SD	SEM
0	0.0844	0.170	0.162	0.139	0.0473	0.0273
120	0.131	0.144	0.131	0.136	0.00747	0.00431
240	0.132	0.137	0.139	0.136	0.00332	0.00191
360	0.230	0.224	0.176	0.210	0.0296	0.0171
480	0.275	0.246	0.210	0.244	0.0325	0.0188

Illumination time, s	[T], μM			Mean	SD	SEM
0	0.0198	0.0156	0.0122	0.0159	0.00379	0.00219
120	0.138	0.226	0.187	0.184	0.0443	0.0256
240	0.238	0.350	0.303	0.297	0.0560	0.0323
360	0.406	0.520	0.502	0.476	0.0612	0.0353
480	0.726	0.571	0.668	0.655	0.0782	0.0451

Illumination time, s	[A], μM			Mean	SD	SEM
0	0.102	0.142	0.128	0.124	0.0199	0.0115
120	0.348	0.431	0.292	0.357	0.0699	0.0404
240	0.539	0.641	0.623	0.601	0.0541	0.0312
360	0.778	0.837	0.813	0.810	0.0298	0.0172
480	1.31	0.975	1.04	1.11	0.178	0.103

Illumination time, s	[Total FBR], μM			Mean	SD	SEM
0	0.272	0.385	0.349	0.336	0.0580	0.0463
120	0.851	1.10	0.939	0.964	0.127	0.0735
240	1.42	1.70	1.51	1.54	0.146	0.0843
360	2.13	2.31	2.14	2.19	0.102	0.0590
480	3.51	3.10	2.81	3.14	0.355	0.205

VITA

TERENCE JOSHUA MOORE

Education:	B.B.A. Management, East Tennessee State University, Johnson City, Tennessee, 2008
	B.S. Chemistry, East Tennessee State University, Johnson City, Tennessee, 2012
	M.S. Chemistry, East Tennessee State University, Johnson City, Tennessee, 2014
Professional Experience:	Graduate Assistant, East Tennessee State University, College of Arts and Sciences, 2012-2013
	Teaching Assistant, East Tennessee State University, College of Arts and Sciences, 2013-2014
	Adjunct Faculty, East Tennessee State University, College of Arts and Sciences, 2014
Publication:	Roginskaya, M., Mohseni, R., Moore, T. J., Bernhard, W. A., and Razskazovskiy, Y. *Radiat. Res.* **2014**, 181, 131-137.
Honors and Awards:	Phi Sigma Pi National Honor Fraternity – Epsilon Xi Chapter, Southern Appalachian Alumni Chapter
	Golden Key International Honour Society
	Outstanding Teaching Assistant, Chemistry Department (2013, 2014)
	Dean's List
	2nd Place, Oral Presentations – Master's Candidates, Natural Sciences Division, 2014 Appalachian Student Research Forum